CHEMICAL INTERVENTION OF INFLUENZA VIRUS MRNA NUCLEAR EXPORT

APPROVED BY SUPERVISORY COMMITTEE

Beatriz Fontoura, Ph.D.

Jerry Shay, Ph.D.

Frederick Grinnell, Ph.D.

John Minna, M.D.

DEDICATION

I would like to thank all those who have helped me complete this project. In particular, I would like to thank my mentor Beatriz Fontoura for accepting me into her lab and under her mentorship, as well as for the years of guidance and direction both scientifically and professionally. The members of the Fontoura Lab, both previous and current, have been a great help in the day-to-day execution of experiments and in discussing my work. Lastly, I have greatly appreciated the input and critical insight of my committee members Jerry Shay, Frederick Grinnell, John Minna, and previously Lawrence Lum.

I also would like to thank those who have invested time in my growth outside of lab. My roommates, Noah and Susie Sorrelle, and my church family at Antioch Community Church have greatly supported me throughout my time as a graduate student. Their constant encouragement has been a welcome sense of home away from my family here in Dallas. I am not sure I would have survived the long journey of graduate school and life in this city without them.

Most importantly, I would like to thank my family back in El Paso. All my siblings, Bob (Robert), Boo (David), Dex (Josh), Dot (Andréa), and Peaches (Sarah), have each been an endless source of inspiration of creativity, intelligence, and care that I could not have experienced anywhere else. My nieces and nephews Amoryna, Bobby, Chloe, Hanalei, Arabella, Cassi, Abram, Abigail, Lexi, and Samuel push me to be a role model they can look up to one day. Lastly, my parents, Robert and Mary Ann. As if raising a knucklehead of a son wasn't enough, they had to deal with all the craziness that comes along with me. There is no way to express how incredibly thankful I am for their unconditional support. Not just for their love and concern during graduate school, but for instilling in me as a child the importance of getting a good education, of having a demeanor marked by humbleness, of sacrificing when the times call for it, and of living a life not for one's self, but for the glory and honor of a gracious and loving God. Thank you mom

and dad for the countless lessons you deliberately taught me, and especially the ones you did not explicitly teach just by living your lives as an example for all your children.

CHEMICAL INTERVENTION OF INFLUENZA VIRUS MRNA NUCLEAR EXPORT

by

MATTHEW AARON ESPARZA

DISSERTATION

Presented to the Faculty of the Graduate School of Biomedical Sciences

The University of Texas Southwestern Medical Center at Dallas

In Partial Fulfillment of the Requirements

For the Degree of

DOCTOR OF PHILOSOPHY

The University of Texas Southwestern Medical Center at Dallas

Dallas, Texas

August, 2020

Chemical Intervention of Influenza Virus mRNA Nuclear Export

MATTHEW AARON ESPARZA, Ph.D.

The University of Texas Southwestern Medical Center at Dallas, 2020

BEATRIZ FONTOURA, Ph.D.

Influenza A viruses are human pathogens with limited therapeutic options, making it crucial to devise strategies for the identification of new classes of antiviral medications. The influenza A virus genome is constituted of 8 RNA segments. Two of these viral RNAs are transcribed into mRNAs that are alternatively spliced. The M1 mRNA encodes the M1 protein but is also alternatively spliced to yield the M2 mRNA during infection. M1 to M2 mRNA splicing occurs at nuclear speckles, and M1 and M2 mRNAs are exported to the cytoplasm for translation. M1 and M2 proteins are critical for viral trafficking, assembly, and budding. We show that influenza virus utilizes nuclear speckles to promote post-transcriptional splicing of its M1 mRNA. We assign previously unknown roles for the viral NS1 protein and cellular factors to an intranuclear trafficking pathway that targets the viral M1 mRNA to nuclear speckles, mediates splicing at these nuclear bodies, and exports the spliced M2 mRNA from the nucleus. In addition, gene knockout of the cellular protein NS1-BP, a constituent of the M mRNA speckle-export pathway, inhibits M mRNA nuclear export without significantly altering bulk cellular mRNA export, providing an avenue to

preferentially target influenza virus. We performed a high-content, image-based chemical screen using single-molecule RNA-FISH to label viral M mRNAs followed by multistep quantitative approaches to assess cellular mRNA and cell toxicity. We identified inhibitors of viral mRNA biogenesis and nuclear export that exhibited no significant activity towards bulk cellular mRNA at non-cytotoxic concentrations. Among the hits is a small molecule that inhibits nuclear export of a subset of viral and cellular mRNAs via the mRNA export factor UAP56 without altering bulk cellular mRNA nuclear export. These findings underscore specific nuclear export requirements for viral mRNA nuclear export. This RNA export inhibitor also impaired replication of diverse influenza virus strains at non-toxic concentrations. Thus, this screening strategy yielded compounds that alone or in combination may serve as leads to new ways of treating influenza virus infection and are novel tools for studying viral RNA trafficking in the nucleus.

TABLE OF CONTENTS

PRIOR PUBLICATIONS……...……x

LIST OF FIGURES……xi

LIST OF ABBREVIATIONS……..xiii

CHAPTER ONE: INTRODUCTION……... 1

INFLUENZA VIRUS: DISEASE AND TREATMENT……..1

OVERVIEW OF THE INFLUENZA A VIRUS…….. 2

MECHANISMS OF VIRAL MRNA TRANSCRIPTION AND RNA REPLICATION……4

VIRAL MRNA SPLICING…….. 6

PROJECT RATIONALE……..9

CHAPTER TWO: MATERIALS AND METHODS……11

CELL CULTURE ……...11

TRANSFECTIONS AND SIRNAS ……...11

NS1-BP KNOCKOUT CELL LINE……...11

VIRUSES ……12

VIRAL REPLICATION AND CYTOTOXICITY ASSAYS ……12

SMRNA-FISH ……...…….13

HIGH-THROUGHPUT SCREEN AND STATISTICS ……16

IMAGE QUANTIFICATION AND STATISTICS……17

COMPOUNDS ……...18

MEASUREMENT OF CELLULAR ATP LEVELS……..19

RNA PURIFICATION AND RT-QPCR……19

CELL FRACTIONATION AND RNASEQ ANALYSIS……..20

GENE SET ENRICHMENT ANALYSIS (GSEA)……21

WESTERN BLOT ……..22

CHAPTER THREE: INFLUENZA VIRAL MRNA SPLICING AND TRAFFICKING …….23

3.1 INFLUENZA VIRUS M MRNA ACCUMULATES AT NUCLEAR SPECKLES……23

3.2 VIRAL M MRNA IS POST-TRANSCRIPTIONALLY SPLICED AT NUCLEAR SPECKLES. ...…….26

3.3 VIRAL NS1 PROTEIN PROMOTES M MRNA SPLICING AND NUCLEAR EXPORT VIA NUCLEAR SPECKLES …….28

3.4 CELLULAR PROTEINS MEDIATE M1 MRNA PROCESSING AT NUCLEAR SPECKLES..……...30

3.5 ALY/REF AND UAP56 COUPLE VIRAL M MRNA NUCLEAR EXPORT TO SPLICING VIA NUCLEAR SPECKLES …….33

3.6 SON INTERACTS WITH M1 MRNA AND WITH FACTORS REQUIRED FOR M1 MRNA PROCESSING ……38

CHAPTER FOUR: IDENTIFICATION OF CHEMICAL COMPOUNDS THAT INHIBIT VIRAL M MRNA NUCLEAR EXPORT ……..40

4.1 HIGH-THROUGHPUT SCREEN TO IDENTIFY INHIBITORS OF VIRAL M MRNA PROCESSING AND NUCLEAR EXPORT ……..40

4.2 SELECTIVE INHIBITION OF VIRAL MRNA NUCLEAR EXPORT ……46

4.3 COMPOUND 2 PHENOCOPIES DOWN-REGULATION OF THE MRNA EXPORT FACTOR UAP56……49

4.4 COMPOUND 2 INHIBITS REPLICATION OF DIVERSE INFLUENZA A VIRUSES …..57

CHAPTER FIVE: DISCUSSION……60

5.1 INFLUENZA VIRUS M1 MRNA TRAFFICKING PATHWAY THROUGH NUCLEAR SPECKLES FOR SPLICING …….60

5.2 VIRAL M MRNA NUCLEAR EXPORT PATHWAY ……...61

5.3 IDENTIFICATION OF SMALL MOLECULE INHIBITORS OF VIRAL M MRNA TRAFFICKING ……..62

5.4 COMPOUND 2 INHIBITS THE UAP56-MEDIATED MRNA EXPORT OF M1 MRNA ...63

5.5 POTENTIAL ANTI-VIRAL DEVELOPMENT AND IMPLICATIONS FOR CELL BIOLOGY……...65

BIBLIOGRAPHY ……..67

PRIOR PUBLICATIONS

Esparza M, Mor A, Niederstrasser H, White K, White A, Zhang K, Gao S, Wang J, Liang J, Sho S, Sakthivel R, Sathe AA, Xing C, Muñoz-Moreno R, Shay JW, García-Sastre A, Ready J, Posner B, and Fontoura BMA. Chemical Intervention of Influenza Virus mRNA Nuclear Export. PLoS Pathog. 2020 April:16(4):e1008407. https://doi.org/10.1371/journal.ppat.1008407

Zhang K, Xie Y, Muñoz-Moreno R, Wang J, Zhang L, Esparza M, Garcia-Sastre A, Fontoura BMA, Ren Y. Structural basis for influenza virus NS1 protein block of mRNA nuclear export. Nat Microbiol. 2019 Oct;4(10):1671-1679

Mor A, White A, Zhang K, Thompson M, Esparza M, Muñoz-Moreno R, Koide K, Lynch KW, Garcia-Sastre A, Fontoura BM. Influenza virus mRNA trafficking through host nuclear speckles. Nat Microbiol. 2016 May 27;1(7):16069

Dang TT, Esparza MA, Main EA, Westcott JM, Pearson GW. ΔNp63α Promotes Breast Cancer Cell Motility through the Selective Activation of Components of the Epithelial-to-Mesenchymal Transition Program. Cancer Res. 2015 Sep 15;75(18):3925-35

Westcott JM, Prechtl AM, Maine EA, Dang TT, Esparza MA, Sun H, Zhou Y, Xie Y, Pearson GW. An epigenetically distinct breast cancer cell subpopulation promotes collective invasion. J Clin Invest. 2015 May;125(5):1927-43

LIST OF FIGURES

FIGURE 1. INFLUENZA VIRUS LIFE CYCLE ……4

FIGURE 2. VIRAL M MRNA PROCESSING AND NUCLEAR EXPORT PATHWAY ……..9

FIGURE 3. INFLUENZA M MRNA IS LOCALIZED AT NUCLEAR SPECKLES ……...24

FIGURE 4. M1 MRNA AND SPLICED M2 MRNA ACCUMULATE AT NUCLEAR SPECKLES AFTER TRANSCRIPTION ……27

FIGURE 5. VIRAL NS1 PROTEIN PROMOTES M1 MRNA SPLICING AT NUCLEAR SPECKLES AND NUCLEAR EXPORT…….29

FIGURE 6. M MRNA SPLICING AT NUCLEAR SPECKLES IS MEDIATED BY HOST FACTORS NS1-BP, HNRNP K AND SON ……..31

FIGURE 7. ALY/REF AND UAP56 DEPLETION INHIBITS M1 AND M2 MRNA NUCLEAR EXPORT AND MEDIATES SPECKLE DEPENDENT M1 TO M2 SPLICING ENHANCEMENT…..34

FIGURE 8. NUCLEAR SPECKLE ASSEMBLY FACTOR SON INTERACTS WITH M1 MRNA AND MEDIATORS OF M1 MRNA SPLICING……..37

FIGURE 9. LOSS OF NS1-BP PROTEIN INHIBITS VIRAL M MRNA NUCLEAR EXPORT WITHOUT SIGNIFICANTLY ALTERING INTRACELLULAR DISTRIBUTION OF BULK CELLULAR POLY(A) RNA ……..41

FIGURE 10. GROWTH RATE OF NS1-BP KNOCKOUT CELLS COMPARED TO WILD-TYPE CELLS ……41

FIGURE 11. SCHEMATIC REPRESENTATION OF A HIGH-THROUGHPUT SCREEN TO IDENTIFY CHEMICAL INHIBITORS OF VIRAL M MRNA PROCESSING AND NUCLEAR EXPORT ……..42

FIGURE 12. IDENTIFICATION OF SMALL MOLECULES THAT INHIBIT VIRAL M MRNA NUCLEAR EXPORT AND/OR DECREASE VIRAL M MRNA LEVELS……..44

FIGURE 13. SCHEMATIC REPRESENTATION OF IDENTIFICATION AND SELECTION OF TOP HITS THAT INHIBIT VIRAL M MRNA NUCLEAR EXPORT AND/OR EXPRESSION ……45

FIGURE 14. CLUSTER ANALYSIS OF CONFIRMED HITS ……46

FIGURE 15. COMPOUND 2 INHIBITS VIRAL MRNA NUCLEAR EXPORT……..48

FIGURE 16. PARTIAL DEPLETION OF THE MRNA EXPORT FACTOR UAP56 SHOW DIFFERENTIAL EXPORT OF VIRAL MRNAS SIMILAR TO COMPOUND 2……50

FIGURE 17. CONTROL FOR CELL FRACTIONATION SHOWN IN FIGURE 16……...51

FIGURE 18. COMPOUND 2 ACTIVITY PHENOCOPIES DOWN-REGULATION OF THE MRNA EXPORT FACTOR UAP56 ……53

FIGURE 19. COMPOUND 2 ALTERS THE LEVELS AND INTRACELLULAR DISTRIBUTION OF A SUBSET OF CELLULAR MRNAS……56

FIGURE 20. COMPOUND 2 INHIBITS VIRAL PROTEIN PRODUCTION AND REPLICATION ….58

FIGURE 21. COMPOUND 2 INHIBITS INFLUENZA VIRUS REPLICATION IN PRIMARY HUMAN BRONCHIAL EPITHELIAL CELLS AT NON-TOXIC CONCENTRATIONS ……..59

FIGURE 22. POSITIVE CONTROL FOR COMPOUND CYTOTOXICITY ……...59

FIGURE 23. COMPOUND JMN3-003 (N-ARYL MERCAPTOBENZIMIDAZOLE) DOES NOT INHIBIT VIRAL MRNA NUCLEAR EXPORT ……66

LIST OF ABBREVIATIONS

IAV	Influenza A Virus
HA	Hemagglutinin
NA	Neuraminidase
NS1	Non-Structural Protein 1
NEP	Nuclear Export Protein
NS2	Non-Structural Protein 2
vRNP	Viral Ribonucleoprotein
NLS	Nuclear Localization Signals
NP	Nucleoprotein
NPC	Nuclear Pore Complex
cRNP	Complementary Ribonucleoprotein
RdRp	RNA-dependent RNA polymerase
svRNA	Short Viral RNA
SF2	Splicing Factor 2
ESE	Exonic Splicing Enhancer
IGC	Interchromatin Granule Clusters
Aly/REF	Aly/RNA Export Factor
NS1-BP	NS1-Binding Protein
smRNA-FISH	Single molecule RNA-fluorescent *in situ* hybridization
MDCK	Madin-Darby Canine Kidney
DMEM	Dulbecco's Modified Eagle Media
FBS	Fetal Bovine Serum
EMEM	Eagle's Minimum Essential Medium
PBS	Phosphate Buffered Saline
sgRNA	Short Guide RNA
BSA	Bovine Serum Albumin
Poly(A) RNA	Polyadenylated RNA
N	Nuclear
C	Cytoplasmic

N/C	Nuclear to Cytoplasmic (ratio)
TPM	Transcripts per Million
DMSO	Dimethyl sulfoxide
MOI	Multiplicity of Infection
cDNA	Complementary DNA
GSEA	Gene Set Enrichment Analysis
qPCR	Quantitative Real-Time PCR
HRP	Horse Radish Perioxidase
SF2 or SRSF2	Serine/Arginine-Rich Splicing Factor 1
SR	Serine/Arginine-Rich Splicing Factor
NXF1-NXT1	Nuclear Export Factor 1-NTF2-related Export Protein 1
SDS-PAGE	Sodium dodecyl sulfate-polyacrylamide gel electrophoresis
DRB	5,6-dichloro-1-β-D-ribofuranosylbenzimidazole
AC_{50}	Activity Concentration 50%
3'UTR	3' Untranslated Region
siRNA	Short Interference RNA
FDR	False Discovery Rate
snoRNA	Small nucleolar RNA
SV40	Simian Vacuolating virus 40
SA	Splicing Acceptor
IFIT1	Interferon Induced Protein with Tetratricopeptide Repeats 1
IRF7	Interferon Regulatory Factor 7
GAPDH	Glyceraldehyde 3-phosphate dehydrogenase

CHAPTER ONE
Introduction

Influenza virus: disease and treatment

Influenza A viruses are human pathogens that cause 291,000 to 646,000 deaths worldwide annually [1]. The largest influenza virus pandemic, the Spanish flu, caused more than 25 million deaths in the first 25 weeks of its detection and over 50 million deaths occurred by the end of the pandemic period. The influenza A virus is also capable of infecting diverse animals, including avian, canine, and swine species, which can also be transmitted to humans. One strain of swine origin was responsible for the most recent influenza pandemic in 2009. Despite the availability of modern-day treatment and medical care, this specific strain caused a large number of influenza-related deaths, more than 180,000 deaths worldwide [2].

Though it has been several decades since influenza virus was identified, available treatments are limited to vaccines and a few antiviral drugs. Currently, vaccines are dependent on the robustness of the one's immune system, being less effective in the elderly population. In addition, seasonal Influenza vaccines rely on the accuracy of predicted circulating population of Hemagglutinin (HA) and Neuraminidase (NA). Antiviral drugs are most effective within the first 48 hours of the infection. In both cases, vaccines and antivirals are limited in effectiveness due to the virus' high mutation rate, which drives resistance [3-5]. This gradual accumulation of genetic changes caused by selective pressures from the immune system is known as antigenic shift. Antigenic shift changes the HA and NA surface protein structures to evade recognition by antibodies in the extracellular space. This same event also allows the virus to infect different species as well as production of the different strain subtypes, including 16 different HA and 9 different NA subtypes.

Of the four FDA-approved Influenza antiviral drugs, three (Oseltamivir, Zanamivir, and Peramivir) target the NA protein, all of which have similar resistance limitations as vaccines against NA. The newest drug, Baloxavir Marboxil, is the only drug that does not target NA, but targets another viral protein PA, an endonuclease that is important for proper viral mRNA synthesis. Despite being approved for clinical use in 2018, virus mutations that confer reduced susceptibility to the drug have already been observed in patients.

Patients infected by influenza carrying these mutations exhibited longer time to alleviate symptoms and shed infectious virus longer than patients infected with virus without these mutations [6]. Due to the lack of sustainable medical options available for treatment of Influenza infections, identification of alternative antiviral strategies is necessary to develop drugs that cannot be quickly resisted. One strategy to do this is to target viral-host interactions that reduce viral replication while having no major adverse effects on the host. In order for the development of such treatments, the field then requires an understanding of how the virus interacts with the cell.

Overview of the influenza A virus

Influenza is a member of the *Orthomyxoviridae* family of RNA viruses, which can be further classified into Influenza A, B, C, and D types. Differences between the influenza types are based on genetic changes that influence what species can be infected and how pathogenic they are in humans. Influenza A is a membrane-bound viral particle forming a spherical structure ~100 nm in diameter. The viral membrane is surrounded by the two surface proteins Hemagglutinin (HA) and Neuraminidase (NA), which function to allow proper entry and budding from the host cell. HA is in greater representation compared to NA, at a ratio of four to one [7]. In addition, the M2 ion channel is found at a much lower abundance than either, at a ratio of one for every 10-100 HA present [8]. M2 is required for proper viral entry, inhibition of cellular autophagy [9], and budding from the host [10, 11]. Located on the interior surface of the viral membrane is the M1 matrix protein. Viral RNAs (vRNAs) make up the viral genome and are bound by nucleoproteins (NP) and the subunits for the viral RNA-dependent, RNA Polymerase (PB1, PB2, and PA). Together, these proteins and vRNAs make up the viral ribonuclear proteins or vRNPs. Other proteins synthesized, which are not structural components of the viral particle but serve other functions important for replication, are Non-Structural Protein 1 (NS1) and Nuclear Export Protein or Non-Structural Protein 2 (NEP/NS2). NS1 protein has a variety of functions, including suppression of host innate immunity [12], regulation of RNA synthesis and translation, regulation of splicing, and RNA nuclear export, preventing host mRNA nuclear

export [13, 14] but promoting viral mRNA nuclear export [14-17]. NS2 plays a role in nuclear export of vRNPs and because of this is important for viral replication [18].

The virus first enters the host cell by receptor-mediated endocytosis, triggered when HA recognizes the α-2,3-linked or α-2,6-linked sialic acid from cellular receptors on the plasma membrane. Before HA is able to interact with receptors it must be cleaved by cellular proteases, processing the uncleaved HA_0 into HA_1 and HA_2 parts that are bound by disulfide bonds. Within the endosome, the low pH (pH 5.0-6.0) induces a conformational change in HA_2, allowing the N-Terminal peptide to insert into the endosomal membrane causing fusion with the viral membrane and entrance of viral components into the host cell. Also while in the endosome, the M2 ion channel on the viral membrane transports hydrogen ions from the endosomal acidic environment into the virus particle resulting in M1 matrix coat protein dissociation and release of the viral genome into the host cell cytoplasm after viral-host membrane fusion [7]. Each of the vRNPs are unique, each carrying 1 of 8 negative-sense, single-stranded vRNA. The proteins that make up the vRNPs contain nuclear localization signals (NLS), though NP is the only necessary and sufficient NLS required for nuclear import. The NP of the vRNP complex associates with the nuclear import receptors karyopherin α and karyopherin β, which dock the vRNP on the nuclear pore complex (NPC) for nuclear import [19]. Once in the nucleus, the vRNAs can be directly transcribed into viral mRNAs.

Once transcribed, the viral mRNAs are exported from the nucleus using host cellular factors [16, 20] and are then translated into proteins in the cytoplasm. The viral proteins carry out functions in the cytoplasm and the nucleus. Later in the viral life cycle, vRNPs are transcribed into positive-strand complementary RNPs (cRNPs), an intermediate that will then be transcribed into vRNPs. The newly synthesized vRNPs are exported from the nucleus into the cytoplasm via M1 protein interaction with the NP and NEP/NS2 proteins. NEP interaction with the cellular CRM1 nuclear export factor mediates nuclear export of vRNPs, which are then localized to the plasma membrane for new virion assembly [18, 21-23]. Membrane-bound proteins, HA, NA, and M2 are also shuttled to the cell surface membrane through the trans-golgi network. M1 matrix protein assists with curving the membrane to initiate budding, while M2

localizes to the membrane neck bridging the budding viral particle and the cell. NA assists in leaving the host cell by cleaving sialic acid from the newly assembled viral particle [10]. This budding is damaging to the cell and produces a cytotoxic effect that eventually lyses the cell.

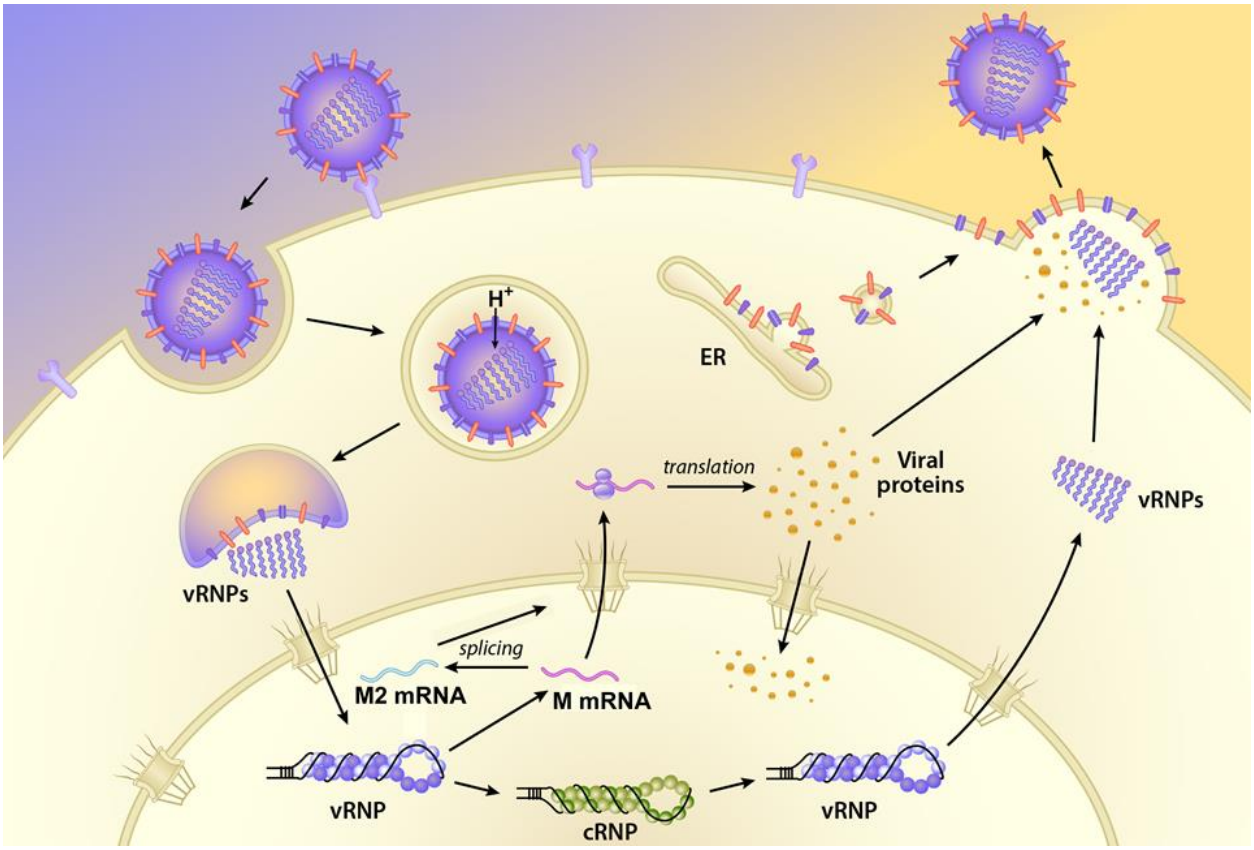

Figure 1. Influenza virus life cycle.
Influenza A virus life cycle begins with hemagglutinin binding to cell surface receptors containing sialic acid. The virus enters the cell through receptor-mediated endocytosis where it transports hydrogen ions from the acidic endosomal environment into the interior of the virus particle. The lower pH triggers fusion of the viral and endosomal membranes and release of the viral genome into the cytoplasm which is imported to the nucleus. In the nucleus, the negative-sense viral RNA packaged in viral ribonucleoproteins (vRNPs) can be transcribed into mRNA. The viral mRNA is then exported out of the nucleus for translation, while specific mRNAs like M and NS mRNAs, undergo splicing before nuclear export. Midway through infection, vRNPs are used as the template to synthesize an intermediate complementary RNP (cRNP), which is transcribed into new vRNPs. The newly synthesized vRNPs are exported from the nucleus to the cytoplasm where, together with viral proteins, localize at the plasma membrane to assemble new viral particles, which then bud from the host cell.

Mechanisms of Viral mRNA transcription and RNA replication

Viral mRNAs are synthesized by the virus' RNA-dependent RNA Polymerase (RdRp), which consists of the subunits PB1, PB2, and PA. With the highly conserved 5' and 3' ends of each vRNA, the complementary sequences form a double stranded segment creating a distinct panhandle structure. The RdRp initially recognizes and binds to the panhandle, promoting transcription initiation [24, 25]. In a separate event, PB2 binds to the 5'-cap of the host RNAs while the endonuclease domain of the PA subunit cleaves 8-14 nucleotides downstream in an act known as cap-snatching [26-28]. The RdRp uses this as a primer to start elongation of the vRNA template until it reaches a segment with a 5-7 nucleotide uracil repeat (U-stretch). The stuttering is caused by steric hindrance of the 5' end of the template still bound to the newly synthesized viral mRNA. The RdRp continues and synthesizes a polyadenylated tail at the end of the viral mRNA [29, 30].

Using the same proteins for transcription in the process of replication, vRNPs are used as the template for the generation of cRNPs. Unlike during the synthesis of mRNA, complementary RNAs (cRNAs) are synthesized by copying the entire vRNA template. In addition, cRNA synthesis is initiated *de novo*, meaning a primer is not required for initiation and elongation. Because no primer is needed, this does not require cap-snatching as a pre-initiation step. Instead, a subdomain located near the active site of PB1 known as a priming loop is used, likely functioning to stabilize the first nucleotide base interaction [31]. As the cRNA is synthesized, cRNPs are organized similarly to vRNPs using NPs and formed into a panhandle structure. This starts shortly after the 5' end of the newly synthesized cRNA emerges from the RdRp. The cRNA is bound by a second polymerase which recruits other viral proteins to start assembly of cRNPs. Continuing cRNA synthesis, steric hindrance is avoided and there is no polyadenylated tail produced despite using the same template for mRNA synthesis. It is hypothesized that this is due to small viral RNAs (svRNAs) that are produced, which correspond to the 5' termini of vRNAs. This is thought to preserve the sequence by forming the promoter *in trans*, allowing the polymerase to reach the end of the vRNA sequence and preventing polyadenylation [32, 33].

In the last stages of the viral life cycle, cRNA is used as the template for generation of genomic vRNA for viral particle packaging. Unlike either mRNA or cRNA synthesis, vRNA synthesis initiation

does not require primers or the priming loop. Instead, it is initiated on the cRNA template at the U4 and C5 positions in a process termed internal initiation. The dinucleotide complex is then shifted to the U1 and C2 positions of the 3' terminus of the cRNA. As the 5' end of the vRNA emerges from the RdRp, a second polymerase also binds [34]. This second RdRp does not need to be catalytically active but is still required for RNA replication [35]. There are different models that suggest the role of the second polymerase. In the *trans*-activating role, the second RdRp functions to recruit NP to assemble new vRNPs and stabilize vRNA. In another model in which the second RdRp is *trans*-acting, the second RdRp performs the same activity as the first, starting with internal initiation. There is then a third polymerase that initiates assembly of the vRNPs [36].

There are a few models as to what determines whether the virus should continue mRNA transcription or to start vRNA replication. In the first model, NP accumulation over the course of the viral life cycle signals to the viral replication proteins to start cRNA synthesis. This is supported by the transcription-to-replication switch occurring with exogenous expression of NP and the observation that the RNA-binding activity is not required for this switch to occur [37]. The second theory is based on the transcription of svRNAs, which are typically synthesized later in the viral life cycle. Since proper cRNA synthesis requires the presence of svRNAs, cRNA synthesis would also occur later in the life cycle about 8-10 hours post-infection when svRNA is available [38]. The last model is that cRNA is continually being produced, but without the necessary amounts of NP and RdRp proteins to stabilize the cRNAs in cRNPs, the RNA is degraded by cellular nucleases. It is not until the later in the life cycle that there is enough proteins to protect the cRNA being made [39].

Viral mRNA splicing

Two of the eight influenza virus RNA segments, M and NS, undergo alternative splicing in addition to generating proteins from the pre-mRNA [40]. In the case of the M1 mRNA, it generates the M1 protein and is alternative spliced into M2, which is translated into the M2 ion channel. The splicing of M1 to M2 occurs late in infection as M2 is a proton channel and its expression early during infection would be toxic

to the host cell, inhibiting the late stages of infection. M1 mRNA is also spliced into $mRNA_3$, which does not encode a peptide, and M4 mRNA, which encodes an isoform of M2 protein and only present in specific viral strains [41]. The other viral mRNA that is alternatively spliced is NS1 mRNA, which is spliced into NS2 mRNA. NS1 to NS2 splicing is regulated by NS1 protein. NS1 interacts with the host splicing factor SF2, directing it to the exonic splicing enhancer (ESE) to promote splicing [42].

Previous work from our lab has shown that M1 to M2 splicing occurs at nuclear speckles [16], also known as interchromatin granule clusters (IGCs). Mammalian cells have ~20-50 nuclear speckles per nucleus, each containing proteins involved with pre-mRNA processing and splicing factors [43, 44]. In most cases, splicing factors leave nuclear speckles to function at active transcription sites in the nucleoplasm [45]. However, polyadenylated RNAs are found at nuclear speckles and a subset of mRNAs require localization to a nuclear speckle for splicing and/or export from the nucleus [46-50]. This is in contrast to the majority of mRNAs that are co-transcriptionally spliced.

Based on our studies of M1 to M2 splicing, we proposed a model that viral NS1 protein interacts with the cellular protein NS1-BP, which along with hnRNP K, targets M1 mRNA from the nucleoplasm to nuclear speckles. U1 snRNP is then recruited to the complex at the M2 5' splice site on M1 mRNA to promote splicing. NS1 and NS1-BP then use the RNA helicase UAP56 and the mRNA export factor Aly/REF to export M1 and M2 mRNAs into the cytoplasm for translation [51]. Though most splicing occurs in the nucleoplasm, these data suggest that the virus utilizes a non-canonical pathway for splicing and nuclear export through nuclear speckles. This is likely a post-transcriptional splicing event as opposed to co-transcriptional splicing. This same pathway is also used by a subset of cellular RNAs, as indicated by another study from our laboratory on NS1-BP interactions with components of the splicing and mRNA export machineries and its function in splicing and nuclear export of a subset of viral and host mRNAs [52].

Disruption of this nuclear speckle-export pathway at different steps of the pathway results in various phenotypes that impair viral M mRNA production, splicing, and export. Infecting cells with a NS1-deficient virus results in decreased production of viral M2 mRNA relative to M1 mRNA as well as an inhibition of M mRNA nuclear export [16]. This result shows that although M1 is being produced, it is not

being spliced or exported. This highlights NS1's role in viral M1 mRNA to M2 mRNA splicing as well as nuclear export, supporting the model that NS1 promotes transport of M1 mRNA to nuclear speckles for splicing and exports M1 and M2 mRNAs from the nucleus. Depletion of nuclear speckle factors NS1-BP, hnRNP K, and SON by siRNA did not change overall M mRNA levels (total M1 mRNA and M2 mRNA levels), but did result in accumulation of M mRNA in nuclear speckles. This effect prevented M mRNA splicing and nuclear export. As a result, viral replication was reduced. These data suggest that without the ability to be spliced, viral M1 mRNA is halted at nuclear speckles and cannot be exported from the nucleus. Interestingly, knockdown of nuclear export factors Aly/Ref and UAP56 also results in accumulation of M mRNA in nuclear speckles in addition to inhibiting nuclear export. One major difference from the previously described phenotype is that there is an increase in splicing rather than a decrease. This result suggests that while M1 mRNA is trapped in the nucleus and with all the required splicing factors intact within the nuclear speckles, the higher concentration of M1 mRNA is readily available for splicing. These experiments show how targeting this pathway disrupts viral M mRNA processing and export which decreases viral replication [16].

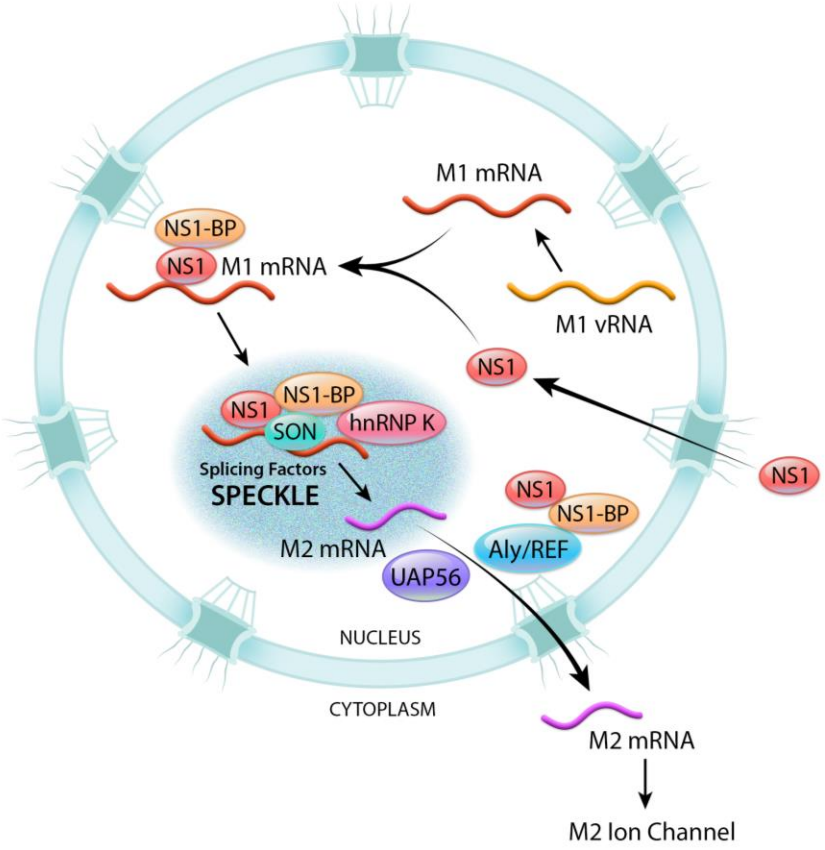

Figure 2. Viral M mRNA processing and nuclear export pathway.
Viral M1 vRNA is transcribed into M1 mRNA using viral RNA polymerase. Viral NS1 protein is imported into the nucleus and binds the cellular NS1-BP protein. The complex then transports M1 mRNA to nuclear speckles where together with hnRNP K and SON mediate M1 mRNA splicing into M2 mRNA. After splicing, M2 mRNA is exported from the nucleus, a process mediated by NS1, NS1-BP, and the export factors UAP56 and Aly/Ref.

Project rationale

Since this splicing-export pathway through nuclear speckles does not impact bulk mRNA but only a subset of viral and cellular mRNAs [16, 52], chemical compounds that would antagonize this process have the potential of not being overly toxic and could inhibit virus replication. Thus, we performed an image-based chemical screen using single-molecule RNA-FISH to detect the viral M mRNA (M1 and M2 mRNAs) and thereby identify chemical compounds that would inhibit different steps of this speckle-export intranuclear pathway but that would not significantly compromise bulk poly(A) RNA. Indeed, we identified chemical compounds that inhibited viral mRNA processing and nuclear export, and which did not

significantly affect bulk cellular mRNA levels or intracellular distribution. This selective approach offers a window of opportunity for targeting virus-host interactions, which favor the mining of compounds that target the virus with less impact to the host. Furthermore, differential requirements for nuclear export of viral mRNAs and for a subset of cellular mRNAs were revealed by one of the top hits, uncovering a new tool for studying these poorly known cell biological processes.

CHAPTER TWO
Materials and Methods
(Contents of Chapters 2-5 were adapted from Nature Microbiology 2016 and PLOS Pathogens 2020)

Cell Culture

Human lung adenocarcinoma epithelial cells (A549) and MDCK cells, obtained from ATCC (American Type Culture Collection), were maintained in high-glucose DMEM (Gibco), 10% FBS (Sigma), and 100 units/mL Pen/Strep antibiotics at 37 °C with 5% CO_2. Primary human bronchial epithelial cells were cultured as reported [53]. A549 cells stably expressing UAP56 E179A mutant were generated as we recently reported [54].

Transfections and siRNAs

siRNAs were reverse transfected with A549 cells using RNAiMAX (Invitrogen) in OptiMEM (ThermoFisher) by the manufacturer's instructions. After 24h transfection, media was replaced with growth media. Knockdown was allowed to continue for 48h before compound treatment or infections occurred. siRNAs used include UAP56 and MISSION siRNA Universal Negative Control #2 (Sigma-Aldrich), ON-TARGETplus siRNAs against SON and ON-TARGETplus Non-targeting Control #2 (Dharmacon, ThermoFisher), and 3'UTR siUAP56 sequence 5'-GCUUCCAUCUUUUGCAUCAUU-3' (Dharmacon).

NS1-BP knockout cell line

The NS1-BP gene was knocked out in A549 cells by genome editing using CRISPR–Cas9. In brief, the genomic target oligos (Forward: CACCGTGCTTATGGCCATTCTCACG, Reverse: AAACCGTGAGAATGGCCATAAGCAC) were cloned into a lentiCRISPRv2 vector. The plasmid was co-transfected into HEK293T cells, obtained from ATCC (American Type Culture Collection), with the packaging plasmids pVSVg and psPAX2, generating lentivirus to infect A549 cells. Then, cells were clonally selected using puromycin (1.0 μg/mL) for 7 days followed by 3 days without selection for

expansion. Clones were isolated and expanded to generate lysates for western blot analysis using anti-NS1-BP antibody. Candidate clones were subjected to genomic sequencing using amplicons flanking the sgRNA-target site. Growth rates were determined by measuring ATP levels. Cells were tested at 24 h, 48 h, 72 h, and 96 h after plating equal number of NS1-BP$^{+/+}$ and NS1-BP$^{-/-}$ cells. ATP was measured by luminescence using CellTiter-Glo (Promega) according to the manufacturer's instructions.

Viruses

Influenza A viruses (A/WSN/33, A/Vietnam/1203/04, A/Panama/99) were generated in embryonated eggs or in MDCK cells after growth from a clonal population of virus at low multiplicity of infection to avoid accumulation of defective virus particles. In MDCK cells, virus was amplified at MOI 0.1-0.001 in infection media containing EMEM (ATCC, 30-2003), 10mM HEPES (Gibco), 0.125% BSA (Gibco), 0.5μg/mL TPCK trypsin (Worthington Biomedical Corporation). Cells were incubated with virus for 1 hour at 37°C, then washed before amplification in infection media. After cell death was observed at 48-72 hours post-infection, supernatants were centrifuged at 1,000 x *g* for 10 minutes to remove cell debris, aliquoted, and stored at -80°C. All virus stocks are controlled for an appropriate ratio of HA/PFU titer and sequenced by RNAseq to confirm the full sequence of the virus.

Viral replication and cytotoxicity assays

A549 cells were infected with A/WSN/33 and A/Vietnam/1203/04 at MOI 0.01, or with A/Panama/99 at MOI 0.1 in the absence or presence of compound 2 at concentrations depicted in the figures. Supernatants were collected from each condition 24 h post-infection and viral particles were tittered by plaque assay as following: MDCK cells were seeded in 6-well plates to reach confluency the next day. At confluency, ten-fold serial dilutions of each sample's supernatant were diluted in PBS containing 100 units/mL Pen/Strep antibiotics, 0.2% BSA, 0.9 mM $CaCl_2$, and 1.05 mM $MgCl_2$. After infection with each dilution, cells were

overlaid with a 1:1 mixture of 2X L-15 media and 2% Oxiod Agar (Final concentration of 1X L-15 media and 1% Agar). Plaques formed at 24 h for A/WSN/33 and A/Vietnam/1203/04, or 48 h for A/Panama/99 were counted and titers determined. Primary human bronchial epithelial cells were infected with A/WSN/33 at MOI 0.1 for 24 h in the absence or presence of compound 2 at depicted concentrations. Supernatants were subjected to plaque assays as described above.

Cytotoxicity was also performed using the MTT assay (Roche), according to the manufacturer's instructions, concurrent with viral replication assay.

smRNA-FISH

smRNA-FISH was performed as previously described [16], which includes the sequences of M1 and NS1 probes except for the HA probes that are listed below. Briefly, cells were grown on glass coverslips (Fisherbrand, Fisher Scientific) coated with 1mL of 0.1% gelatin (Sigma-Aldrich). Cells were fixed with 4% paraformaldehyde (PFA, Electron Microscopy Sciences) in PBS for 15 min before incubation in 70% ethanol for 12 h at 4°C. Coverslips were then placed in wash buffer for 5 min, containing Nuclease Free Water, 2x SSC Buffer (Sigma), and 10% formamide. (Sigma). The coverslips where then removed and incubated in hybridization buffer containing FISH probe. Hybridization occurred at 37 °C for 4 h, then cells were washed with wash buffer for 30 min at 37 °C. Coverslips were then washed twice for 5 min in PBS and stained with 1 µg/ml Hoechst 33258 (Molecular Probes/Life Technologies) for 10 min. Coverslips were briefly washed with PBS before mounting in ProLong Gold antifade reagent (Life Technologies).

<u>HA mRNA Probes:</u>

Forty-eight, 20nt DNA probes labeled with Quasar 570 (BIOSEARCH TECHNOLOGIES) were designed to hybridize with the Influenza WSN full length HA mRNA. Sequences include:

Probe #	**Probe (5'-> 3')**

1	catattgtgtctgcatctgt
2	ttgagttgttcgcatggtag
3	gccacattcttctcgaatat
4	gtcttcgagcaggttaacag
5	ttacatagtttcccgttgtg
6	caattgtagtggggctattc
7	catccggtgatgttacattt
8	tgagtcgcattctggatttc
9	cattctcagagtttggtgtt
10	tcagttcctcatagtcgatg
11	gatactgagctcaattgctc
12	ccatgaactttccttgggaa
13	gagcatgatactgttactcc
14	gtaaaaactgctttttcccc
15	ttcgtcagccatagcaaatt
16	aattggtcagctttgggtat
17	tttccctttattgttcacat
18	tgatgaacaccccatagtac
19	gggtgaatctcctgttataa
20	cccatgttgatcttttactt
21	gcaaggtccagtaatagttc

22	tattagattaccagttgcct
23	tcagtgcgaaagcataccat
24	tgatgatgccggactcaaac
25	tcatgcattgacgcgtttga
26	gtgtttgacacttcgtgtta
27	gattgctgtttatagatccc
28	gactgggtgtatattctgga
29	tgacatattttgggcactct
30	gtaaccatcctcaatttggt
31	ggatgggatgtttcttagtc
32	ctccaaatagacctctgtat
33	cccctcaataaaaccagcaa
34	aaccataccatccatctatc
35	ttttttgatccgctgcatag
36	tttgtaatcccgttaatggc
37	ctcgataacagagttcacct
38	tgtccaaatgtccagaaacc
39	ggctttttactttctcgtac
40	tccgatttctttggcattat
41	tcattgtcacacttgtggta
42	aagtcccatttcttacactt

43	ctatcttttccctgttcaac
44	cccattgattccaatttcac
45	tggcgacagttgagtagatc
46	gagaccaaaagcaccagtga
47	acatccagaaactgattgcc
48	atgcatattctgcactgcaa

High-throughput screen and statistics

To identify chemical inhibitors of viral M mRNA processing and nuclear export, A549 cells were treated with 232,500 chemical compounds available from the University of Texas Southwestern Medical Center High Throughput Screening core facility. Cells were treated with 2.5 μM compound for 30 minutes and incubated at 37°C in 5% CO_2. Cells were then infected with influenza A/WSN/33 virus at MOI of 2 and returned to incubation as before. At 7.5 hours post-infection, cells were fixed with 4% paraformaldehyde and subjected to RNA-FISH. To localize M mRNA, we used forty-five FISH probes labeled with Quasar 570 that cover the entire M mRNA segment, as previously reported [16]. Nuclei were stained with 1 μg/mL Hoechst 33342 dye. M mRNA distribution between the nucleus and the cytoplasm was detected using the IN Cell Analyzer 6000 (GE Healthcare, Marlborough MA). Multiple fields per well were taken at 20X magnification using the Hoechst and dsRed widefield fluorescence filters. Image analysis was performed in a GE IN Cell Analyzer Workstation 3.7.3 (GE Healthcare) using the multi-target analysis template. Individual nuclei were segmented using a top-hat filter on the Hoechst channel with the default sensitivity setting. For samples detecting the M1 mRNA, the cell body was segmented using the region growing method on the M1 mRNA channel. This method uses the nuclei as the seed and then expands outwards until the edge of the stain is reached. For samples detecting poly(A) RNA, the poly(A) RNA channel was instead used to define the cell body region using the region growing method. For each segmented nucleus

and cell pair, the mean and total signal intensities of the nuclear and cytoplasmic chambers were calculated for the poly(A) RNA (where applicable) and M1 mRNA channels. The mean nuclear to mean cytoplasmic (N/C) ratio was then calculated for both mRNA probes for each cell. Finally, the average N/C ratios per well were calculated and used for hit identification. The results were imported into the GeneData Screener™ (Basel, Switzerland; version 13.0.6) software analysis suite to normalize and summarize the overall M mRNA intensity as well as nuclear to cytosolic ratio in terms of a Z-score as previously described [55, 56].

In the primary screen, compounds with a robust Z-score of less than -3 for intensity were considered hits affecting virus replication. Compounds with a Z-score greater than 3 in the nuclear/cytosolic ratio were selected as hits for inhibition of nuclear export. Any compound that lowered the nuclear count to a Z-score of -3 or lower was considered cytotoxic and not included in follow-up experiments. Compounds (1,125) that had the highest activity were selected for confirmation and retested in triplicate at a compound concentration of 2.5 μM. All imaging confirmation and follow-up assays included a bulk poly(A) RNA probe linked to Quasar 670 for FISH imaging. As with the M mRNA probe, total intensity and N/C ratio were also measured for the poly(A) RNA probe. The 600 compounds with the highest activity from the confirmation assay were subjected to 12 point dose response curves ranging from 0.5 nM to 50 μM at 0.5 log dose intervals. Of the 600 compounds tested, 413 compounds had a measureable effect on bulk poly(A) RNA and were excluded from further testing. The remaining 187 compounds that inhibited viral mRNA nuclear export and/or decreased viral mRNA levels but had no substantial effect on the host cell poly(A) RNA were categorized into 3 major phenotypes. These include 22 compounds that retained viral M mRNA in the nucleus, 33 compounds that decreased viral M mRNA levels, and 132 compounds that decreased overall levels and inhibited nuclear export of viral M mRNA. Clustering analysis of confirmed hits was performed with Pipeline Pilot v16 (Biovia, Inc.) using ECFP4 fingerprints [57].

Image quantification and statistics

Total cell fluorescence intensity or fluorescence intensity in the nucleus and cytoplasm analysis for Figures 9, 15, 16, and 23. Images were obtained using AxioVs40 (4.8.2.0) then deconvolved with AutoQuant (3.1.2) software. Deconvolved images were analyzed using Imaris (Bitplane) (9.1.2). The Surfaces tool was used to segment fluorescence within the cytoplasm and nucleus of each cell quantified. Statistical analyses for imaging studies and qPCR data in the figures mentioned above were performed using the two-sample, two-tailed, *t*-test.

Compounds

Compound 2-thiobenzimidazole was initially purchased from TimTec (HTS04595) as well as synthesized in-house. JMN3-003 was synthesized as previously described [58]. All compounds were dissolved in dimethylsulfoxide (DMSO). Compound 2 was synthesized and characterized as following:

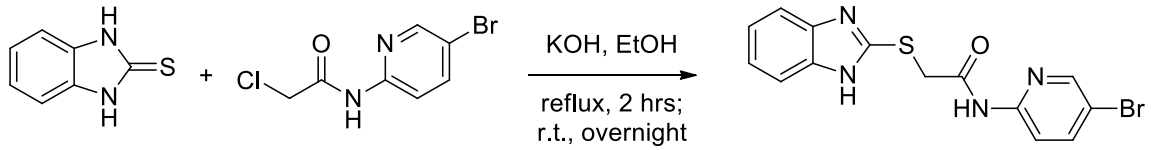

SW053772 (Compound 2)

2-((1H-benzo[d]imidazol-2-yl)thio)-N-(5-bromopyridin-2-yl)acetamide

A mixture of 2-mercaptobenzimidazole (30.0 mg, 0.2 mmol, 1.0 equiv.) and crushed potassium hydoxide (11.2 mg, 0.2 mmol, 1.0 equiv.) in 2 mL of ethanol was kept at reflux for 2 hours. The reaction mixture was cooled down to room temperature, N-(5-bromopyridin-2-yl)-2-chloroacetamide (49.9 mg, 0.2 mmol, 1.0 equiv.) was added, and the reaction was stirred for overnight. The resulting reaction mixture was concentrated under reduced pressure. 2.0 mL of saturated ammonium chloride solution and 2.0 mL of dichloromethane were added to the residue. The organic layer was separated, washed with 2.0 mL of brine, then dried over sodium sulfate, filtered and concentrated under reduced pressure. The crude was further

purified by silica gel chromatography using 60% of ethyl acetate in hexane to afford 54 mg white solid as product, yield 74%.

^{1}H NMR ($CDCl_3$, 400 MHz)

δppm 8.31 – 8.24 (m, 1H), 8.03 (d, J = 8.8 Hz, 1H), 7.72 (ddd, J = 8.9, 2.8, 1.5 Hz, 1H), 7.48 (br, 2H), 7.20 – 7.08 (m, 3H), 4.03 (s, 2H).

^{13}C NMR ($CDCl_3$, 400 MHz)

δppm 168.23, 149.92, 149.48, 148.78, 140.57, 122.95, 122.35, 115.53, 114.86, 109.97, 36.24.

MS

MS (ESI) *m/z* = 363.0 ($[M+H]^+$), $C_{14}H_{11}BrN_4OS$ requires 363.0

Measurement of cellular ATP levels

ATP was measured by luminescence using the CellTiter-Glo kit (Promega) according to the manufacturer's instructions.

RNA purification and RT-qPCR

Total RNA was isolated from A549 cells using the RNeasy Plus Mini Kit (Qiagen) and reverse transcribed into cDNA by SuperScript II reverse transcriptase (Invitrogen), each according to the manufacturers' protocols. Samples were then amplified in a LightCycler 480 quantitative real-time PCR (qPCR) system (Roche) using SYBR Green I (Roche) and sequence specific primers.

RT-PCR Primer Sequences:

M1 Forward- ATCAGACATGAGAACAGAATGG

Reverse- TGCCTGGCCTGACTAGCAATATC

M2	Forward: CGAGGTCGAAACGCCTATCAGAAAC
	Reverse: CCAATGATATTTGCTGCAATGACGAG
NS1	Forward: TGGAAAGCAAATAGTGGAGCG
	Reverse: GTAGCGCGATGCAGGTACAGAG
NS2	Forward: CAAGCTTTCAGGACATACTGATGAG
	Reverse: CTTCTCCAAGCGAATCTCTGTAGA
HA	Forward: TCTATTTGGAGCCATTGCTGG
	Reverse: TGCTTTTTTGATCCGCTGCA
18S	Forward: GTAACCCGTTGAACCCCATT
	Reverse: CCATCCAATCGGTAGTAGCG
β-actin	Forward: CCGCGAGAAGATGACCCAGAT
	Reverse: CGTTGGCACAGCCTGGATAGCAACG
SPTLC3	Forward: GGAATTGGAACCCTGTTTGGC
	Reverse: GTCTCTGATTCGCATGTAAAGGT
CEACAM19	Forward: GCCCAGCCTACAGACAGTG
	Reverse: GCAGCAAGAGATCCAATGATGG
VTCN1	Forward: TCTGGGCATCCCAAGTTGAC
	Reverse: TCCGCCTTTTGATCTCCGATT
UQCC	Forward: GGAGAAAACTGACTTCGAGGAAT
	Reverse: TCCAGACGTGGAGTAGGGTTA
UAP56	Forward: CTTTGAGCATCCGTCAGAAGT
	Reverse: AGTGTGACACATCACCAGTACA

Cell fractionation and RNAseq analysis

Cells were treated with 0.1% DMSO or 2.5 μM compound 2 for 9 hours. Nuclear and cytoplasmic fractions were obtained using the NE-PER Nuclear and Cytoplasmic Extraction Reagents (Thermo Fisher Scientific).

Total RNA was isolated total cell lysates, nuclear and cytoplasmic fractions using the RNeasy Plus Mini Kit (Qiagen). RNA samples were then analyzed in the Agilent 2100 Bioanalyzer to determine RNA quality (RIN Score 8 or higher). RNA concentration was determined using the Qubit fluorometer. A TruSeq Stranded Total RNA LT Sample Prep Kit (Illumina) was used to prepare 4 μg of DNAse-treated RNA for poly(A) RNA purification and fragmentation before strand specific cDNA synthesis. cDNA libraries were a-tailed and ligated to indexed adapters. Samples were then PCR amplified and purified with Ampure XP beads and validated with the Agilent 2100 Bioanalyzer. Samples were quantified again by Qubit before being normalized and pooled to be ran on the Illumina HiSeq 2500 using SBS v3 reagents. Raw FASTQ files were analyzed using FastQC v0.11.2 [59] and FastQ Screen v0.4.4 [60], and reads were quality-trimmed using fastq-mcf (ea-utils/1.1.2-806) [61]. The trimmed reads were mapped to the hg19 assembly of the human genome (the University of California, Santa Cruz, version from igenomes) using STAR v2.5.3a [62]. Duplicated reads were marked using Picard tools (v1.127; **https://broadinstitute.github.io/picard/**), the RNA counts generated from FeatureCounts [63] were TMM normalized [64], and differential expression analysis was performed using edgeR [64]. Expression data is represented as TPM (Transcripts per Million). Genes with mRNA TPM values of zero in either the control or experiment conditions were removed from the analysis. Log2 of the average TPM values for the remaining genes of each condition (total, nuclear, and cytoplasmic) were calculated. Only mRNAs with Log2TPM > -1 were considered for further analysis to remove experimental background noise. The TPM readings of the experiment compared with control samples were used to calculate the positive and negative fold changes from their ratios. The differentially expressed mRNAs with fold changes of + or – 1.5 FC were subjected to GSEA to obtain the enriched pathways.

Gene Set Enrichment Analysis (GSEA)

Pathway and network analysis were conducted using Gene Set Enrichment Analysis (GSEA) [65] software and the functional datasets were CP: Canonical pathways from the MSigDB [66, 67].

Western blot

Cell lysis was performed in 250mM Tris HCl pH 6.8, 40% Glycerol, and 8% SDS. Western blot was performed as previously described [68]. Antibodies used in this study to detect viral proteins include Influenza A virions (Meridian Life Science B65141G), M1 and M2 (Thermo MA1-082), NA (GeneTex GTX125974), PA (GeneTex GTX118991), PB1 (Santa Cruz sc-17601), PB2 (Santa Cruz sc-17603), and NS1 (a gift from J.A. Richt, National Animal Disease Center, Iowa) [69]. Antibodies against cellular proteins include β-actin (Sigma A5441) and UAP56 [Anti-BAT1 (C-TERMINAL antibody produced in rabbit, Millipore SAB1307254). Horseradish peroxidase (HRP)-conjugated secondary antibodies include donkey anti-rabbit, sheep anti-mouse (GE Healthcare NA934V and NA931V, respectively), and donkey anti-goat (Jackson Immunoresearch 705–035003). Quantification of protein band intensity was performed using Image Studio software (LI-COR Imaging). Each protein band was normalized to its corresponding loading control. Values listed below each band represent relative band intensity to its corresponding control.

CHAPTER THREE
Influenza Viral mRNA Splicing and Trafficking

3.1 Influenza Virus M mRNA Accumulates at Nuclear Speckles.

The entire section 3 presented here has been published in *Nature Microbiology [16]*. To spatially and temporally define the mechanisms involved in influenza virus M1 mRNA alternative splicing and export, we first followed M1 mRNA distribution using single molecule RNA-FISH (smFISH) in infected cells. Forty-six FISH probes covering the full length M1 mRNA of the influenza A/WSN/33 virus strain were generated to detect single M1 mRNA transcripts during influenza virus infection (Fig. 3a). While these 46 probes can recognize M1 and its alternative spliced forms M2 and $mRNA_3$, they can only detect M1 at the single molecule level due to the small size of the other spliced forms that are recognized in bulk. The signal detected with the 46 probes are then labeled as M mRNA. We observed that at 3h post-infection single M1 mRNA transcripts are detected in the nucleus and in the cytoplasm indicating efficient transcription and nuclear export of M1 mRNA (Fig. 3b). Notably, M mRNA significantly accumulates at intranuclear foci ~4-5h post-infection (Fig. 3b). RNA-FISH and immunofluorescence staining against M mRNA and SC35 protein, respectively, showed that M mRNA is enriched at nuclear speckles (Fig. 3c) as SC35 is a SR protein, known splicing factor, and nuclear speckle marker[43]. Other influenza A virus strains, A/Texas/36/91 and A/Puerto Rico/8/34, also show M mRNA localization at nuclear speckles. Approximately 6h post-infection, M mRNA enrichment at nuclear speckles is reduced and most of the M mRNA is detected in the cytoplasm, indicating efficient nuclear export (Fig. 3b,d).

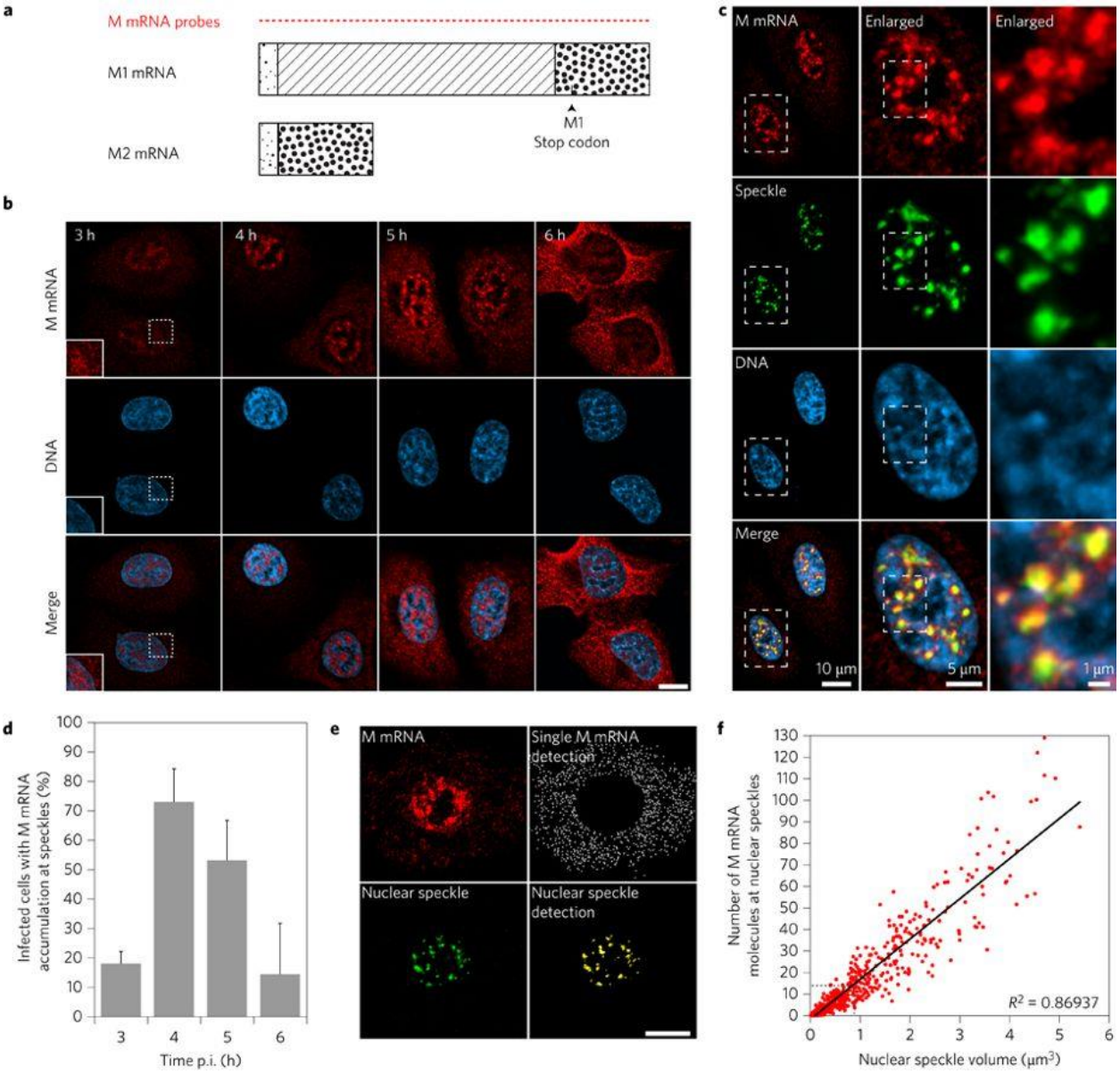

Figure 3. Influenza M mRNA is localized at nuclear speckles.

a. Schematic representation of M1 and M2 mRNAs. The hatched section in M1 mRNA represent an intron that is spliced out to generate M2 mRNA. Forty-six FISH probes (labelled with Quasar 570, M mRNA Probes) that cover the entire M1 and M2 mRNAs were synthesized. **b.** These probes monitored the distribution of M mRNA at 3, 4, 5 and 6 h during A/WSN/33 infection of A549 cells at a multiplicity of infection (MOI) of 10. Insets: enlargement of an area in the nucleus and cytoplasm. Images are representative of three independent experiments. Scale bar, 10 µm. **c**, M mRNA accumulates at nuclear speckles, which are marked by SC35 immunofluorescence staining (Pearson's correlation coefficient between the M mRNA channel and the 'Speckle' channel in the nucleus = 0.72). The marked rectangular region was enlarged and is shown in the middle panel. Further enlargement is shown in the right panel. Images are representative of three independent experiments. **d.** The percentage of cells with speckle mRNA accumulation was quantified. Values are percentage means ± s.d. of at least 99 cells that were counted in three independent experiments for each time point. p.i., post infection. **e.** M mRNA quantification at nuclear speckles. Fluorescent signal emerging from labelled M mRNA transcripts was detected in the cytoplasm

(single M mRNA detection, white dots) while the M mRNA signal emerging from the nucleus was masked based on Hoechst staining. Nuclear speckles were also marked (nuclear speckle detection, yellow punctate). Images are representative of three independent experiments. Scale bar, 10 μm. **f**. Quantification of M mRNA copy number at nuclear speckles marked with SC35 antibody. M mRNA fluorescence intensity sum inside speckles was divided by the average intensity sum of individual cytoplasmic M mRNA transcripts. Cells were infected for 4 h and RNA-FISH was quantified as in **e**. The number of M mRNA at nuclear speckles was plotted according to the nuclear speckle volume. Dotted lines in the graph indicate the average nuclear speckle volume and the corresponding M mRNA copy number. A total of 682 nuclear speckles were analyzed in 16 cells.

To determine the number of viral M mRNA molecules at nuclear speckles, we first quantified the fluorescence signal emerging from single mRNA molecules that could be detected in the cytoplasm (Fig. 3e). In the same cells, we used SC35 labeling to locate nuclear speckles and quantify the overall intensities of RNA-FISH labeled M mRNAs inside the nuclear speckle volume (Fig. 3e). The M mRNA fluorescent signal at individual speckles was then divided by the average intensity of a single M1 mRNA. In general, nuclear speckles vary in size ranging from one to several micrometers in diameter [43]. We detected and analyzed 682 SC35 labeled nuclear speckles in 16 cells (average of 42.6 nuclear speckles per nucleus) and measured the volume of these nuclear speckles. We found that the average volume of a single nuclear speckle is 0.82 μm^3 (Diameter = 1.16 μm). We then calculated the accumulation of M mRNAs with respect to the nuclear speckle volume (Fig. 3f). We show that there is a linear correlation between nuclear speckle volume and the number of M mRNAs enriched at nuclear speckles (R^2=0.869). Additionally, we found that inside the average size nuclear speckle, the bulk M mRNA signal is equivalent to ~ 13 M1 mRNA molecules. Thus, we estimate that hundreds of viral M mRNA transcripts enter/pass through nuclear speckles during infection.

Next we tested whether the viral NS mRNA, which is also alternatively spliced, accumulates inside nuclear speckles. For this purpose we generated an additional set of probes covering the entire NS mRNA. We then followed both NS mRNA and M1 mRNA (see below the description of specific M1 mRNA probes) distribution during infection. At 3h post-infection most of NS mRNA had already been exported to the cytoplasm while M1 mRNA was mainly in the nucleus. In contrast to M1 mRNA, NS mRNA was not

enriched at nuclear speckles. This may indicate a major difference between M and NS mRNA biogenesis pathways and that M mRNA specifically utilizes nuclear speckles for RNA processing.

3.2 Viral M mRNA is Post-transcriptionally Spliced at Nuclear Speckles.

To investigate if the viral M1 mRNA is actively spliced at nuclear speckles, we generated M1 and M2 probes that specifically label the unspliced M1 mRNA and the spliced M2 mRNA, respectively (Fig. 4a). We then monitored both M1 and M2 mRNAs at 4h post-infection and found that significant pools of both mRNAs were localized at nuclear speckles (Fig. 4b,c). M1 mRNA also co-localized with U5 snRNA and Prp8 at nuclear speckles, indicating accumulation at speckles that contain high concentration of key catalytic components of the splicing reaction (Fig. 4d) [70]. In addition, we were also able to detect $mRNA_3$ at nuclear speckles, demonstrating the presence of another spliced product of M1 mRNA at this nuclear body. Thus, the presence of both M1 mRNA and the spliced M2 mRNA and $mRNA_3$ at nuclear speckles suggests that splicing of the M1 mRNA may occur at nuclear speckles. To reveal whether viral M1 mRNA splicing occurs co- or post-transcriptionally at nuclear speckles, we co-labeled single M vRNA segments using RNA-FISH and tracked accumulation in SC35 marked speckles. At 4h post-infection, when M mRNAs are enriched at nuclear speckles, we did not detect single M vRNAs at nuclear speckles but they can be adjacent to these nuclear bodies (Fig. 4e-g). In fact, comparative imaging analysis of the M vRNA channel and the speckle channel shows low Pearson's coefficient of 0.17. These findings suggest that the M1 mRNA is first generated upon M vRNA transcription in the nucleoplasm and then M1 mRNA associates with nuclear speckles for post-transcriptional splicing.

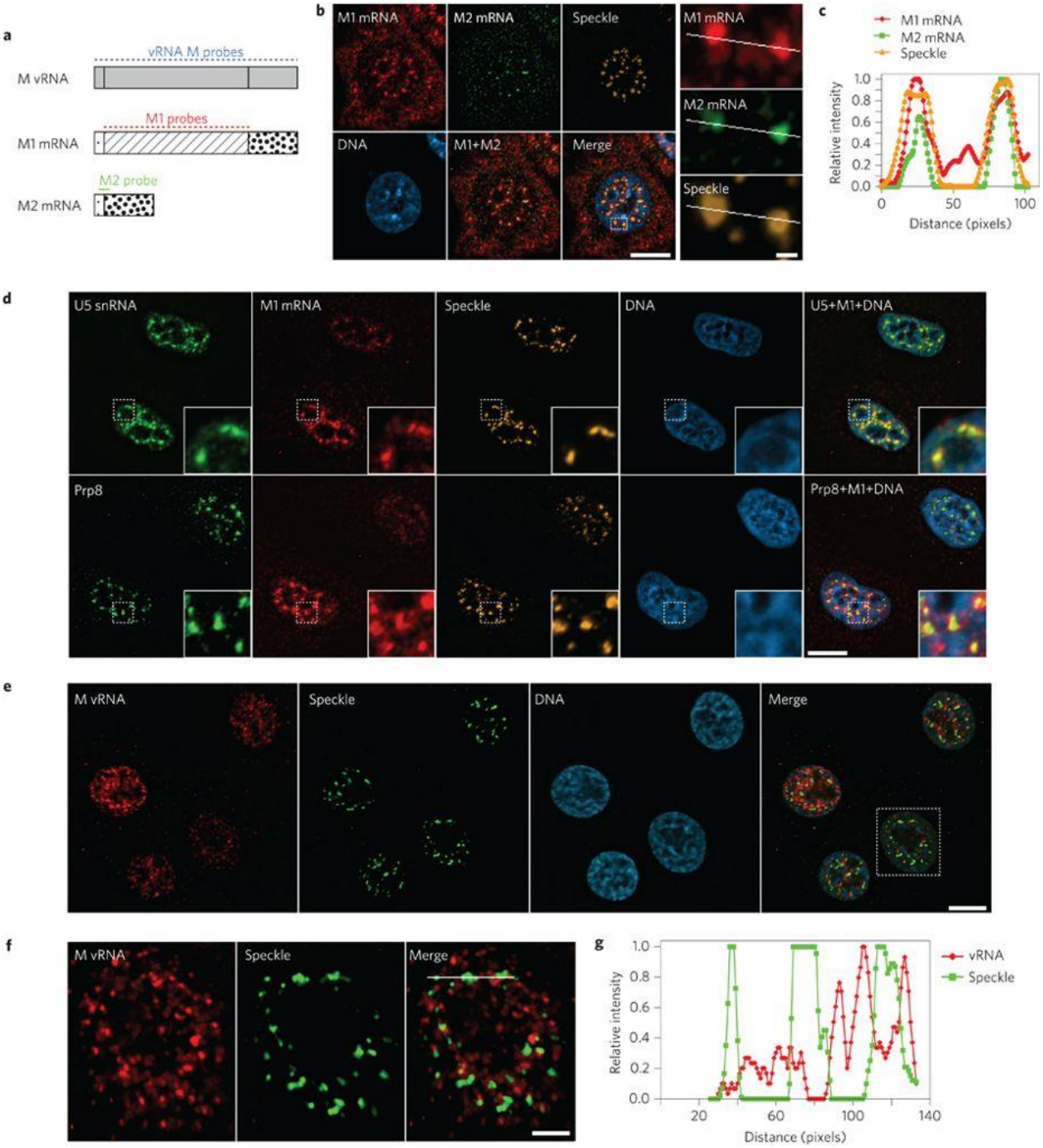

Figure 4. M1 mRNA and spliced M2 mRNA accumulate at nuclear speckles after transcription.
a. Schematic representation of three sets of probes that were synthesized to specifically detect the M vRNA and M1 and M2 mRNAs. Forty-six FISH probes labelled with Quasar 670 were synthesized to label the entire M vRNA segment. Thirty-one FISH probes labelled with Quasar 670 were synthesized to cover the M1 mRNA intron region. The M2 mRNA was detected using a single probe labelled with two Quasar 570 fluorophores. This probe binds the exon junction region of M2 mRNA. **b.** M1 and M2 probes were used in RNA FISH experiments performed at 4 h post-infection. Nuclear speckles were marked with SC35 antibody. A single cell was enlarged to demonstrate the M1 and M2 mRNA enrichment at nuclear speckles.

The squared region shown in 'Merge' was further enlarged and the M1, M2 and 'Speckle' channels are shown on the right. **c,** Relative intensity of the three channels along the white line in **b**. **d.** U5 snRNP components, U5 snRNA and Prp8, were co-labelled with M1 mRNA at 4 h post-infection. Nuclear speckles were marked with SC35 antibody (top) or SON antibody (bottom). **e,** M vRNA probes were used in RNA FISH experiments performed at 4 h post-infection. Nuclear speckles were marked with SC35 antibody. **f.** For the square region marked in **e**, 'Merge' was enlarged and M vRNA, 'Speckle' and 'Merge' are shown. **g.** Relative intensity of the M vRNA and 'Speckle' signal along the white line in f ('Merge'). Images in **b** and d–f are representative of three independent experiments. Scale bar (**b**, right panel), 1 μm. Scale bar (**f**), 5 μm. All other scale bars, 10 μm.

3.3 Viral NS1 Protein Promotes M mRNA Splicing and Nuclear Export Via Nuclear Speckles.

M1 mRNA splicing has been linked to the viral NS1 protein [71] and M1 mRNA can interact with NS1 [71-73]. Additionally, NS1 has been previously shown to alter the SC35 punctate pattern, suggesting that NS1 may induce changes in nuclear speckle structure and function [74]. Hence, we tested whether NS1 is involved in M mRNA localization and splicing at nuclear speckles using an influenza virus strain that lacks NS1 (WSN ΔNS1) [75]. Because NS1 is also responsible for suppressing the innate immune system, these infection studies were performed both in VERO cells which are interferon-deficient and therefore allow replication of this mutant virus, and in A549 cells, which are immune-competent. This would differentiate any perturbation in M mRNA localization and splicing observed as being due to immune suppression or as separate NS1 activity. We found that the lack of NS1 protein significantly reduced accumulation of M mRNA at nuclear speckles (Fig. 5a, b) and diminished M1 mRNA splicing (Fig. 5c, d) in both cell types. Furthermore, after 6h post-infection, we observed a decrease in M mRNA nuclear export in cells infected with WSN ΔNS1 (Fig. 5e, f). Consequently, these effects contribute to the decrease in M1 and M2 protein levels in cells infected with virus lacking NS1 as compared to cells infected with wild-type virus. These results point to a specific and previously unknown function of NS1 in promoting M1 mRNA localization at nuclear speckles, which lead to M1 to M2 splicing. This function of NS1 seems to be independent from its inhibitory role of interferon expression since M mRNA mislocalization and splicing-export defects observed upon WSN ΔNS1 infection occurred in both A549 and VERO cells.

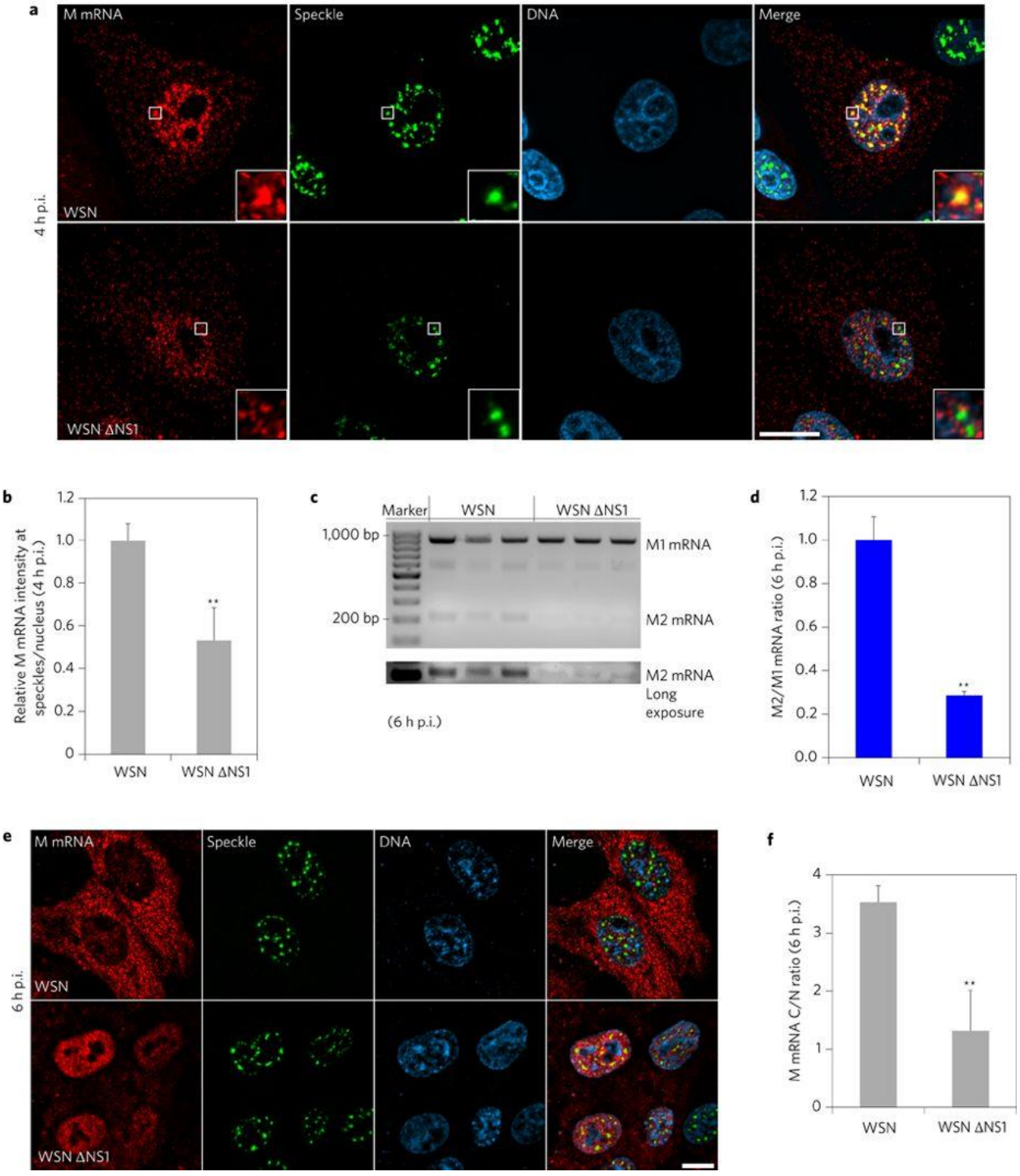

Figure 5. Viral NS1 protein promotes M1 mRNA splicing at nuclear speckles and nuclear export. **a.** Vero cells were infected with WSN virus or mutated virus that lack NS1 (WSN ΔNS1) at an MOI of 10. After 4 h, cells were fixed and M mRNA was labelled by RNA-FISH. Speckles were marked by immunofluorescence with SON antibody. Insets: enlargements of the marked white squares, showing nuclear speckle areas. Scale bar, 10 μm. **b.** Quantification of M mRNA intensity at speckles after WSN or WSN ΔNS1 infection. Data represent three independent experiments. M mRNA intensity sum at speckles was normalized to the intensity sum in the nucleus. Normalized intensities at speckles of wild-type virus-

infected cells were set to 1, and the relative fold change in WSN ΔNS1 virus-infected cells is shown. Values are means ± s.d. measured in 25 WSN and 29 WSN ΔNS1 infected cells. p.i., post infection. **c.** Vero cells were infected with WSN virus or WSN ΔNS1 at an MOI of 1 for 6 h. Purified RNA was subjected to RT-PCR and the products were run on agarose gel. Data represent three independent experiments. **d.** RT-qPCR quantification of M2/M1 mRNA ratio in WSN or WSN ΔNS1 Vero infected cells. The average M2/M1 mRNA ratio from cells infected with WSN (M2/M1 mRNA = 0.62) was set to 1 and the relative average M2/M1 mRNA ratio in WSN ΔNS1 infected cells is shown. Values are means ± s.d. for ratios from three independent experiments. **e.** Vero cells were infected with WSN virus or WSN ΔNS1. After 6 h, cells were fixed and M mRNA was labelled by RNA-FISH. Speckles were marked by immunofluorescence with SON antibody. Scale bar, 10 μm. **f.** Quantification of M mRNA cytoplasmic to nuclear ratio (C/N) was determined after 6 h of WSN or WSN ΔNS1 infection. Values are means ± s.d. measured in 41 WSN and 50 WSN ΔNS1 infected cells. Images shown in **a** and **e** are representative of three independent experiments. **t-test $P < 0.01$.

3.4 Cellular Proteins Mediate M1 mRNA Processing at Nuclear Speckles.

We have previously shown that the cellular protein NS1-BP, which interacts with the viral NS1 protein [76], forms a complex with the cellular hnRNP K protein and they are required for proper M1 mRNA splicing into M2 mRNA [77]. NS1-BP and hnRNP K are RNA binding proteins involved in viral RNA splicing and the latter has also been linked to cellular pre-mRNA splicing [78-81]. Thus, we tested whether NS1-BP and hnRNP K have a role on M mRNA localization at nuclear speckles. First, we show that a pool of both NS1-BP and hnRNP K is found at nuclear speckles. NS1-BP has been previously found at nuclear speckles [76]**.** In NS1-BP depleted cells, M mRNA accumulation at nuclear speckles was reduced after 4h post-infection but the cytoplasmic to nuclear M mRNA ratio C/N was not altered. At 6h post-infection, we observed an inhibition of M mRNA nuclear export in cells depleted of NS1-BP (Fig. 6a, b). The observed M mRNA mislocalization shown here and the splicing defects we reported upon NS1-BP knockdown [77] are similar to what we showed in cells infected with WSN ΔNS1 (Fig. 5). These data suggest that NS1 and NS1-BP may function together to recruit M1 mRNA to nuclear speckles for splicing and support the concept that M1 mRNA that is generated at 4-6 h post-infection is not efficiently exported without being processed at nuclear speckles.

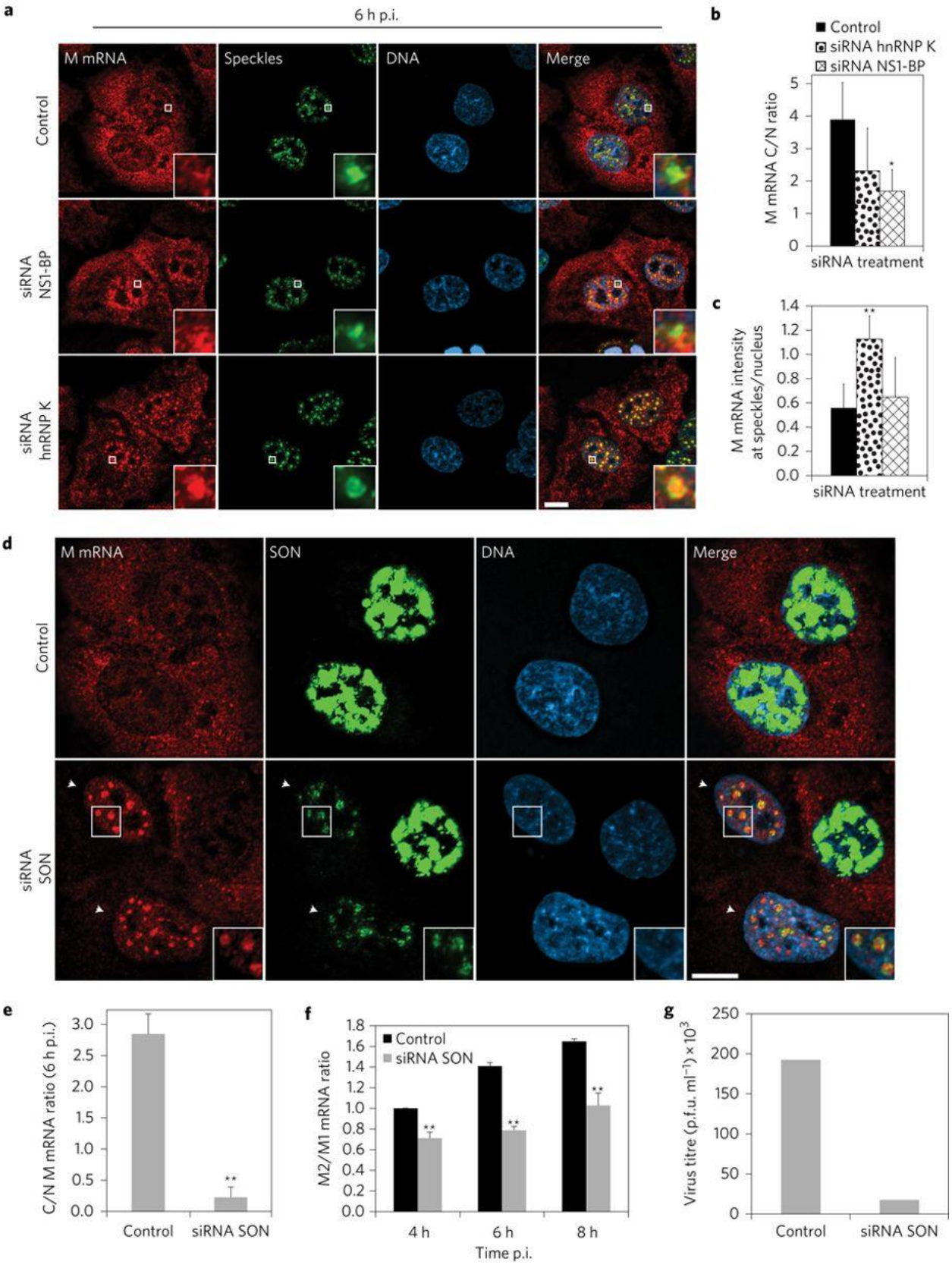
a
6 h p.i.
M mRNA
Speckles
DNA
Merge
Control
siRNA NS1-BP
siRNA hnRNP K
b
Control
siRNA hnRNP K
siRNA NS1-BP
M mRNA C/N ratio
siRNA treatment
c
M mRNA intensity at speckles/nucleus
siRNA treatment
d
M mRNA
SON
DNA
Merge
Control
siRNA SON
e
C/N M mRNA ratio (6 h p.i.)
Control
siRNA SON
f
Control
siRNA SON
M2/M1 mRNA ratio
4 h
6 h
8 h
Time p.i.
g
Virus titre (p.f.u. ml⁻¹) × 10³
Control
siRNA SON

Figure 6. M mRNA splicing at nuclear speckles is mediated by host factors NS1-BP, hnRNP K and SON.
a. A549 cells were transfected with control siRNA, hnRNP K siRNA or NS1-BP siRNA. After 72 h, cells were infected with WSN at an MOI of 10 for 6 h. Cells were then fixed for M mRNA labelling by RNA-FISH. Nuclear speckles were marked with SON antibody. Insets: enlarged nuclear speckle region. Scale bar, 10 μm. **b,c.** The distribution of M mRNA in the nuclear and cytoplasmic compartments (**b**) and at speckles (**c**) was quantified. Values are means ± s.d. of at least 20 cells that were analyzed for each treatment. **d.** A549 cells were transfected with control siRNA or SON siRNA. After 48 h, cells were infected with WSN at an MOI of 10 for 6 h. Cells were subjected to RNA-FISH. Nuclear speckles were marked with SON antibody. The SON signal was intensified to show the abnormal speckle structure that forms in SON-depleted cells (marked by white arrows). Insets from cells depleted of SON show an enlarged area with abnormally shaped nuclear speckles. Scale bar, 10 μm. **e.** Quantification of M mRNA cytoplasmic to nuclear ratios (C/N ratios). Values are means ± s.d. measured in 61 cells transfected with control siRNA and in 27 cells transfected with SON siRNA and infected with WSN. p.i., post infection. **f.** RT-qPCR quantification of M2/M1 mRNA ratios from cells transfected with control siRNA or SON siRNA and infected for 4, 6 and 8 h. The average M2/M1 mRNA ratio from cells treated with control siRNA at 4 h post-infection (M2/M1 mRNA = 0.59) was set to 1 and the relative average M2/M1 mRNA ratios at the depicted time points are shown. Values are means ± s.d. from three independent experiments. **g.** WSN replication was determined after 24 h in control cells or in SON-depleted cells. Virus titer was determined by plaque assay. Values are means from two independent experiments. Images in **a** and **d** are representative of three independent experiments. *t-test $P < 0.05$, **t-test $P < 0.01$.

We then depleted hnRNP K, which interacts with NS1-BP [77]. In contrast to NS1-BP depletion and similar to control cells, hnRNP K depleted cells efficiently accumulated M mRNA at nuclear speckles 4h post-infection. However, at 6h post-infection we found a significant enrichment of M mRNA at nuclear speckles in hnRNP K depleted cells (Fig. 6a,c) whereas most of M mRNA is not present at nuclear speckles during this time in the control infected cells, as it has already been exported to the cytoplasm (Fig. 6a-c). Since M mRNA enters and accumulates at speckles for a prolonged time in hnRNP K knockdown cells, but does not efficiently splice [77], hnRNP K appears to function on M1 to M2 mRNA splicing at nuclear speckles. Although M mRNA accumulation at nuclear speckles upon hnRNP K knockdown is prolonged, the nucleoplasmic M mRNA pool was not enriched, so the C/N ratio of M mRNA was not significantly altered relative to control cells (Fig. 6a, b). In hnRNP K and NS1-BP knockdown cells, the mislocalization phenotypes may be specific to the viral M mRNA, as cellular GAPDH mRNA localization remained unchanged after NS1-BP and hnRNP K depletion.

To further determine the importance of nuclear speckles for M1 to M2 splicing and export, we perturbed nuclear speckle structure by knocking down the SON protein. SON was shown to be a

scaffold/structural nuclear speckle factor and its depletion leads to dispersion of splicing factors from nuclear speckles to the nucleoplasm [82, 83]. SON was also shown to regulate cell cycle progression, development, and disease [82, 83]. In control cells where SON is not depleted, we found that most of the M mRNA is in the cytoplasm at 6h post-infection (Fig. 6d, e). In contrast, in SON depleted cells the M mRNA is accumulated at nuclear speckles that contain low levels of SON (Fig. 6d), while the distribution of GAPDH mRNA remains unchanged. Although some M mRNA was detected in the cytoplasm of SON depleted cells, the C/N ratio of M mRNA was significantly reduced (Fig. 6e), indicating defect in M mRNA nuclear export in these cells. SON knockdown also reduced the M2/M1 mRNA ratio during infection (Fig. 6f). As a result, SON depletion reduced virus replication as compared to control cells (Fig. 6g). This effect is consistent with a previous screen that identified SON as an essential cellular protein for influenza virus replication [84]. Together, these findings reveal a novel role for the SON protein in the influenza virus life cycle, supporting the concept of M1 mRNA splicing at nuclear speckles.

3.5 Aly/REF and UAP56 Couple Viral M mRNA Nuclear Export to Splicing via Nuclear Speckles.

There is some evidence that the TREX components UAP56 and Aly/REF proteins are involved in the release of certain cellular mRNAs from nuclear speckles [47]. In the model of mRNA nuclear export, UAP56 is recruited to the nascent transcript and in turn recruits Aly/REF. UAP56 is then displaced by the NXF1-NXT1 mRNA export receptors and Aly/REF enhances NXF1-NXT1 binding to the RNA [85]. NXF1-NXT1 then mediates the mRNA translocation through the nuclear pore complex. We show that Aly/REF is present at nuclear speckles and UAP56 has been previously localized at these nuclear bodies [86]. Additionally, Aly/REF and UAP56 have been shown to be involved in nuclear export of M1 and M2 mRNAs [20]. Thus, we tested whether depletion of these factors would lead to a change in M mRNA localization or splicing. By monitoring M1 and M2 mRNA, we found that in both Aly/REF and UAP56 siRNA treated cells M1 and M2 mRNA accumulated at nuclear speckles and in the nucleoplasm after 6h, in contrast to control in both A549 and VERO cells (Fig. 7a-d; Fig. 9a). Surprisingly, RT-qPCR analysis of the M2/M1 mRNA ratio revealed that M1 mRNA splicing was significantly enhanced by the Aly/REF and

UAP56 knockdown (Fig. 7e). Despite this splicing enhancement, both M1 and M2 mRNAs were significantly blocked in the nucleus upon depletion of Aly/REF and UAP56, which resulted in low levels of M1 and M2 proteins. Thus, M1 mRNA nuclear export block seems to prolong the accumulation of M1 mRNA at nuclear speckles, which likely enhanced M1 mRNA splicing.

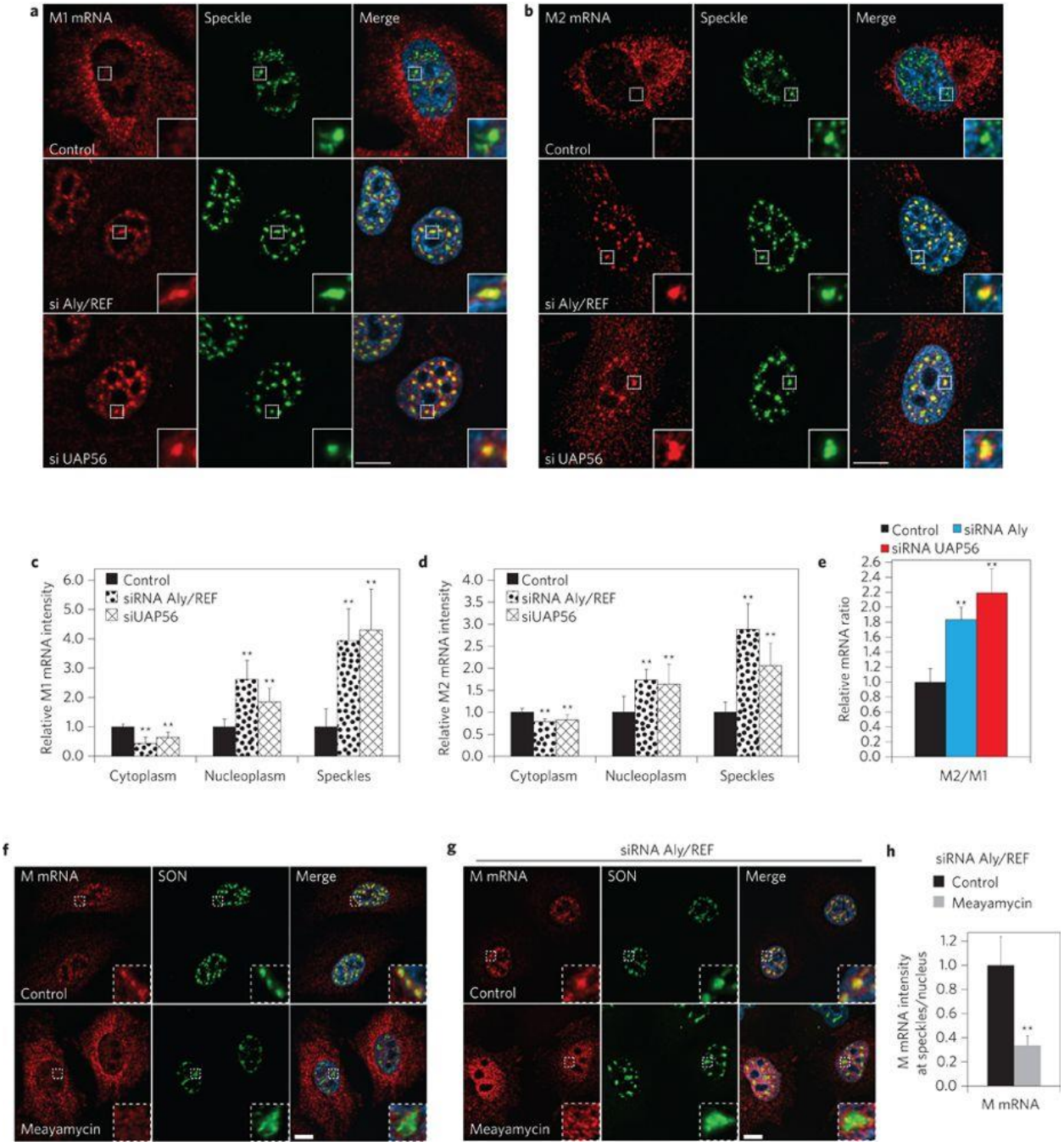

Figure 7. Aly/REF and UAP56 depletion inhibits M1 and M2 mRNA nuclear export and mediates speckle dependent M1 to M2 splicing enhancement.

a,b. A549 cells were transfected with control siRNA, Aly/REF siRNA or UAP56 siRNA. After 48 h, cells were infected with WSN at an MOI of 10 for 6 h. M1 (**a**) and M2 (**b**) mRNA labelling was performed by RNA-FISH. Nuclear speckles were marked with SON antibody. **c,d.** Distribution of M1 (**c**) and M2 (**d**) mRNAs in the cytoplasm, nucleoplasm and nuclear speckles. The intensity sum in each compartment was normalized to the general fluorescence intensity in the cell. Values obtained from cells transfected with control siRNA were set to 1, and the relative fold changes in Aly/REF and UAP56 siRNA transfected cells are shown. Values are means ± s.d. of at least nine cells that were analyzed for each condition. **e.** RT-qPCR quantification of M2/M1 mRNA ratio in cells transfected with control siRNA, Aly/REF siRNA or UAP56 siRNA and infected for 6 h. Values are means of ratios ± s.d. from three independent experiments. **f.** A549 cells were treated with 100 nM meayamycin or 0.1% DMSO (control) for 2 h and infected with WSN at an MOI of 10 for 1 h. Virus was removed and 100 nM meayamycin or 0.1% DMSO was added for 3 h. Cells were subjected to RNA-FISH. Nuclear speckles were marked with SON antibody. **g.** A549 cells were transfected with control siRNA or Aly/REF siRNA. After 48 h, cells were processed as in **f**. **h.** M mRNA intensities at nuclear speckles in cells (treated as in **g**) were quantified. The M mRNA signal at speckles was normalized to the average speckle volume measured within each cell. Values obtained from cells transfected with Aly/REF siRNA (control) were set to 1, and the relative fold changes in meayamycin-treated cells depleted of Aly/REF are shown. Values are means ± s.d. of at least nine cells that were analyzed for each condition. Images shown in **a**, **b**, **f** and **g** are representative of three independent experiments. All insets are enlargement of nuclear speckle areas. All scale bars, 10 μm.

We next inhibited splicing of M mRNA to determine whether this perturbation would affect its nuclear speckle localization. We used the splicing inhibitor meayamycin that binds SF3b and therefore prevents the formation of protein-RNA complexes essential for early spliceosome assembly [87]. M mRNA localization was assessed by RNA-FISH in the absence or presence of this chemical probe. In agreement with previous findings, meayamycin, like its analogue spliceostatin A, increased nuclear speckle sizes (Fig. 8f-g) [88]. Additionally, we found that meayamycin treatment promotes premature nuclear export of M mRNA (Fig. 7f) in addition to inhibiting M1 to M2 splicing. To prevent this premature nuclear export effect and still inhibit M mRNA splicing, we took advantage of the Aly/REF phenotype, which inhibits M mRNA nuclear export and increases both accumulation of M mRNA at nuclear speckles and splicing (Fig. 7a-e and Fig. 7g control), and treated cells with both Aly/REF siRNA and meayamycin (Fig. 7g). We found that meayamycin treatment prevents M mRNA nuclear speckle accumulation and splicing even in Aly/REF depleted cells that contain high levels of nuclear M1 mRNAs (Fig. 7g, h). When meayamycin was removed from the medium, M2 mRNA could again be detected after an additional 4 hours. Examination of both M1

and M2 mRNA distribution by RNA-FISH revealed that M1 and M2 mRNA speckle localization was restored upon meayamycin removal. These results indicate that the accumulation of M1 mRNA at nuclear speckles is not a random process but rather a mechanism to induce M1 mRNA splicing.

Next we examined the effect of Aly/REF and UAP56 depletion during WSN ΔNS1 virus infection. As expected, both WSN and WSN ΔNS1 infected cells depleted from Aly/REF and UAP56 exhibited a significant M mRNA nuclear export defect (Fig. 8a, b). Importantly, the nuclear speckle accumulation and splicing enhancement seen after Aly/REF and UAP56 knockdown in WSN ΔNS1 infected cells were reduced as compared to WSN infected cells (Fig. 8a-d). These results indicate that the splicing enhancement in Aly/REF and UAP56-deficient cells is dependent on nuclear speckle accumulation and reinforces the new role of NS1 described here as a driver of M mRNA to speckles to undergo splicing.

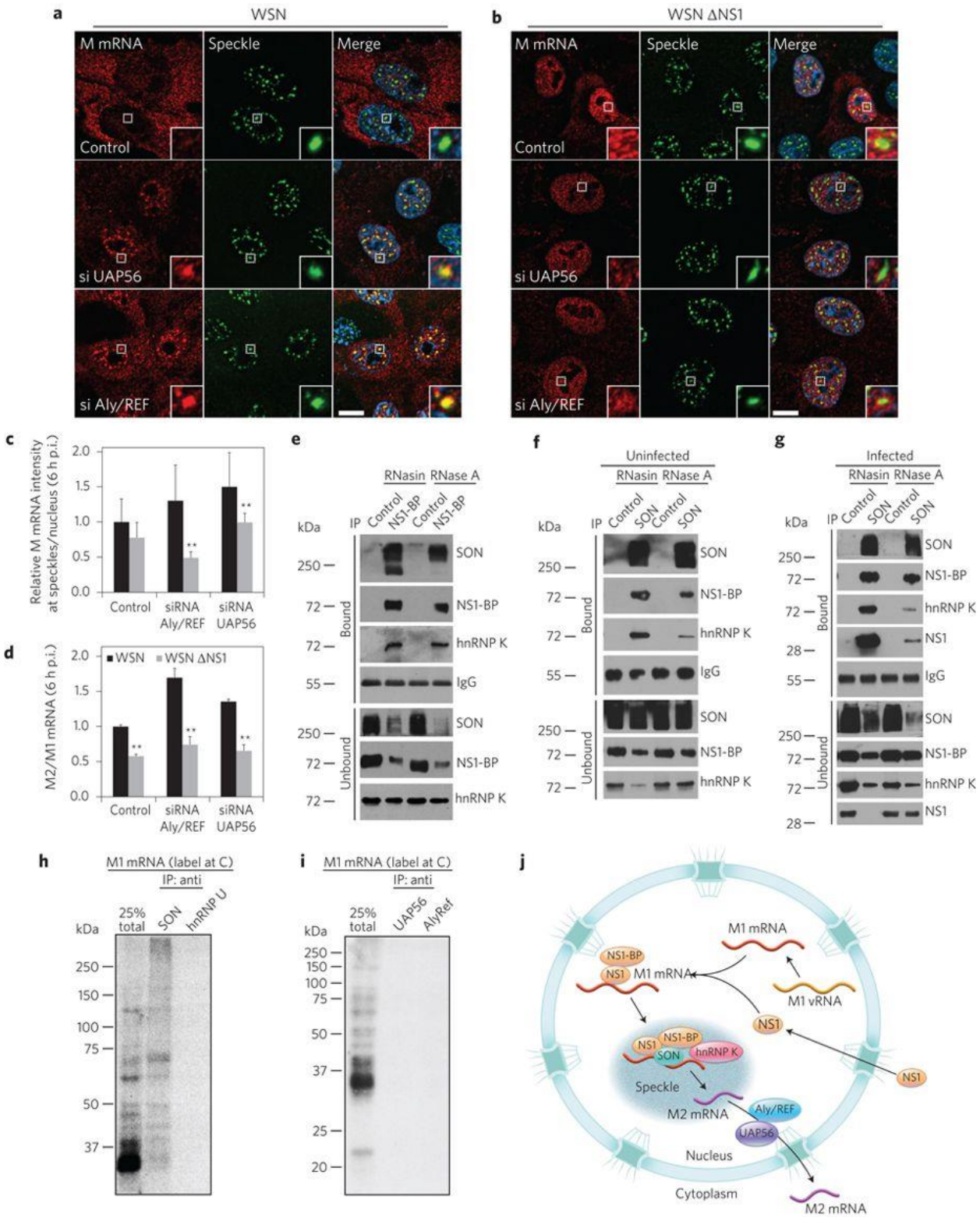

Figure 8. Nuclear speckle assembly factor SON interacts with M1 mRNA and mediators of M1 mRNA splicing.

a,b. Vero cells were transfected with control siRNA, Aly/REF siRNA or UAP56 siRNA. After 48 h, cells were infected with WSN (**a**) or WSN ΔNS1 (**b**) at an MOI of 10 for 6 h. Cells were then fixed for M mRNA labelling by RNA-FISH. Nuclear speckles were marked with SON antibody. Insets are enlargement of areas showing nuclear speckles. Images shown in **a** and **b** are representative of three independent experiments. Scale bars, 10 μm. c, The accumulation of M mRNA at nuclear speckles was quantified and compared between WSN- and WSN ΔNS1-infected cells transfected with siRNA as in **a** and **b**. Values are means ± s.d. of at least 11 cells that were analyzed in each treatment. p.i., post infection. **d.** RT-qPCR quantification of M2/M1 mRNA ratio in Vero cells transfected with control siRNA, Aly/REF siRNA or UAP56 siRNA and infected for 6 h with WSN or WSN ΔNS1 at an MOI of 1. The average M2/M1 mRNA ratio from control siRNA transfected cells infected with WSN (M2/M1 mRNA = 0.495) was set to 1, and the relative average M2/M1 ratios at the depicted conditions are shown. Values are means ± s.d. from three independent experiments. **t-test $P < 0.01$. **e–g.** Cell extracts from uninfected or infected A549 cells treated with RNase inhibitor (RNasin) or with RNase A were subjected to immunoprecipitations with antibodies specific to NS1-BP or SON. Immunoprecipitates (bound) and unbound fractions were subjected to western blot using antibodies specific to the depicted proteins. **h,i.** SON binds directly to M1 mRNA. The entire M1 mRNA was radiolabeled uniformly at C residues, incubated with JSL1 nuclear extract under splicing conditions, crosslinked with 254 nm light and digested with RNase. The reaction was then either resolved by SDS–PAGE (25% total) or incubated in separate reactions with the antibodies indicated (IP: anti-). Total reaction or immunoprecipitated proteins were resolved by SDS–PAGE. **j.** Model for influenza virus M1 mRNA trafficking and splicing. Data shown in **e–i** are representative of three independent experiments.

3.6 SON Interacts with M1 mRNA and with Factors Required for M1 mRNA Processing.

We then investigated whether NS1 and the cellular proteins involved in M1 mRNA localization and splicing at nuclear speckles physically interact with SON, a major player in nuclear speckle assembly and alternative splicing [82, 83]. The major form of the SON protein is ~263 kD and runs as a broad band in SDS- PAGE as it is likely post-translationally modified. Lower molecular weight forms of SON are predicted to be alternative spliced forms. We show that NS1-BP and hnRNP K interact with SON in non-infected or infected cells (Fig. 8e-g). In addition, NS1 was pulled-down by SON antibody (Fig. 8g). To this end, NS1 protein from influenza B virus has also been shown to interact with nuclear speckle domains [89], further indicating the importance of this intranuclear body to the different strains of influenza virus. The NS1-BP and hnRNP K interactions with SON were detected by immunoprecipitations performed with either anti-NS1-BP antibody or anti-SON antibody in the presence or absence of RNA (Fig. 8e-g). In uninfected cells, the interactions of SON with NS1-BP (Fig. 8e) or SON with hnRNP K (Fig. 8f) were partially dependent on RNA. During infection, interactions of SON with hnRNP K and with NS1 showed partial RNA

dependence as well (Fig. 8g). Then, we tested whether SON directly interacted with M1 mRNA. M1 mRNA was capped, ^{32}P-labeled, and incubated with nuclear extracts. This was followed by UV treatment to crosslink RNA-protein interactions. RNA was digested and immunoprecipitations were performed with antibodies specific to SON, hnRNP U, Aly/REF and UAP56. hnRNP U was used as negative control based on our previous work, which demonstrated direct interaction of hnRNP K with M1 mRNA and lack of interaction with hnRNP U [77]. As shown in Figure 8h, SON (~263 kD broad band) and its putative alternative spliced forms directly bound M1 mRNA whereas hnRNP U, Aly/REF and UAP56 did not interact with M1 mRNA (Fig. 8h,i). Lack of direct interaction between Aly/REF or UAP56 with M1 mRNA is not surprising as they likely require adaptor proteins to bind RNA. Thus, SON interaction with NS1, NS1-BP and hnRNP K in addition to directly bind M1 mRNA support the functional data that indicates M1 mRNA splicing at nuclear speckles.

CHAPTER FOUR
Identification of Chemical Compounds that Inhibit Viral M mRNA Nuclear Export

4.1 High-throughput screen to identify inhibitors of viral M mRNA processing and nuclear export

The entire section 4 presented here has been published in *PLoS Pathogens [90]*. In the previous chapter, we identified that knockdown of the cellular NS1-BP protein inhibits influenza virus M mRNA splicing and nuclear export through host nuclear speckles [16]. We have now knocked out NS1-BP using the CRISPR/Cas9 system (Fig. 9a) and these cells show a slight reduction in growth rate (Fig. 10). We then subjected wild-type and NS1-BP knockout cells to single-molecule RNA fluorescence *in situ* hybridization (smRNA-FISH) to detect influenza virus M1 mRNA in infected cells (Fig. 9b-d) and oligo-dT *in situ* hybridization to label bulk cellular poly(A) RNA in the absence of infection (Fig. 9e-g). While viral M1 mRNA nuclear export is substantially inhibited in the absence of NS1-BP (Fig. 9b-d), as expected based on our previous results with siRNA [16], bulk cellular poly(A) RNA distribution between the nucleus and cytoplasm was not altered in the absence of NS1-BP, but total intracellular levels were increased (Fig. 9e-g). These results indicate that the viral M mRNA uses a distinct mechanism to be exported from the nucleus to the cytoplasm, which is not shared by the bulk of the cellular mRNA. Thus, we postulated that it should be possible to identify specific inhibitors of this unique mechanism that would impact nuclear export of the influenza virus M RNA without significantly affecting bulk cellular RNA processing and expression.

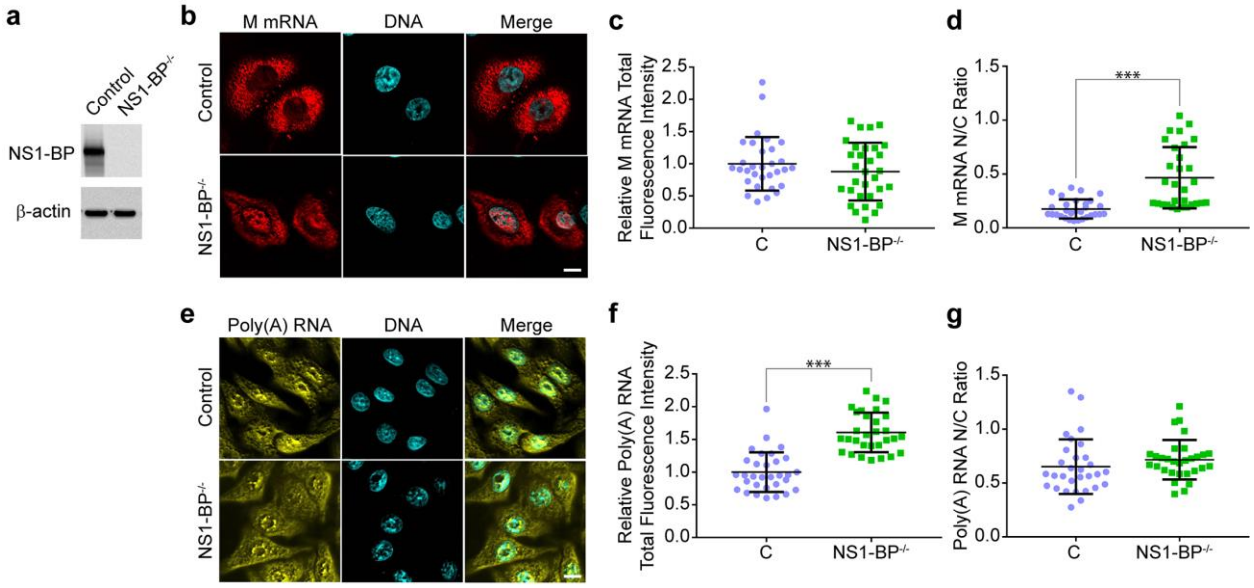

Figure 9. Loss of NS1-BP protein inhibits viral M mRNA nuclear export without significantly altering intracellular distribution of bulk cellular poly(A) RNA.

a. Disruption of the NS1-BP gene by CRISPR-Cas9 system yielded A549 cells lacking NS1-BP protein. Cell lysates from control or NS1-BP knockout cells were subjected to western blot analysis with antibodies against NS1-BP antibody or β-actin, as control. **b.** Wild-type or NS1-BP$^{-/-}$ A549 cells were infected with influenza virus (A/WSN/33) at MOI 2 for 6h. Single-molecule RNA fluorescence *in situ* hybridization (smFISH) was performed to detect influenza virus M mRNA. Hoechst staining labeled nuclei. Scale bar = 10 μm. **c,d.** Quantification of total fluorescence intensity of M mRNA in the nucleus and cytoplasm of wild-type or NS1-BP$^{-/-}$ cells (**c**), or nuclear-to-cytoplasmic (N/C) ratios of M mRNA in these cells (**d**) from panel B. **e.** Non-infected wild-type or NS1-BP$^{-/-}$ A549 cells were subjected to RNA-FISH to label poly(A) RNA. **f,g.** Quantification of total fluorescence intensity of poly(A) RNA in the nucleus and cytoplasm of wild-type or NS1-BP$^{-/-}$ cells (**f**), or nuclear-to-cytoplasmic (N/C) ratios of poly(A) RNA in these cells (**g**) from panel **e**. Thirty cells were quantified for each condition. These data are representative of three independent experiments. ***p<0.001.

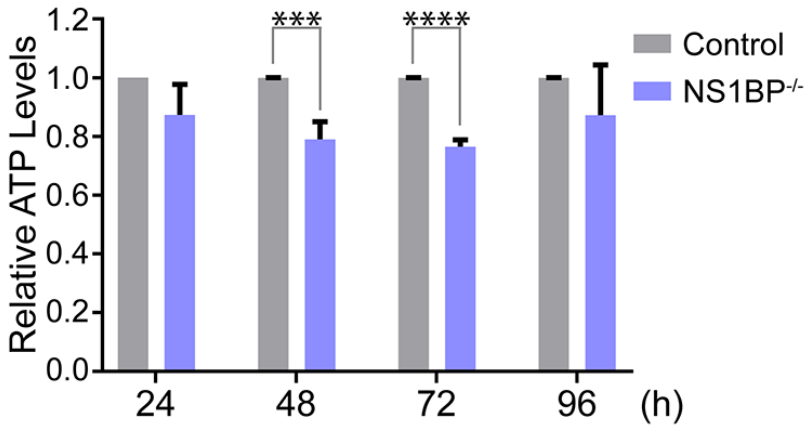

Figure 10. Growth rate of NS1-BP knockout cells compared to wild-type cells.

Cell growth of NS1-BP wild-type and knockout cells was monitored at 24, 48, 72, and 96 hours as determined by CellTiter-Glo. Four independent experiments were performed. Graph shows mean +/- SD. ***p<0.001, ****p<0.0001.

Next, we performed a high-throughput screen to select inhibitors of viral M mRNA processing and nuclear export. By adapting our previously reported protocol to visualize the M mRNAs during virus infection [16], we designed a high-throughput screening assay to identify compounds that alter M mRNA expression and trafficking without significantly compromising bulk cellular poly(A) RNA levels or intracellular distribution. The high throughput screen was performed using a chemical library of 232,500 compounds. As shown in Figure 11, cells were incubated with compounds and then infected with influenza virus (WSN) for 7.5 h.

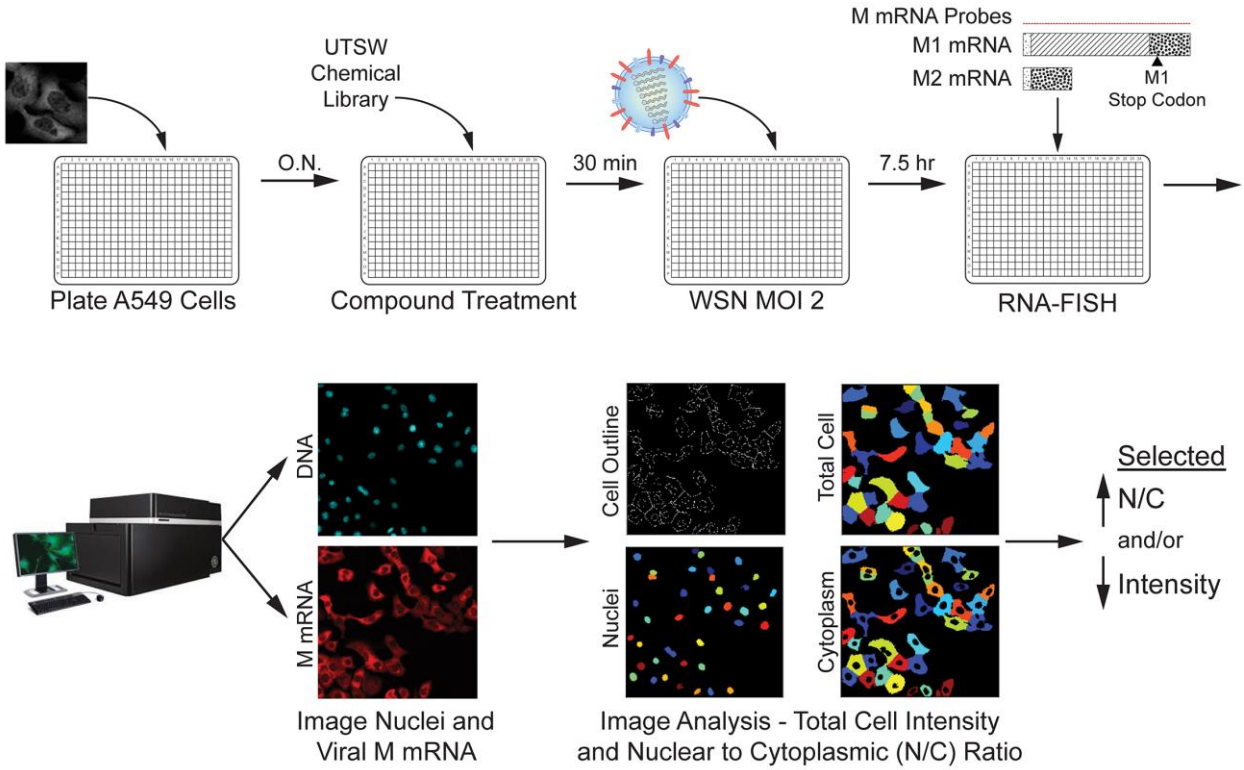

Figure 11. Schematic representation of a high-throughput screen to identify chemical inhibitors of viral M mRNA processing and nuclear export.
Screen was performed using a chemical library of 232,500 compounds in A549 cells. Cells were incubated with compounds for 30 min and, for robust imaging analysis, ~ 100% of the cells were infected with

influenza virus (WSN), at MOI 2 for 7.5h. Viral M mRNA was detected by smRNA-FISH and images were systematically taken in a high throughput microscope (IN Cell Analyzer 6000). Samples on 384-well black clear-bottom plates were imaged at 20X magnification using the Hoechst and dsRed filters. 4 fields of view per well were collected for each channel. The distribution of fluorescent signal between the nucleus (N) and the cytoplasm (N/C ratio) as well as total cell signal intensity were quantified using GE IN Cell Analyzer Workstation (version 3.7.3) and Pipeline Pilot (version 9.5; Biovia). Data was imported into the GeneData's Screener™ software analysis suite for quality control to ensure that data quality is high for all plates in each experimental run ($Z' > 0.4$).

Cells were then subjected to smRNA-FISH and images were analyzed by quantifying the distribution of fluorescence signal between the nucleus (N) and the cytoplasm (N/C ratio) as well as total cell fluorescence intensity. In a control experiment, N/C ratios were identified for DMSO negative-control and DRB (5,6-dichloro-1-beta-*D*-ribofuranosylbenzimidazole) positive control (Fig. 12a,b), which inhibits cellular processive transcription by RNA polymerase II and also prevents nuclear export of a subset of influenza virus mRNAs, including M mRNA [91]. Compounds with high N/C ratios (Z-score ≥ 3 compared to the robust test population median on each plate), indicating nuclear export block of viral M mRNA (Fig. 12c), were selected for follow-up screening. In addition, our screen revealed compounds that selectively decreased viral RNA signal (fluorescence intensity), indicating down-regulation of viral M mRNA levels (Z-score ≤ -3 compared to the median of the test population on each plate, Fig. 12d).

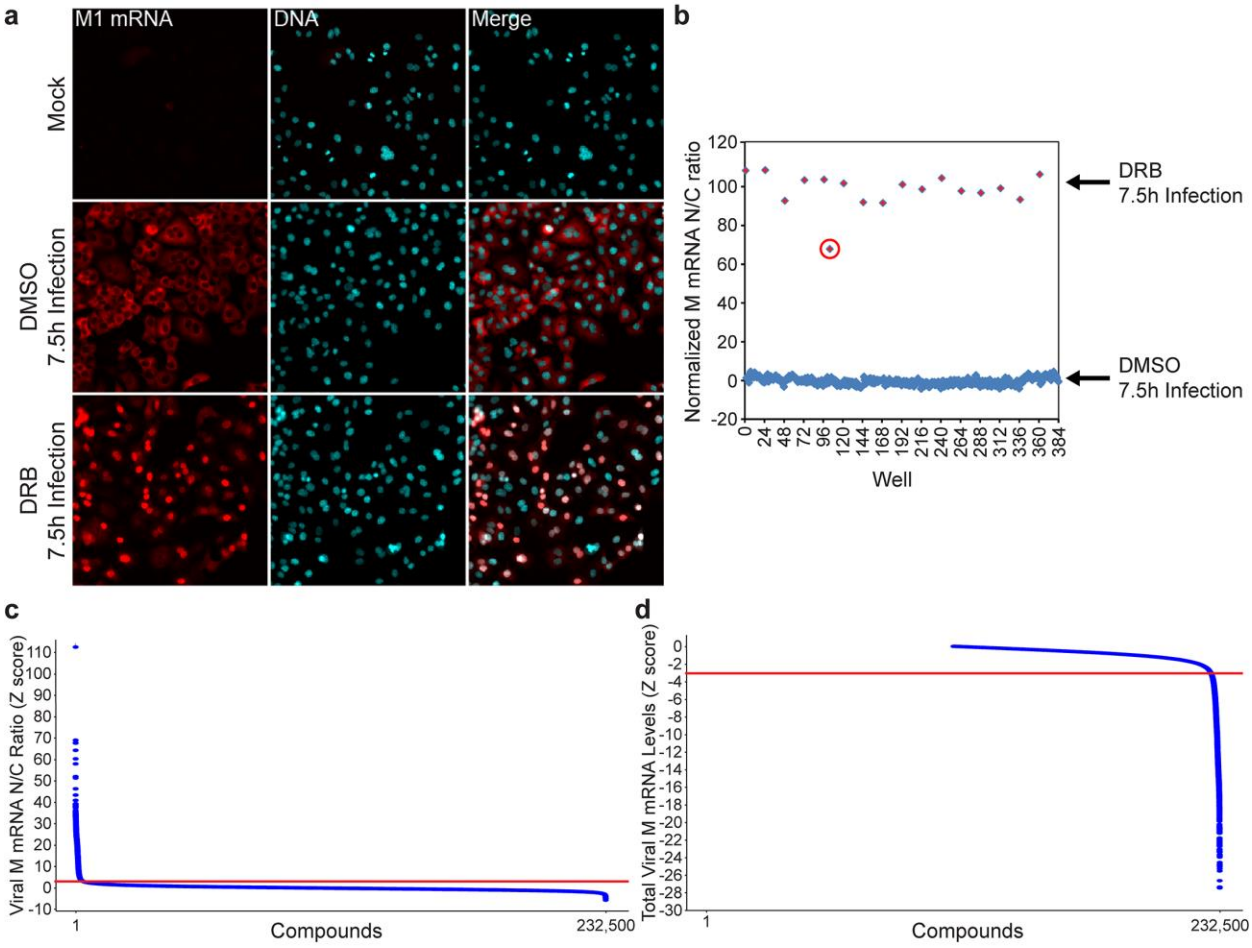

Figure 12. Identification of small molecules that inhibit viral M mRNA nuclear export and/or decrease viral M mRNA levels.

a. Representative images showing uninfected cells; cells infected with A/WSN/33 and pretreated with 0.5% DMSO (control), which show viral M mRNA exported into the cytoplasm, in red; and cells infected with A/WSN/33 pre-treated with 2.5 μM of the transcription inhibitor DRB (5,6-dichloro-1-β-D-ribofuranosylbenzimidazole). DRB served as positive control for viral M mRNA nuclear retention. **b.** Distribution of nuclear (N) to cytosolic (C) (N/C ratio) of all wells in a mock assay plate showing the assay window and sensitivity. DMSO wells were normalized to 0 and DRB positive control wells were normalized to 100. The circled red diamond shape represents a lower dose of DRB and shows lower normalized N/C ratio than the other diamonds representing the full control dose of DRB. **c.** Rank-sorted Z-score of the Nuclear to Cytoplasmic (N/C) ratio of viral M mRNA in A549 cells after individual treatment with 232,500 compounds (2.5 μM). Each N/C value is expressed as a Z-score, indicating the number of standard deviations from the median plate ratio. Points above the red line at Z-score 3 represent compounds that were considered hits in the primary screen. **d.** Rank-sorted Z-score of the total intensity of viral M mRNA after compound treatment. Each value is expressed as a Z-score, indicating the number of standard deviations from the median plate intensity. Points below the red line at Z-score -3 represent compounds selected as hits in the primary screen. To better visualize the distribution of compounds within the desired range (Z-score < -3), the Z-score range of the graph has been focused to view data points that show decrease in viral M mRNA fluorescence.

Furthermore, we have also identified compounds that inhibited both viral M mRNA nuclear export and decreased total viral M mRNA levels (Fig. 13). Compounds that reduced nuclei count were considered cytotoxic (Z-score threshold < -3, See Fig. 13). In total, 4,688 of the 232,500 compounds tested were hits in the primary screen. The 4,688 compounds were clustered based on chemical structure and the 1,125 compounds (824 that inhibited M mRNA nuclear export and 301 that decreased M mRNA levels) with the highest Z-scores from each cluster were chosen for confirmation. The top 600 compounds, including both phenotypic classes, were then subjected to dose response assays to determine their potency. At this stage, we also assessed poly(A) RNA by RNA-FISH to detect potential compound effects on host bulk poly(A) RNA levels or nuclear export. Compounds that altered bulk poly(A) RNA were excluded (AC_{50} < 8 μM). Thus, only compounds that blocked viral M mRNA nuclear export or biogenesis and did not substantially affect host bulk mRNA, at non-toxic concentrations, were selected. 413 of the 600 compounds altered bulk poly(A) RNA and were excluded, thus leaving a total of 187 compounds for follow-up studies (Fig. 13). Importantly, these 187 confirmed hits represent 187 structurally diverse clusters, and each cluster contains the top hit and related less active analogs (Fig. 14).

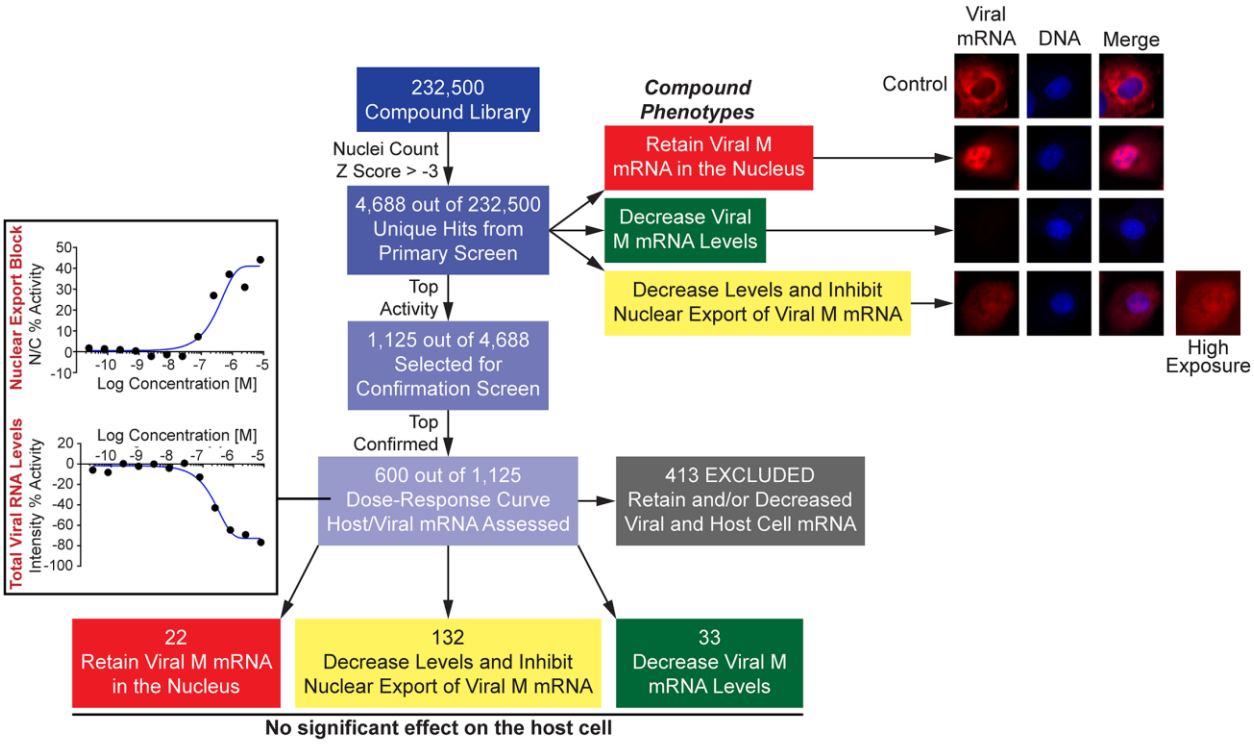

Figure 13. Schematic representation of identification and selection of top hits that inhibit viral M mRNA nuclear export and/or expression.
Out of the 232,500 compounds tested in the primary screen, we selected compounds with Z-scores ≥ 3 for the N/C ratio and compounds that decreased viral mRNA levels with Z-scores ≤ -3. Compounds that reduced nuclear count significantly (Z-score < -3) were considered cytotoxic and were eliminated from further consideration. Of those remaining, the 1,125 compounds with the highest Z-scores were chosen for confirmation studies. The top 600 compounds from single-dose confirmation studies were further evaluated in a 12-point dose response study to assess the potency (AC_{50} – concentration at 50% activity). Examples of dose-response curves showing phenotypes of hits that induced viral M mRNA nuclear export block (increased N/C) and decrease in viral M mRNA levels (decreased intensity) are depicted. During this step, bulk cellular poly(A) RNA localization and intensity were also assessed by smRNA-FISH to determine the effect of these compounds on host cell mRNA (intensity and N/C ratio). Compounds that inhibited viral mRNA nuclear export and/or decreased viral mRNA levels but had no significant effect on the host cell poly(A) RNA were then selected for additional assays.

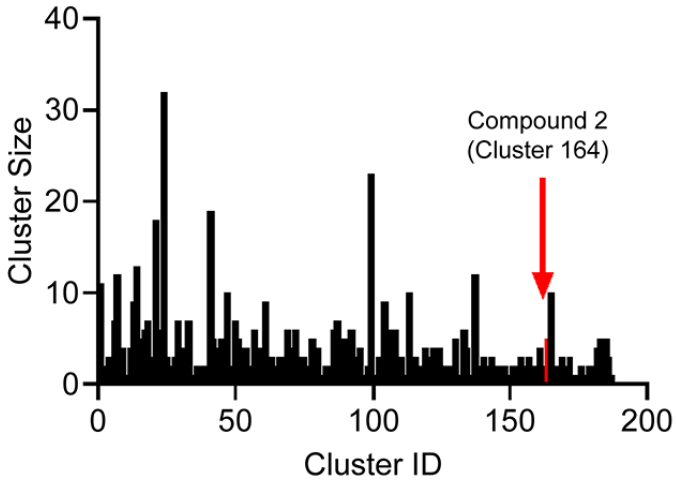

Figure 14. Cluster analysis of confirmed hits.
The 187 compounds identified for follow up studies are the most active members of 187 clusters. Within each active cluster, there are related analogs with lesser activity. In this figure, we show the 187 clusters (arbitrarily numbered 1 to 187) on the x-axis and the number of related analogs for each cluster plotted on the y-axis. Cluster size ranged from 1 to 32 members. Singleton clusters comprised 31% of the structural clusters (chemotypes). Compound 2 is a member of cluster 164 (indicated in red), which has 5 members. Clustering was performed with Pipeline Pilot v16 (Biovia, Inc.) using ECFP4 fingerprints.

4.2 Selective Inhibition of viral mRNA nuclear export

For follow-up studies, we first selected compounds with the lowest AC_{50} in dose-response curves that showed retention of viral M mRNA in the nucleus by measuring nuclear to cytoplasmic ratios as in Figure 13. Among the top hits is compound 2, which is a 2-((1H-benzo[d]imidazole-2-yl)thio)-N-(5-bromopyridin-2-yl) acetamide (Fig. 15a). We re-tested this compound in smRNA-FISH to confirm the

intracellular distribution of viral M mRNA and also extended our analysis to other influenza virus mRNAs, including HA and NS, as well as bulk poly(A) RNA and cellular GAPDH mRNA. Image quantification was performed by determining the mRNA fluorescence intensity in whole cells or in the nucleus and cytoplasm, which is expressed as N/C ratios. We found that compound 2 did not affect the total levels of bulk cellular poly(A) RNA (Fig. 15b,c) and slightly decreased its nuclear to cytoplasmic ratio (Fig. 15b,d). The total levels of cellular GAPDH mRNA were also slightly decreased by compound 2 (Fig. 15b, e) and its nuclear to cytoplasmic distribution was not affected (Fig. 15b, f). Thus, compound 2 slightly promoted cellular poly(A) RNA export. In contrast, compound 2 robustly inhibited nuclear export of viral M mRNA (Fig. 15g-i) and HA mRNA (Fig. 15j-l). Compound 2 did not alter total M mRNA fluorescence intensity (Fig. 15g, h) but induced nuclear retention of M mRNA (Fig. 15g, i). A similar result was obtained for the HA mRNA (Fig. 15j-l). The total levels of the NS mRNA were not altered by compound 2 (Fig. 15m, n), but this compound induced a weak nuclear retention of NS mRNA (Fig. 15m, o) as compared to the effective inhibition of M and HA mRNAs (Fig. 15g-l). These results highlight differences in requirements for nuclear export of specific influenza virus mRNAs. To assess whether compound 2 had any effect on M1 to M2 splicing, we quantified the relative ratio of M2 to M1 mRNAs in the absence or presence of compound 2 by qPCR. We found no effect of compound 2 on M1 to M2 splicing as opposed to knockdown of the splicing co-factor and nuclear speckle assembly factor SON, which was used as a positive control (SON promotes M1 to M2 splicing at nuclear speckles [16]; See Fig. 15p). In addition, compound 2 only slightly inhibited NS1 to NS2 splicing (Fig. 15q). Cellular ATP levels were also assessed as a surrogate for cytotoxicity and showed no significant change in ATP levels (Fig. 15r). Thus, these findings indicate that compound 2 robustly targets nuclear export of a subset of mRNAs at non-toxic concentrations.

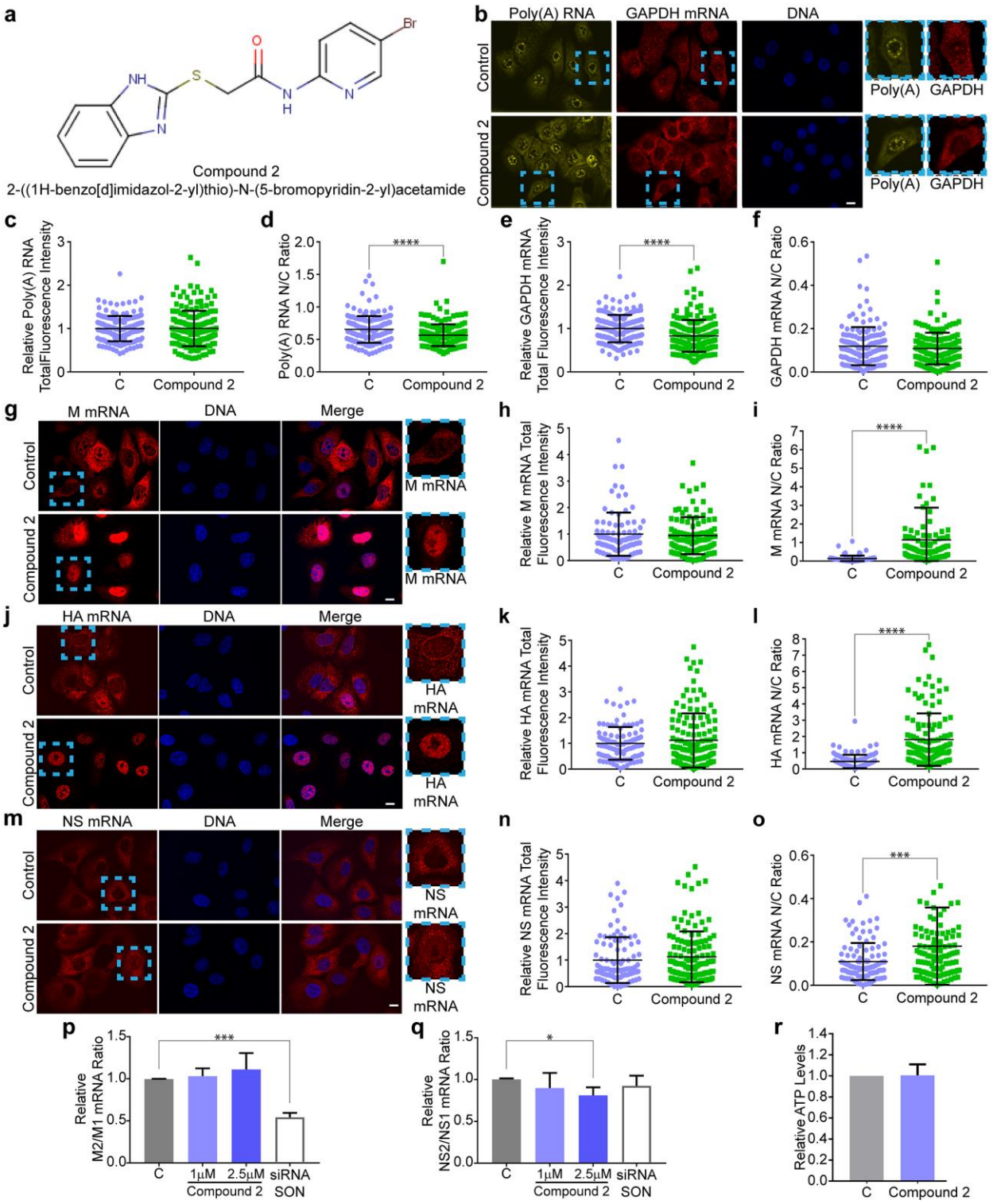

Figure 15. Compound 2 inhibits viral mRNA nuclear export.

a. Structure of compound 2. **b.** RNA-FISH and smRNA-FISH followed by fluorescence microscopy were performed in cells treated with 0.1% DMSO or 2.5 μM compound 2 to detect poly(A) RNA and GAPDH mRNA, respectively, in uninfected cells. **c-f.** Total fluorescence intensity or nuclear to cytoplasmic fluorescence intensity (N/C ratio) were quantified for poly(A) RNA and GAPDH mRNA in the absence or

presence of compound 2. For **c** (C, *n*=174 cells; Compound 2, *n*=181), **d** (C, *n*=172 cells; Compound 2, *n*=181 cells), **e** (C, *n*=166 cells; Compound 2, *n*=181 cells), and **f** (C, *n*=151 cells; Compound 2, *n*=160 cells). **g.** Cells were treated as in **b** except that smRNA-FISH was performed with probes to detect M mRNA in cells infected with WSN at MOI 2 for 8 h. **h,i.** Total fluorescence intensity or nuclear to cytoplasmic fluorescence intensity (N/C ratio) were quantified for M mRNA in the absence or presence of compound 2. For **h** (C, *n*=91 cells; Compound 2, *n*=104 cells) and **i** (C, *n*=101 cells; Compound 2, *n*=95 cells). **j.** Cells were treated as in **g** except that smRNA-FISH was performed with probes to detect HA mRNA. **k,l.** Total fluorescence intensity or nuclear to cytoplasmic fluorescence intensity (N/C ratio) were quantified for HA mRNA in the absence or presence of compound 2. For **k** (C, *n*=104 cells; Compound 2, *n*=137 cells) and **l** (C, *n*=101 cells; Compound 2, *n*=126 cells). **m.** Cells were treated as in **g** except that smRNA-FISH was performed with probes to detect NS mRNA. **n,o.** Total fluorescence intensity or nuclear to cytoplasmic fluorescence intensity (N/C ratio) were quantified for M mRNA in the absence or presence of compound 2. For **n** (C, *n*=96 cells; Compound 2, *n*=135 cells), and **o** (C, *n*=106 cells; Compound 2, *n*=113 cells). At least three independent experiments were performed for each imaging analysis. **p,q.** Relative mRNA ratios of M2 to M1 **p** and NS2 to NS1 **q** were determined by qPCR from RNA obtained from cells infected as in **g** and treated with 0.1% DMSO, 1 μM, or 2.5 μM compound 2. The nuclear speckle assembly factor SON was knocked down with siRNAs as positive control for inhibition of M1 to M2 mRNA splicing. Three independent experiments were performed. C, control. **r** Cellular ATP levels were measured in cells treated with 0.1% DMSO or 2.5 μM of compound 2 at 24 h. Four independent experiments were performed and each contained 6 technical replicates. Graphs shows data points and mean +/- SD. *$p<0.05$; ***$p<0.001$, ****$p<0.0001$.

4.3 Compound 2 phenocopies down-regulation of the mRNA export factor UAP56

We then tested the effect of compound 2 on the M mRNA nuclear export pathway. We and others have previously shown that M mRNA nuclear export is inhibited by knockdown of the mRNA export factor UAP56 [16, 20, 92]. This effect is also shown here with increasing concentrations of siRNAs that target UAP56 (Fig. 16a-c), emphasizing that UAP56 is critical for M mRNA nuclear export. When UAP56 mRNA was knocked down with 25 nM siRNA, a slight reduction in total levels of bulk poly(A) RNA (Fig. 16d,e) and partial inhibition of bulk cellular poly(A) RNA nuclear export (Fig. 16d,f) were detected. We then analyzed the total levels and intracellular distribution of viral M, HA, and NS1 mRNAs upon depletion of UAP56 with low concentrations of siRNA, which reduced UAP56 mRNA and protein levels in a dose-dependent manner (Fig. 16g, h). Upon UAP56 depletion, purified RNA from total cell extracts, nuclear and cytoplasmic fractions were subjected to qPCR (controls for cell fractionation are shown in Fig. 17). Knockdown of UAP56 with 1 nM siRNA only slightly reduced the total levels of M and NS1 mRNAs and did not affect the levels of HA mRNA (Fig. 16i). However, this level of UAP56 down-regulation was sufficient to significantly block M mRNA in the nucleus while the intracellular distribution of NS1 and HA

mRNAs were not affected (Fig. 16j). When the siRNA concentration targeting UAP56 was increased to 20 nM, total levels of M and NS1 mRNAs were reduced but HA mRNA level was not altered (Fig. 16i). Nevertheless, M mRNA nuclear export was further blocked, HA mRNA export is also inhibited, and no effect was observed with NS1 mRNA (Fig. 16j). This preferential blockage of M and HA mRNAs by partial depletion of UAP56 is similar to compound 2 effect on viral mRNA export (Fig. 15g-o). A similar pattern of preferential viral mRNA export upon UAP56 depletion has been previously described [92], but high levels of UAP56 siRNA have been shown to inhibit NS1 mRNA export [20].

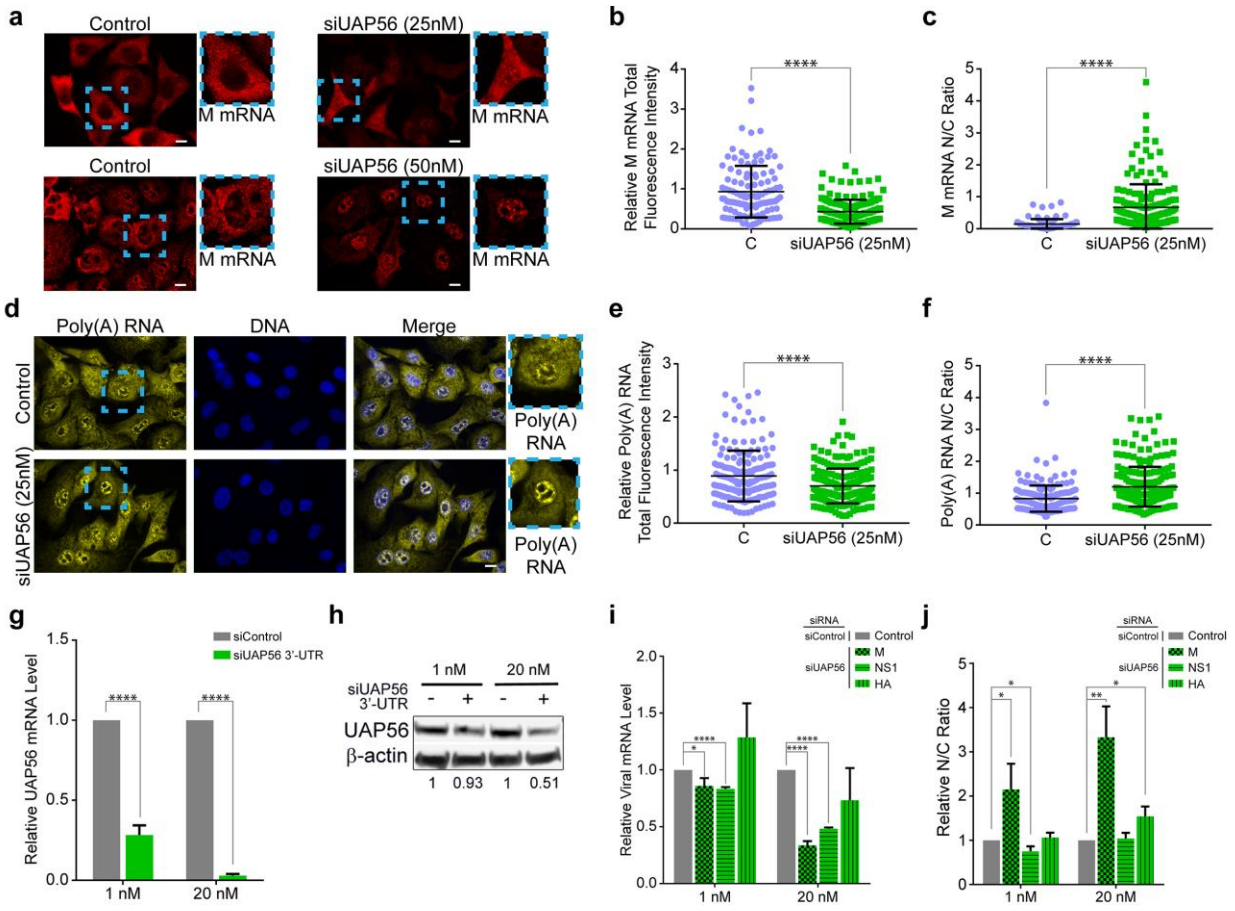

Figure 16. Partial depletion of the mRNA export factor UAP56 show differential export of viral mRNAs similar to compound 2.

a. smRNA-FISH followed by fluorescence microscopy was performed to detect M mRNA in A549 cells treated with control siRNA or with two concentrations (25 nM and 50 nM) of siRNAs that target the coding region of UAP56 or control siRNA followed by infection with WSN at MOI 2 for 8h. **b.** Total fluorescence intensity or nuclear to cytoplasmic fluorescence intensity (N/C ratio) **c.** were quantified for images in **a** in which cells were treated with 25 nM siRNA targeting UAP56. For **b** (C, *n*=117 cells; siRNA UAP56, *n*=171 cells) and **c** (Control, *n*=97 cells; siRNA UAP56, *n*=166 cells). Graphs show data points and mean +/- SD. ****p<0.0001. **d.** A549 cells were treated with 25 nM siRNA targeting UAP56 or control siRNA

as in **a**. RNA-FISH was performed to detect poly(A) RNA. Total fluorescence intensity (**e**) or nuclear to cytoplasmic fluorescence intensity (**f**) were quantified for images in **d**. For **e** (C, *n*=171 cells; siRNA UAP56, *n*=213 cells) and **f** (Control, *n*=172 cells; siRNA UAP56, *n*=208 cells). Graphs show data points and mean +/- SD. ****p<0.0001. **g-j.** A549 cells were treated with 1 nM or 20 nM siRNA targeting the 3'UTR of the UAP56 mRNA or with control siRNA and then infected with WSN at MOI 2 for 8h. **g.** Purified RNA from total cell lysates was subjected to qPCR to measure UAP56 mRNA levels. **h.** Cell lysates were also subjected to western blot to detect UAP56 protein and β-actin as control. Quantification of protein bands normalized to their loading control is shown at the bottom of the blots. **i.** Purified RNA from total cell lysates in **g** were subjected to qPCR to measure viral mRNA levels. **j.** Purified RNA from nuclear and cytoplasmic fractions from cells treated as in **g-j** were subjected to qPCR to measure viral mRNA levels in both fractions and determine their nuclear to cytoplasmic ratios (N/C). Control for cell fractionation is shown in Fig. 17. *n*=3. Graphs are mean +/- SD. *p<0.05, **p<0.01, ****p<0.0001.

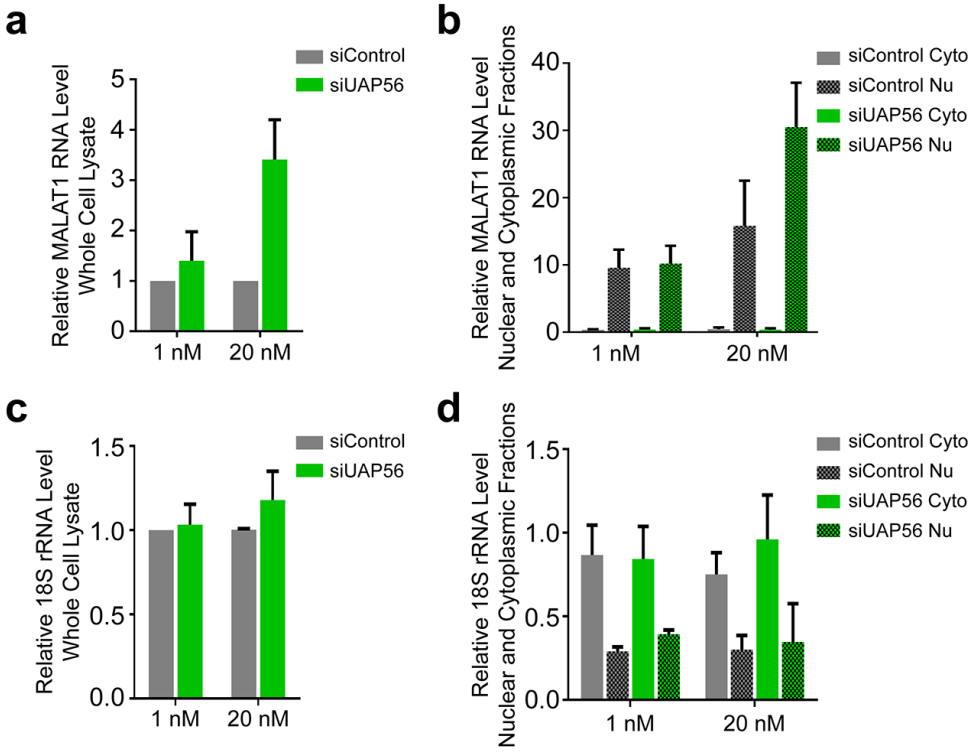

Figure 17. Control for cell fractionation shown in Figure 16.
A549 cells were treated with 1 nM or 20 nM siRNA targeting the 3'UTR of the UAP56 mRNA or with control siRNA and then infected with WSN at MOI 2 for 8h. Purified RNA from total cell extract (**a**) or nuclear and cytoplasmic fractions (**b**) was subjected to qPCR to detect MALAT1 (a long non-coding RNA localized in the nucleus) as a nuclear marker. **c.** Purified RNA from **a** was also used to detect total levels of 18S RNA or determine its nuclear to cytoplasmic distribution (**d**). 18S RNA is preferentially localized in the cytoplasm. Three independent experiments were performed. Graphs show mean +/- SD. Cyto, cytoplasm; Nuc, nucleus.

To further corroborate these data, we tested the effect of a catalytically inactive mutant of UAP56 (E197A) [93-95] on nuclear export of viral M, HA, NS1, and poly(A) RNA. We have generated cells stably

expressing UAP56 (E197A), as we recently reported [54]. These cells were treated with control siRNA or with siRNA that targets the 3'UTR of UAP56 – this siRNA depletes endogenous UAP56 and not UAP56 mutant [54]. The efficiency of this siRNA is shown in Figure 16g and h. Control cells and UAP56 (E197A) mutant cells were then subjected to RNA-FISH to label poly(A) RNA (Fig. 18a-c) or infected with WSN followed by smRNA-FISH to detect M, HA, and NS1 mRNAs (Fig. 18d-l) followed by fluorescence microscopy. In the UAP56 mutant cells treated with siRNA control, the total levels of these mRNAs are not altered while nuclear export of M and HA mRNAs is preferentially blocked, poly(A) RNA export is slightly inhibited, and NS1 mRNA export is not altered (Fig. 18). When these mutant UAP56 cells were then treated with siRNA against endogenous UAP56, the total levels of M and HA mRNAs were reduced (Fig. 18e,h) and the levels of poly(A) RNA and NS1 mRNA were not altered (Fig. 18b,k). On the other hand, nuclear export of M mRNA was severely blocked, poly(A) RNA and HA mRNA export was also inhibited, and NS1 mRNA was only slightly altered (Fig. 18c-l). Taken together, these results show that compound 2 phenocopies partial down-regulation of UAP56 activity as shown by either depleting UAP56 with low levels of siRNA (Fig. 16g, h, j) or by expressing UAP56 mutant in the presence of endogenous UAP56 (UAP56–E197A + siRNA control) (Fig. 18). Since UAP56 is a critical mRNA export factor for viral M mRNA, these results further corroborate the screening strategy to identify inhibitors of the M mRNA nuclear export such as compound 2. Additionally, the differential effect of down-regulating UAP56 activity on nuclear export of certain viral mRNAs further emphasize the concept of preferential usage of specific mRNA export factors or adaptors by a subset of mRNAs.

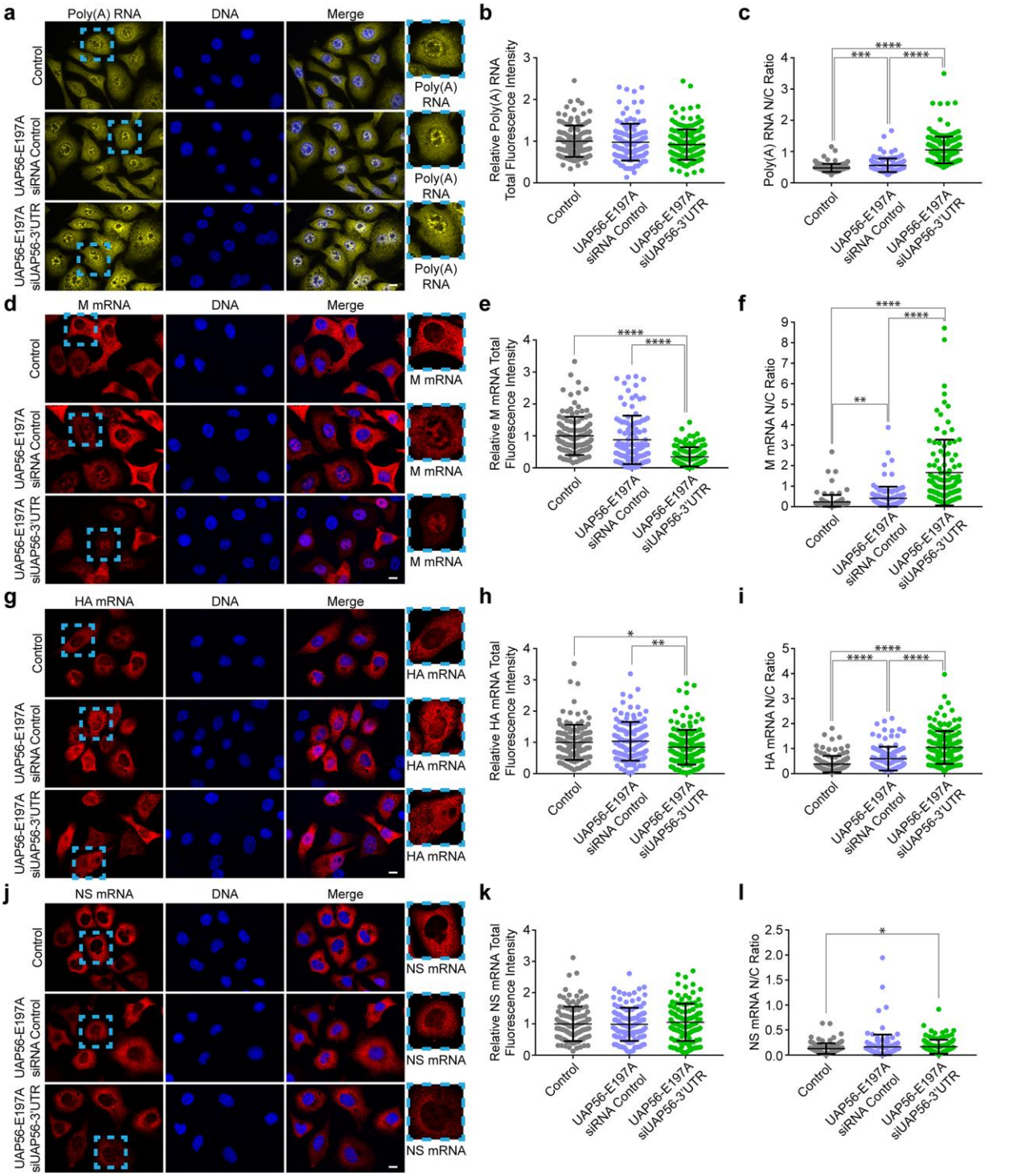

Figure 18. Compound 2 activity phenocopies down-regulation of the mRNA export factor UAP56. A549 cells or A549 cells stably expressing UAP56 E179A mutant were untreated or treated with control siRNA or with siRNA targeting the 3'UTR of UAP56 to knockdown endogenous UAP56 mRNA. Cells were then infected with WSN at MOI 2 for 8h followed by RNA-FISH to detect poly(A) RNA (**a-c**) or smRNA-FISH to detect M (**d-f**), HA (**g-i**), and NS (**j-l**) mRNAs. For **b-c** (C, *n*=128 cells; UAP56-E197A+siRNA Control, *n*=117 cells; UAP56-E197A_siUAP56-3'UTR, *n*=170 cells). For **e-f** (C, *n*=121 cells; UAP56-E197A+siRNA Control, *n*=106 cells; UAP56-E197A_siUAP56-3'UTR, *n*=108 cells). For

h-i (C, *n*=124 cells; UAP56-E197A+siRNA Control, *n*=118 cells; UAP56-E197A_siUAP56-3'UTR, *n*=151 cells). For **k-l** (C, *n*=113 cells; UAP56-E197A+siRNA Control, *n*=119 cells; UAP56-E197A_siUAP56-3'UTR, *n*=115 cells). Graphs show data points and mean +/- SD. *p<0.05, **p<0.01, ***p<0.001 ****p<0.0001.

To quantitatively assess a potential impact of compound 2 on a subset of cellular RNAs and determine their identity, we performed RNA-sequencing (RNA-seq) analysis of purified poly(A) RNA obtained from whole cells, nuclear fractions, and cytoplasmic fractions either treated with DMSO (control) or with 2.5 μM of compound 2. As expected, RNAs that are known to be retained in nucleus, such as MALAT1, are primarily nuclear, and mRNAs that are distributed in the nucleus and cytoplasm, such as GAPDH mRNA, are shown in both compartments. A total of 19,799 unique RNAs were sequenced and the cutoff was 1.5-fold change to be considered differentially expressed in the presence of compound 2. We show that compound 2 altered the nuclear to cytoplasmic distribution of a small subset of cellular RNAs, including mRNAs and non-coding RNAs (Fig. 19a). Among the non-coding RNAs were small nucleolar RNAs (snoRNAs), miRNAs, and long non-coding RNAs. While snoRNAs are not polyadenylated, pre-snoRNA polyadenylation has been shown to link different steps of snoRNA processing [96]. Similarly, pre-miRNAs are polyadenylated and some long non-coding RNAs also have poly(A) tails, explaining their presence in our poly(A) RNA selection. We found that the nuclear to cytoplasmic distribution of 194 RNAs were altered upon compound 2 treatment (Fig. 19a). Among these RNAs, 96 were preferentially retained in the nucleus (high nuclear/cytoplasmic ratio) (Fig. 19a, yellow) and 98 were more cytoplasmic compared to control cells (Fig. 19a, blue). Within the RNAs blocked in the nucleus, 48 out of the 96 RNAs were not altered at their total levels (Fig. 19a, gene name marked in red) indicating nuclear export block similar to the viral M and HA mRNAs upon compound 2 treatment (Fig. 15g-l). In the category of preferentially exported to the cytoplasm, 36 out of the 98 cellular RNAs were not affected at their total levels, suggesting enhanced nuclear export (Fig. 19a, gene name marked in red). Regarding the additional RNAs that had both altered total levels and nuclear to cytoplasmic ratios, the regulation may or may not involve nuclear transport as other RNA processing steps could be also compromised, which is a topic for future

investigation. This RNAseq analysis also revealed the subset of RNAs up-regulated (103 RNAs) and down-regulated by compound 2 (829 RNAs) (Fig. 19b). Among these groups, a small number of mRNAs (13 up-regulated and 47 down-regulated) are also known to be regulated by the viral NS1 protein, as shown in infections performed with WSN compared to WSNΔNS1 [97]. In the category of down-regulated RNAs, gene set enrichment analysis (GSEA) showed tyrosine metabolism altered by compound 2 (p-value = $2.23x10^{-5}$ and a FDR q-value = $4.98x10^{-2}$). Figure 19c-f show examples of selected mRNAs whose total levels as well as nuclear and cytoplasmic distribution were assessed by qPCR and were consistent with our RNAseq results. Thus, these results indicate an effect of compound 2 on a subset of RNAs and not on bulk poly(A) RNA.

a

RNAs with altered Nuclear/Cytoplasmic distribution in the presence of compound 2

GENE_NAME	N/C_Compound 2 versus DMSO	GENE_NAME	N/C_Compound 2 versus DMSO	GENE_NAME	N/C_Compound 2 versus DMSO	GENE_NAME	N/C_Compound 2 versus DMSO
SNORD95	8.78	MIR4648	2.04	CYP2E1	-3.15	IFFO1	-2.16
ATP5EP2	7.98	LOC644656	2.03	FAM167B	-2.65	FOLR1	-1.91
SNORA51	6.88	MIR3620	2.02	PMCH	-4.33	C10orf55	-1.83
AKR1CL1	5.44	NXNL2	2.02	LOC643669	-2.73	KDM5B-AS1	-2.04
MIR4758	5.09	P2RY1	2.01	LINC00304	-4.26	AHSG	-2.07
RNU86	5.05	RCAN3AS	2.00	LOC100129858	-2.67	MIR3615	-1.90
C1orf227	4.38	ROCK1P1	1.98	CECR5-AS1	-2.86	LRRC48	-1.87
LOC100130557	4.35	HTR1B	1.98	DLEU2L	-2.75	OR51E1	-1.74
ANXA2P3	4.15	NR2E3	1.96	ATP6V0A4	-2.76	PPEF1	-1.72
SAP25	4.00	NACA2	1.95	RBP7	-3.95	CD83	-1.79
NUDT9P1	3.93	HTR7P1	1.94	SPATA6L	-3.11	LPAR2	-2.03
PAR5	3.92	MIR568	1.94	REP15	-3.31	LOC100130987	-2.17
MIR181A2HG	3.89	TTC3P1	1.92	SNORD89	-3.06	LRRC36	-1.88
TNFRSF6B	3.81	PLAC1	1.92	C5AR1	-2.28	PLEKHG4B	-1.70
RNF138P1	3.75	LOC100130093	1.90	C1QTNF3	-3.38	SNORD19B	-1.91
FETUB	3.75	ZNF695	1.86	LCN12	-3.41	LGALS9C	-2.61
LOC441461	3.69	LINC00472	1.85	SLA2	-2.35	LINC00460	-1.74
NBEAP1	3.63	LOC100131096	1.84	PON1	-2.05	GIMAP2	-1.68
SFTA1P	3.52	GBX2	1.83	MIR2110	-2.91	SNORD38B	-2.63
C10orf131	3.43	POLN	1.82	CLPSL2	-2.19	CAPN8	-1.62
MIR4687	3.33	OR51E2	1.81	NPIPL3	-2.16	C7orf53	-1.86
NACAP1	3.10	SCARNA9	1.80	TMEM255B	-2.19	LRRC66	-1.81
UBE2MP1	3.07	SLFN11	1.79	DKFZP434K028	-2.35	TNFRSF25	-1.83
FTH1P3	2.76	TNFRSF19	1.77	CNIH2	-3.23	LOC100270804	-1.74
CLRN3	2.73	ZNF256	1.76	PPP1R32	-2.33	LGALS9B	-1.72
SNORA3	2.72	MIR25	1.76	MFNG	-2.85	MIR147B	-1.87
SPEF1	2.70	SNORD65	1.76	MIR5196	-3.90	LOC100270746	-1.99
LY96	2.61	ZBTB26	1.75	PYCARD	-2.81	ANXA2P1	-1.57
SNORA6	2.57	LINC00589	1.75	GSTA2	-2.64	SYNE3	-1.95
C8orf31	2.51	LOC440173	1.75	LPAL2	-2.73	ANKRD36B	-1.87
TAS2R19	2.50	SNORD25	1.75	N4BP2L2-IT2	-2.25	ADSSL1	-1.65
MIR5006	2.46	SNORA53	1.75	PPP1R16B	-1.96	SAPCD1	-1.88
SNORA48	2.45	HIST1H4E	1.74	MIR4658	-1.90	RBP1	-1.56
LOC100131564	2.44	CYP2C9	1.72	CLEC2D	-2.21	PPM1J	-1.60
LOC387723	2.44	LOC100506451	1.70	MIR497HG	-1.88	MZB1	-2.02
ZNF607	2.41	SHROOM2	1.69	C19orf73	-2.03	CYGB	-1.58
WNT10B	2.40	ENO1-AS1	1.68	NPHP1	-2.05	HIST2H2AC	-2.40
SNORD28	2.37	RNF180	1.68	CCDC162P	-2.22	MPZ	-1.66
ZNF141	2.36	JMJD7	1.64	SERTAD4-AS1	-1.93	ST7L	-1.54
LIME1	2.27	ZC3HAV1L	1.63	DENND2D	-1.83	MAP1LC3B2	-2.00
SNORD23	2.26	LPP-AS2	1.61	FAM71F2	-2.28	TSC22D1-AS1	-1.57
SPINK4	2.21	GIP	1.60	FLJ13197	-1.91	SFTPD	-2.04
ARHGAP11B	2.16	TYMP	1.60	CRABP2	-1.96	FKBP1AP1	-1.69
LINC00858	2.14	AGT	1.58	LOC728323	-1.88	ARMC2	-1.57
HIST1H2BJ	2.13	TMEM151A	1.57	MIR611	-2.72	TBX20	-2.54
ANKRD34A	2.08	FAM222A	1.54	SRRM5	-2.35	GNB3	-1.94
CT62	2.08	RIMKLB	1.54	LOC100862671	-1.76	MIR635	-2.17
C1RL-AS1	2.04	MTRNR2L2	1.53	KCND1	-1.93	FAM71E1	-1.71
				MEF2B	-2.31	EIF3CL	-1.60

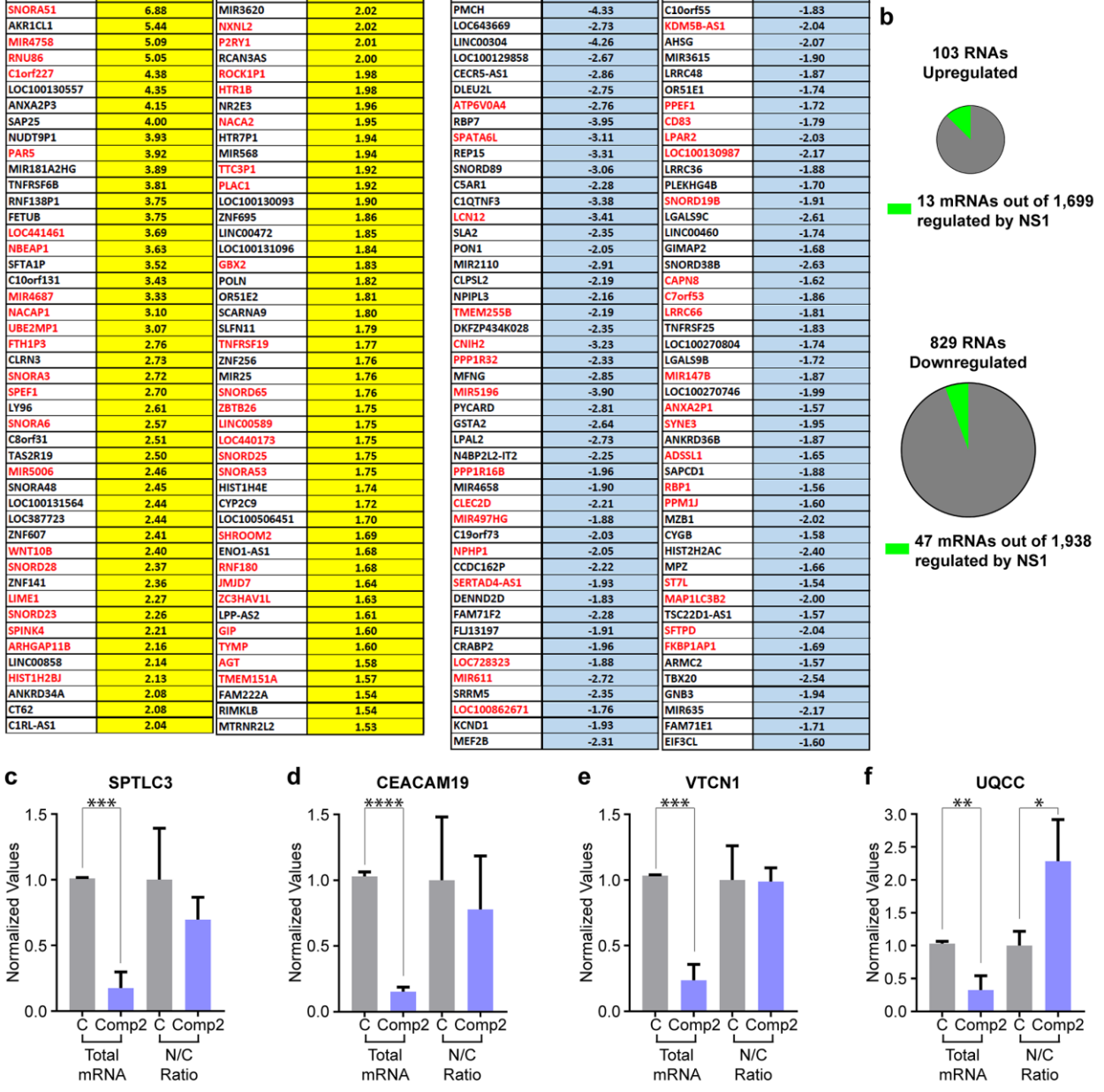

Figure 19. Compound 2 alters the levels and intracellular distribution of a subset of cellular mRNAs. Poly(A) RNA from total cell lysates, nuclear and cytoplasmic fractions untreated or treated with compound 2 was subjected to RNAseq analysis. Two biological duplicates were analyzed and the cut off is 1.5 fold for all analysis. RNAs selected were hits in both samples. **a.** RNAs that are nuclear retained (yellow) or preferentially exported to the cytoplasm (light blue) are shown. Marked in red are RNAs whose total levels were not altered. **b.** The number of RNAs that are up-regulated or down-regulated by compound 2 are shown. Marked in green are the number of RNAs known to be regulated by NS1 during infection. **c-f.** Selected mRNAs were also analyzed by qPCR to corroborate the RNAseq analysis. Relative mRNA levels and nuclear to cytoplasmic ratios of SPTLC3 (**c**), CEACAM19 (**d**), VTCN1 (**e**), and UQCC (**f**) were

determined by qPCR from RNA obtained from total cell lysates, nuclear and cytoplasmic fractions treated with 0.1% DMSO or 2.5 μM compound 2 for 9 h. Three independent experiments were performed. C, control; Comp 2, Compound 2. Graphs show mean +/- SD. *p<0.05, **p<0.01, ***p<0.001 ****p<0.0001.

4.4 Compound 2 inhibits replication of diverse influenza A viruses

Since nuclear export of key viral mRNAs is blocked by compound 2 and given that these mRNAs encode critical proteins for the virus life cycle, it is expected that viral protein levels and replication would be altered by this compound. Indeed, there is a decrease in the levels of the viral M1 and M2 proteins as well as NA and HA proteins upon 2.5 μM compound treatment (Fig. 20a). We then tested compound 2 for inhibition of virus replication and cytotoxicity. As expected, compound 2 inhibited replication of diverse influenza A virus strains at concentrations in which it did not significantly alter cell viability (Fig. 20b-d). Compound 2 also inhibited viral replication in primary human bronchial epithelial cells (Fig. 21). Another compound from our chemical library, ivermectin, is shown as positive control for cytotoxicity at the concentrations used for compound 2 (Fig. 22). In summary, compound 2 preferentially inhibited nuclear export of a subset of mRNAs and further revealed specific requirements for nuclear export of a subset of viral and cellular mRNAs.

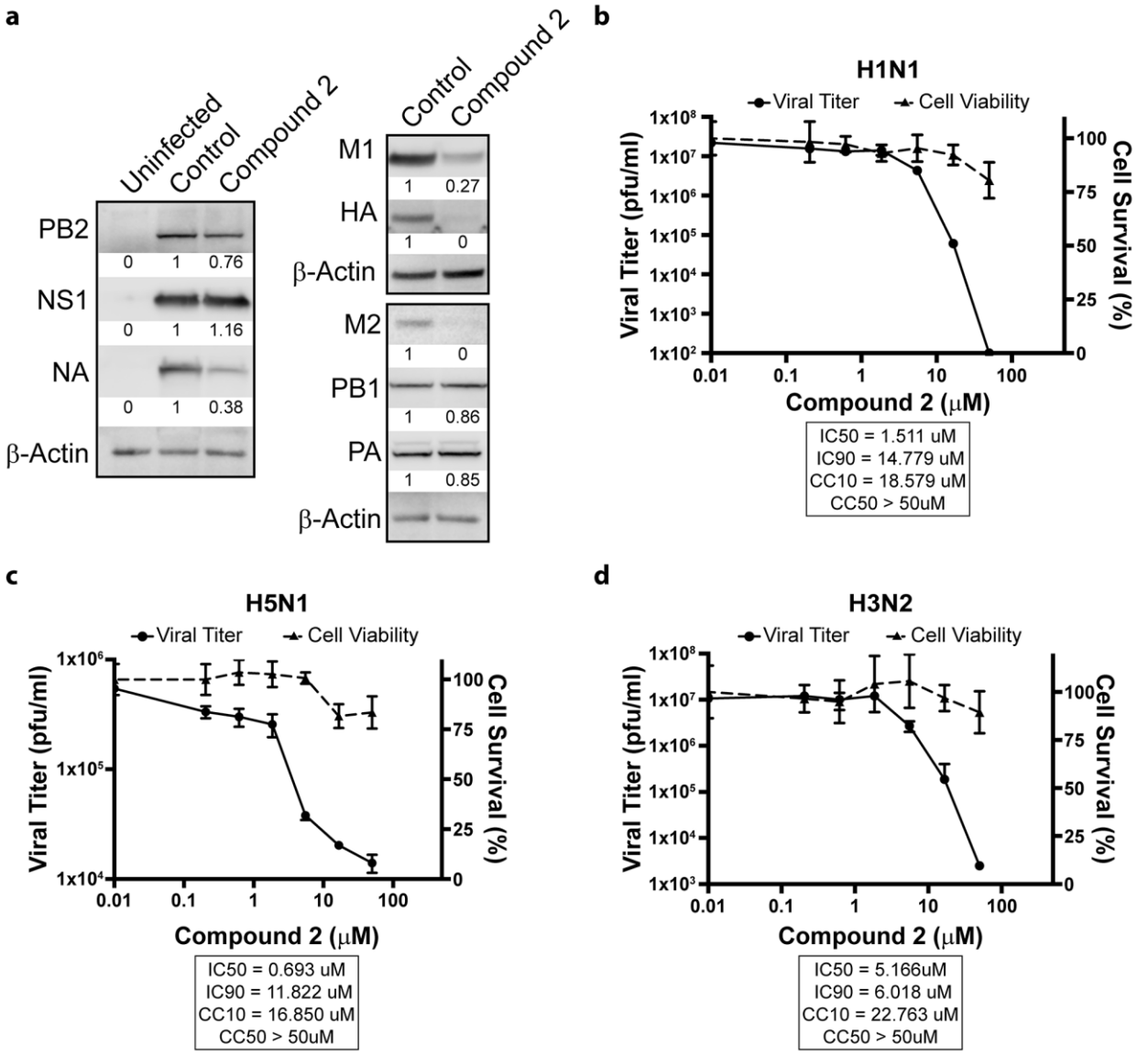

Figure 20. Compound 2 inhibits viral protein production and replication.
a. A549 cells were pre-treated with either 0.1% DMSO or 2.5μM compound 2 before infection with A/WSN33 at MOI 2 for 8 h. Cell lysates were subjected to western blot analysis to detect viral proteins including PB1, PB2, PA, NA, NS1, M1, M2, and HA. β-Actin was used as a loading control. This blot is a representative of three independent experiments. **b-d.** Effect of compound 2 on cell viability and viral replication of (**b**) A/WSN/33 (H1N1), (**c**) A/Vietnam/1203/04 (H5N1), and (**d**) A/Panama/99 (H3N2) influenza A virus strains. Cell viability was determined by the MTT assay in cells treated for 24 h (H1N1 and H5N1) or 48 h (H3N2). Viral titer was determined by plaque assay in cells infected for 24 h (H1N1 and H5N1) or 48 h (H3N2) at MOI 0.01. Three independent experiments were performed. Error bars are SD.

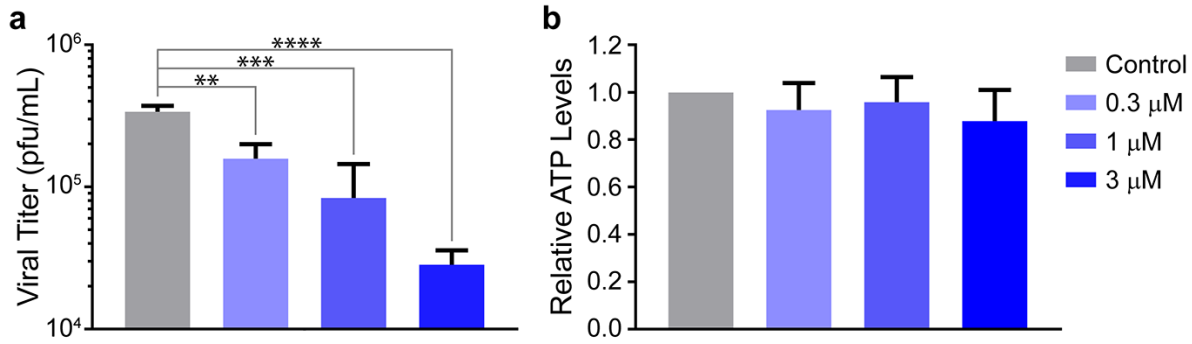

Figure 21. Compound 2 inhibits influenza virus replication in primary human bronchial epithelial cells at non-toxic concentrations.
a. Viral titer was determined by plaque assay in primary human bronchial epithelial cells (HBEC) infected with A/WSN/33 for 24 h in the absence or presence of compound 2 at the depicted concentrations. **b.** Cell viability was monitored at 24 h after treatment with 0.1% DMSO or compound 2 at the depicted concentrations using CellTiter-Glo. Three independent experiments were performed. Graph shows mean +/- SD. **p<0.01. ***p<0.001, ****p<0.0001

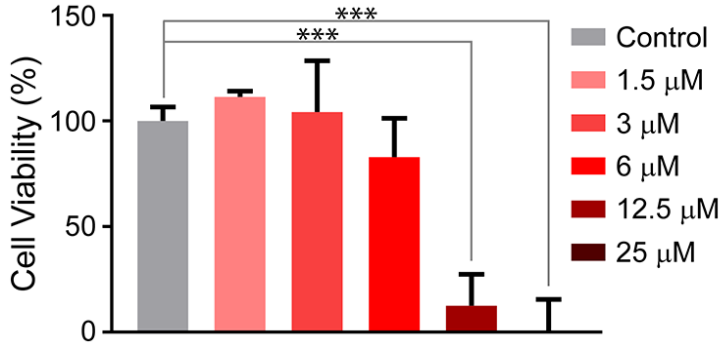

Figure 22. Positive control for compound cytotoxicity.
A549 cells were incubated with ivermectin, a compound present in our chemical library, at the depicted concentrations for 48 h. Cell viability was determined by the MTT assay. Three independent experiments were performed. Graph shows mean +/- SD. ***p<0.001.

CHAPTER FIVE
Discussion

5.1 Influenza virus M1 mRNA trafficking pathway through nuclear speckles for splicing

The identification of the viral mRNA splicing pathway shown here indicates that M1 mRNA trafficking to nuclear speckles is dependent on the viral NS1 protein and the cellular NS1-BP protein. These findings support a model in which NS1 interacts with NS1-BP and directs the M1 mRNA to nuclear speckles during infection for hnRNP K-dependent splicing into M2 mRNA. It has been previously reported that NS1 can bind M1 mRNA and regulate M1 mRNA splicing [71]. Here, we revealed a previously unknown function of NS1 as a mediator of M1 mRNA targeting to nuclear speckles and found that this promotes M1 to M2 mRNA splicing (Fig. 8j). This may explain the unique M1 mRNA splicing kinetics in which M1 production predominates early in infection when NS1 synthesis is low, and then M1 to M2 mRNA splicing is likely enhanced by the high levels of NS1 at late stages of infection [98]. M2 protein has been shown to be cytotoxic to cells when expressed alone [99], which suggests that M2 levels need to be tightly regulated during infection. Furthermore, M2 is critical for viral budding [100], indicating that timing of expression is likely important for production of infectious viral particles, as premature synthesis could lead to defective particles.

The localization of M mRNA into speckles and M1 to M2 mRNA splicing also appears to be coupled to nuclear export. When M1 mRNA localization into intact speckles was impaired by infection with NS1-deficient virus or by depletion of NS1-BP or SON, we observed an accumulation of unspliced M1 mRNA in the nucleus. This effect may be related to previous reports suggesting that mRNA splicing can enhance mRNA nuclear export [101-104]. While our findings indicate that NS1 promotes viral M1 mRNA targeting to nuclear speckles for splicing into M2 mRNA that is efficiently exported to the cytoplasm, NS1 is known to inhibit cellular mRNA export to prevent proper host gene expression and antiviral response [14, 105-107], which happens later than the infection times used here. Together, these results indicate a differential role for NS1 in the nuclear export of viral versus host mRNAs, which may

occur via different RNA-protein interactions. Another possibility is that the actions of NS1 on intranuclear trafficking of M mRNA are indirect, as NS1 is known to be a multifunctional protein involved in regulation of gene expression at the RNA and protein levels [15].

5.2 Viral M mRNA nuclear export pathway

Regarding M mRNA nuclear export, we showed that the cellular mRNA export factors Aly/REF and UAP56 are required for M1 and M2 mRNA export to the cytoplasm. In addition, knockdown of Aly/REF and UAP56 support the compartmentalized M1 mRNA splicing at nuclear speckles. Depletion of these mRNA export factors enhanced the accumulation of M1 and M2 mRNAs at nuclear speckles and increased M1 to M2 mRNA splicing. Since M1 mRNA was blocked in the nucleus, the pool of M1 mRNA available for splicing is high and therefore may explain the increased levels of M1 mRNA splicing. Upon meayamycin treatment of Aly/REF depleted cells, where nuclei were highly enriched with M1 mRNA, nuclear speckle accumulation of M1 mRNA was significantly reduced and a diffusive pattern was observed. This suggests that initial spliceosome assembly, and specifically U2 snRNP deposition on M1 mRNA, is required for M1 mRNA nuclear speckle accumulation and splicing as meayamycin analogues were shown to bind the SF3b complex [88]. Importantly, enhancement of M1 mRNA splicing by Aly/REF and UAP56 knockdown was found to be dependent on entry into nuclear speckles, which was mediated by the viral NS1 protein. This finding underscores the importance of NS1 protein as a mediator of M1 mRNA targeting and splicing at nuclear speckles.

Active spliceosomes are present in nuclear speckles and appear to be involved in post-transcription splicing [108]. Here we found that M vRNAs that serve as templates for the generation of M1 mRNA were not present at nuclear speckles. This indicates that M1 mRNA is not generated at nuclear speckles but is transcribed in the nucleoplasm before being transported to be post-transcriptionally spliced at this nuclear body. At steady state, active spliceosomes residing at nuclear speckles represent ~9-25% of the entire active splicesome population [108] as most cellular pre-mRNAs are spliced at transcribing genes[109, 110] and

not inside nuclear speckles [43]. Thus, influenza virus subverts nuclear speckles to likely usurp splicing factors present in high concentration to promote efficient splicing, and possibly inhibit host gene expression and antiviral response. Alternatively, the virus may utilize specific factors that are active at nuclear speckles for its M1 mRNA processing. The localization of M1 mRNA at nuclear speckles is consistent with a previous study showing differential intranuclear fractionation and splicing of M1 mRNA into M2 mRNA and $mRNA_3$ when the M segment was expressed using a SV40 recombinant virus as opposed to M1 mRNA splicing during influenza virus infection [111]. Thus, transcription of M1 mRNA by the specific influenza virus polymerase machinery and other viral factors may dictate M1 mRNA splicing at nuclear speckles. Finally, due to the importance of regulating mRNA production, splicing, and nuclear export for viral replication, inhibition of this specific viral mRNA pathway through nuclear speckles may provide a strategy for identification of antivirals that we were able to utilize.

5.3 Identification of small molecule inhibitors of viral M mRNA trafficking

Based on our knowledge of viral M mRNA trafficking through host nuclear speckles for splicing and nuclear export [16, 51, 52, 68], we designed a high-throughput screening strategy that led to the identification of small molecules that interfered with specific steps of this pathway. Our image-based chemical screen, which uses single-molecule RNA-FISH, identified three classes of inhibitors that either decreased viral M mRNA levels (class 1), or blocked it in the nucleus (class 2), or both (class 3). Our primary HTS assay proved to be quite robust, as exemplified by an average Z' value of 0.63 for the N/C ratio when comparing the DMSO (vehicle) control to a positive control, DRB. To ensure that we sampled all of the chemical space identified by the screen, we clustered the initial set of hits into chemical series for compounds that decreased the M mRNA fluorescence intensity (552 clusters, intensity reduced > 25%) and for compounds that decreased the N/C ratio (~1300 clusters, N/C ratio > 25%). We then selected cluster representatives from both groups as described above (See Results.) Hit confirmation studies identified ~600 compounds that fell into the three phenotypic classes described above. These compounds were

subsequently reviewed for chemical attractiveness (e.g. absence of problematic substructures or PAINS, synthetic tractability, etc.). In this report, we highlight an inhibitor that preferentially prevented nuclear export of a subset of viral mRNAs (class 2), resulting in their accumulation in the nucleoplasm. Since this small molecule (and others like it identified by the screen) did not substantially alter bulk cellular mRNA levels or their intracellular distribution and were not cytotoxic at active concentrations, they may serve as leads for potential antiviral therapy. Therefore, these data revealed a window of opportunity to target a pathway that processes a subset of viral and cellular mRNAs [16, 52]. In addition, compound 2's differential nuclear export inhibition of viral mRNAs and cellular mRNAs demonstrates specific requirements within the mRNA export machinery for nuclear export and provides a tool to distinguish these pathways in future studies.

5.4 Compound 2 inhibits the UAP56-mediated mRNA export of M1 mRNA

The differential effect of compound 2 on viral M mRNA nuclear export, phenocopying down-regulation of UAP56 activity, further corroborates its action on the UAP56-NXF1-mediated mRNA export pathway. This would be predicted based on the screening strategy presented here. UAP56 is known to recruit the mRNA export factor Aly/REF to the mRNA, which then binds the mRNA export receptor NXF1•NXT1. This interaction displaces UAP56 from the mRNA and NXF1•NXT1 then docks the mRNP to the nuclear pore complex for export into the cytoplasm [112]. Prior to docking at the nuclear pore complex, the M mRNA is spliced at nuclear speckles and then exported to the nucleoplasm for translocation through the nuclear pore complex [16]. UAP56 is localized at nuclear speckles and in the nucleoplasm [86] and is required for exit of M mRNA from nuclear speckles to the nucleoplasm, as we have previously shown [16]. The localization and export function of UAP56 in the nucleoplasm and at nuclear speckles may involve different factors/adaptors. In contrast to M mRNA [16] and a subset of cellular mRNAs [46-50] whose splicing and/or export occur at nuclear speckles, most cellular mRNAs are spliced in the nucleoplasm prior to being exported from the nucleus. Compound 2 targets the viral M mRNA nuclear export without affecting its splicing at nuclear speckles. Therefore, it is likely that this small molecule is targeting a step

between nuclear speckles and the nuclear pore complex, resulting in the accumulation of viral M mRNA throughout the nucleoplasm. Since bulk cellular mRNAs were not substantially affected by the compound at a concentration that it robustly inhibited M and HA mRNA nuclear export, it is possible that this compound is specifically targeting a step or location that affects a subset of cellular mRNAs. In fact, RNAseq analysis shows effect of compound 2 on nuclear export and total levels of a subset of cellular RNAs. This is consistent with the data in which partial depletion of UAP56 or expression of a UAP56 mutant in the catalytic domain in the presence of endogenous UAP56 preferentially blocked viral M and HA mRNA nuclear export without substantially altering NS1 mRNA or bulk cellular mRNAs. These differential effects by partially decreasing the levels of an mRNA export factor reveal a window of opportunity to therapeutically target the mRNA export machinery without inducing major cytotoxicity to the host cell.

Among the subset of cellular mRNAs whose total levels are up-regulated or down-regulated by compound 2 without changes in intracellular distribution, are a few mRNAs known to be regulated by the viral NS1 protein. In the category of up-regulated mRNAs are members of the type-I interferon response system, including IFIT1 and IRF7 [113]. IFN response is known to be suppressed by the NS1 protein therefore both IFIT1 and IRF7 mRNAs are up-regulated in cells infected with the influenza virus lacking NS1 protein [97]. Regarding the down-regulated mRNAs, which were enriched in mRNAs that encode proteins involved in tyrosine metabolism, it is possible that the decrease in tyrosine metabolism inhibits virus replication. Tyrosine is a critical amino acid for viral proteins, such as tyrosine 132 phosphorylation of M1 protein which controls its nuclear import and virus replication [114]. Additionally, virus replication is blocked by receptor tyrosine kinase inhibitors [115]. Furthermore, 47 mRNAs in this down-regulated category are also regulated by NS1. Together, these data suggest that inhibition of influenza virus replication by compound 2 may be a combinatory effect of inhibition of viral mRNA export and induction of antiviral response which, at least in part, involves the type-I interferon system.

5.5 Potential anti-viral development and implications for cell biology

Compound 2 is an alkylated mercaptobenzimidazole featuring an aminopyridine amide. No biological activities have been attributed to this compound previously. However, a structurally related series of N-aryl mercaptobenzimidazoles have been described as inhibitors of influenza viruses and myxoviruses [58, 116]. We show that the most potent compound of this series had no effect on M mRNA nuclear export (Fig. 23), indicating that this series operates through a distinct mechanism(s). Accordingly, compound 2 represents an attractive starting point for additional drug discovery efforts. In addition, the screen presented here yielded compounds with various phenotypes – inhibitors of viral M mRNA biogenesis, processing, and/or nuclear export – thus, this strategy expands the landscape for targeting influenza virus at multiple steps of the virus M mRNA intranuclear pathway. As robust viral therapy will likely rely on combination of drugs, this strategy provides multiple leads for drug development. This combinatorial process also contributes to enhance efficacy against diverse viral strains as these compounds may differentially target influenza virus strains. These small molecules are also valuable tools for further understanding new cell biology. They will likely uncover critical regulatory steps and novel factors involved in a yet understudied viral mRNA processing and export pathway.

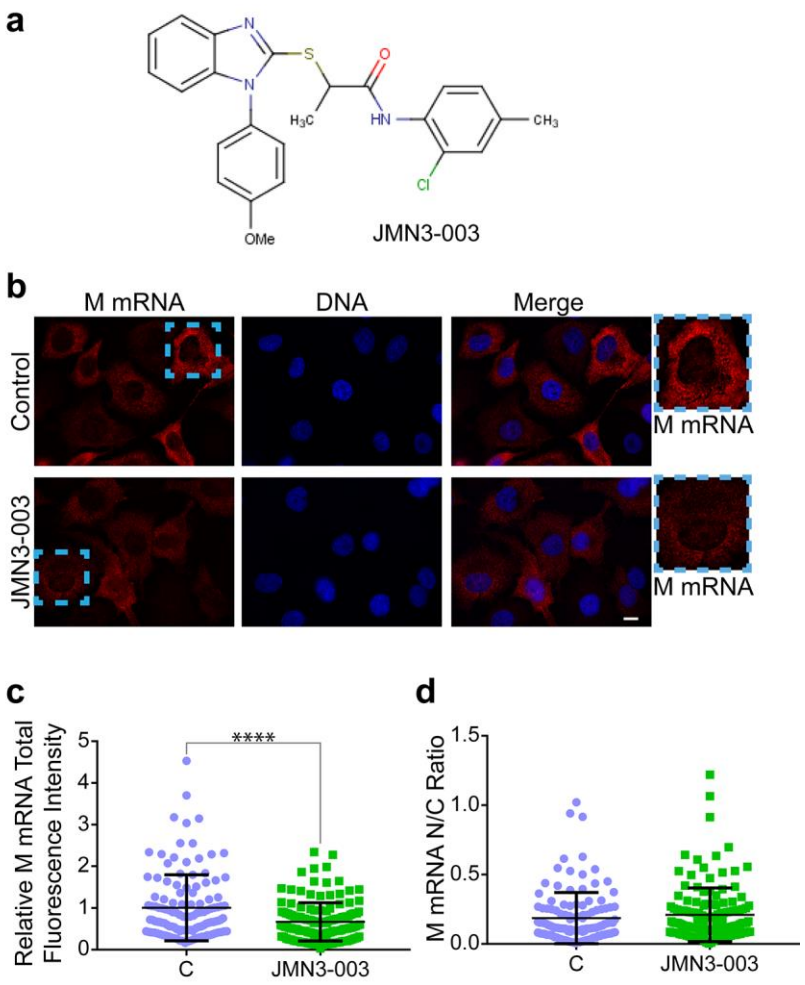

Figure 23. Compound JMN3-003 (N-aryl mercaptobenzimidazole) does not inhibit viral mRNA nuclear export.

a. Structure of compound JMN3-003. **b.** smRNA-FISH followed by fluorescence microscopy was performed to detect M mRNA in cells treated with 0.1% DMSO or 2.5μM JMN3-003. These treatments started 1 hour before infection with WSN at MOI 2 for 8 h. Total fluorescence intensity **c.** or nuclear to cytoplasmic fluorescence intensity (N/C ratio) **d.** of M mRNA was quantified for images in **b**. For both **c** and **d** (C, *n*=123 cells; JMN3-003, *n*=141 cells). Graphs show data points and mean +/- SD. ****p<0.0001. This compound decreased total viral M mRNA levels but did not retain viral M mRNA in the nucleus as compound 2.

BIBLIOGRAPHY

1. Luliano, A.D., et al., *Estimates of global seasonal influenza-associated respiratory mortality: a modelling study.* Lancet, 2018. **391**(10127): p. 1285-1300.
2. Medina, R.A. and A. Garcia-Sastre, *Influenza A viruses: new research developments.* Nature reviews. Microbiology, 2011. **9**(8): p. 590-603.
3. Hayden, F.G., et al., *Baloxavir Marboxil for Uncomplicated Influenza in Adults and Adolescents.* N Engl J Med, 2018. **379**(10): p. 913-923.
4. Krammer, F., A. Garcia-Sastre, and P. Palese, *Is It Possible to Develop a "Universal" Influenza Virus Vaccine? Potential Target Antigens and Critical Aspects for a Universal Influenza Vaccine.* Cold Spring Harb Perspect Biol, 2018. **10**(7).
5. Uyeki, T.M., et al., *Clinical Practice Guidelines by the Infectious Diseases Society of America: 2018 Update on Diagnosis, Treatment, Chemoprophylaxis, and Institutional Outbreak Management of Seasonal Influenza.* Clin Infect Dis, 2018.
6. Takashita, E., et al., *Baloxavir marboxil, a novel cap-dependent endonuclease inhibitor potently suppresses influenza virus replication and represents therapeutic effects in both immunocompetent and immunocompromised mouse models.* PLoS ONE, 2019. **14**(5).
7. Palese, P. and M.L. Shaw, *Orthomyxoviridae: The virus and their replication.* Fields Virology 5th, 2007. **Knipe, D.M., et al.**(Lippincott Williams & Wilkins, Philadelphia, USA): p. 1647-1689.
8. Zebedee, S.L. and R.A. Lamb, *Influenza A virus M2 protein: monoclonal antibody restriction of virus growth and detection of M2 in virions.* J Virol, 1988. **62**(8): p. 2762–2772.
9. Gannage, M., et al., *Matrix protein 2 of influenza A virus blocks autophagosome fusion with lysosomes.* Cell Host Microbe, 2009. **6**(4): p. 367-80.
10. Rossman, J.S., et al., *Influenza virus M2 protein mediates ESCRT-independent membrane scission.* Cell, 2010. **142**(6): p. 902-13.
11. Tripathi, S., et al., *Meta- and Orthogonal Integration of Influenza "OMICs" Data Defines a Role for UBR4 in Virus Budding.* Cell Host Microbe, 2015. **18**(6): p. 723-35.
12. Garcia-Sastre, A., et al., *Influenza A virus lacking the NS1 gene replicates in interferon-deficient systems.* Virology, 1998. **252**(2): p. 324-30.
13. Chen, Z., Y. Li, and R.M. Krug, *Influenza A virus NS1 protein targets poly(A)-binding protein II of the cellular 3'-end processing machinery.* Embo J, 1999. **18**(8): p. 2273-83.
14. Satterly, N., et al., *Influenza virus targets the mRNA export machinery and the nuclear pore complex.* Proc Natl Acad Sci U S A, 2007. **104**(6): p. 1853-8.
15. Ayllon, J. and A. Garcia-Sastre, *The NS1 protein: a multitasking virulence factor.* Curr Top Microbiol Immunol, 2015. **386**: p. 73-107.
16. Mor, A., et al., *Influenza Virus mRNA Trafficking Through Host Nuclear Speckles.* Nat Microbiol, 2016. **1**((7):16069. doi: 10.1038/nmicrobiol.2016.69.).
17. Zhang, K., et al., *Structural basis for influenza virus NS1 protein block of mRNA nuclear export.* Nat Microbiol, 2019. **4**(10): p. 1671-1679.
18. Neumann, G., M.T. Hughes, and Y. Kawaoka, *Influenza A virus NS2 protein mediates vRNP nuclear export through NES-independent interaction with hCRM1.* Embo J, 2000. **19**: p. 6751-6758.
19. O'Neill, R.E., et al., *Nuclear import of influenza virus RNA can be mediated by viral nucleoprotein and transport factors required for protein import.* J Biol Chem, 1995. **270**(39): p. 22701-4.
20. Read, E.K. and P. Digard, *Individual influenza A virus mRNAs show differential dependence on cellular NXF1/TAP for their nuclear export.* J Gen Virol, 2010. **91**(Pt 5): p. 1290-301.

21. O'Neill, R.E., J. Talon, and P. Palese, *The influenza virus NEP (NS2 protein) mediates the nuclear export of viral ribonucleoproteins.* EMBO J, 1998. **17**(1): p. 288-296.
22. S., H., et al., *A second CRM1-dependent nuclear export signal in the influenza A virus NS2 protein contributes to the nuclear export of viral ribonucleoproteins.* J Virol, 2013. **87**(2): p. 767-778.
23. H., A., et al., *Crystal structure of the M1 protein-binding domain of the influenza A virus nuclear export protein (NEP/NS2).* EMBO J, 2003. **22**(18): p. 4646-4655.
24. Flick, R., et al., *Promoter elements in the influenza vRNA terminal structure.* RNA, 1996. **2**(10): p. 1046-1057.
25. Desselberger, U., et al., *The 3' and 5'-terminal sequences of influenza A, B and C virus RNA segments are highly conserved and show partial inverted complementarity.* Gene, 1980. **8**(3): p. 315-328.
26. Dias, A., et al., *The cap-snatching endonuclease of influenza virus polymerase resides in the PA subunit.* Nature, 2009. **458**(7240): p. 914-918.
27. Fechter, P. and G.G. Brownlee, *Recognition of mRNA cap structures by viral and cellular proteins.* J Gen Virol, 2005. **86**: p. 1239-1249.
28. Yuan, P., et al., *Crystal structure of an avian influenza polymerase PA(N) reveals an endonuclease active site.* Nature, 2009. **458**(7240): p. 909-913.
29. Zheng, H., et al., *Influenza A virus RNA polymerase has the ability to stutter at the polyadenylation site of a viral RNA template during RNA replication.* J Virol, 1999. **73**(6): p. 5240-5243.
30. Poon, L.L., et al., *Direct evidence that the poly(A) tail of influenza A virus mRNA is synthesized by reiterative copying of a U track in the virion RNA template.* J Virol, 1999. **73**(4): p. 3473-3476.
31. Te Velthuis, A.J., et al., *The role of the priming loop in Influenza A virus RNA synthesis.* Nat Microbiol, 2016. **1**(5).
32. Umbach, J.L., et al., *Influenza A virus expresses high levels of an unusual class of small viral leader RNAs in infected cells.* mBio, 2010. **1**(4).
33. Perez, J.T., et al., *Influenza A virus-generated small RNAs regulate the switch from transcription to replication.* Proc Natl Acad Sci U S A, 2010. **107**(25): p. 11525-30.
34. Deng, T., F.T. Vreede, and G.G. Brownlee, *Different de novo initiation strategies are used by influenza virus RNA polymerase on its cRNA and viral RNA promoters during viral RNA replication.* J Virol, 2006. **80**(5): p. 2337-48.
35. York, A., et al., *Isolation and characterization of the positive-sense replicative intermediate of a negative-strand RNA virus.* Proc Natl Acad Sci U S A, 2013. **110**(45): p. E4238-45.
36. Jorba, N., R. Coloma, and J. Ortin, *Genetic trans-complementation establishes a new model for influenza virus RNA transcription and replication.* PLoS Pathog, 2009. **5**(5).
37. Newcomb, L.L., et al., *Interaction of the influenza a virus nucleocapsid protein with the viral RNA polymerase potentiates unprimed viral RNA replication.* J Virol, 2009. **83**: p. 29-36.
38. Perez, J.T., et al., *A small-RNA enhancer of viral polymerase activity.* J Virol, 2012. **86**(24): p. 13475-85.
39. Vreede, F.T., T.E. Jung, and G.G. Brownlee, *Model suggesting that replication of influenza virus is regulated by stabilization of replicative intermediates.* J Virol, 2004. **78**(17).
40. Knipe, D.M. and P.M. Howley, *Fields Virology.* 2013. **Sixth Ed. Vol. 1. pp.** : p. 1487-1531.
41. Wise, H.M., et al., *Identification of a novel splice variant form of the influenza A virus M2 ion channel with an antigenically distinct ectodomain.* PLoS pathogens, 2012. **8**(11): p. e1002998.
42. Robb, N., et al., *Splicing of influenza A virus NS1 mRNA is independent of the viral NS1 protein.* J Gen Virol, 2010. **91**: p. 2331-40.
43. Spector, D.L. and A.I. Lamond, *Nuclear speckles.* Cold Spring Harb Perspect Biol, 2011. **3**(2).
44. Mao, Y.S., B. Zhang, and D.L. Spector, *Biogenesis and function of nuclear bodies.* Trends Genet, 2011. **27**(8): p. 295-306.

45. Tilgner, H., et al., *Deep sequencing of subcellular RNA fractions shows splicing to be predominantly co-transcriptional in the human genome but inefficient for lncRNAs.* Genome research, 2012. **22**(9): p. 1616-25.
46. Akef, A., et al., *Trafficking of mRNAs containing ALREX-promoting elements through nuclear speckles.* Nucleus, 2013. **4**(4): p. 326-40.
47. Dias, A.P., et al., *A role for TREX components in the release of spliced mRNA from nuclear speckle domains.* Nat Commun, 2010. **1**: p. 97.
48. Ishihama, Y., et al., *The dynamics of pre-mRNAs and poly(A)+ RNA at speckles in living cells revealed by iFRAP studies.* Exp Cell Res, 2008. **314**(4): p. 748-62.
49. Melcak, I., et al., *Prespliceosomal assembly on microinjected precursor mRNA takes place in nuclear speckles.* Mol Biol Cell, 2001. **12**(2): p. 393-406.
50. Wang, K., et al., *Intronless mRNAs transit through nuclear speckles to gain export competence.* J Cell Biol, 2018. **217**(11): p. 3912-3929.
51. Thompson, M.G., et al., *Co-regulatory activity of hnRNP K and NS1-BP in influenza and human mRNA splicing.* Nat Commun, 2018. **9**(1): p. 2407.
52. Zhang, K., et al., *Structural-functional interactions of NS1-BP protein with the splicing and mRNA export machineries for viral and host gene expression.* Proc Natl Acad Sci U S A, 2018. **115**(52): p. E12218-E12227.
53. Peters-Hall, J.R., et al., *Proliferation of adult human bronchial epithelial cells without a telomere maintenance mechanism for over 200 population doublings.* The FASEB Journal, 2019. **00**: p. 1-13.
54. Hondele, M., et al., *DEAD-box ATPases are global regulators of phase-separated organelles.* Nature, 2019. **573**(7772): p. 144-148.
55. Zhang, Y., et al., *Inhibition of the prostaglandin-degrading enzyme 15-PGDH potentiates tissue regeneration.* Science, 2015. **348**(6240).
56. Zhijin Wu, Dongmei Liu, and Yunxia Sui, *Quantitative Assessment of Hit Detection and Confirmation in Single and Duplicate High-Throughput Screenings.* J. Biomol. Screening, 2008. **13**(2): p. 159-167.
57. Rogers, D. and M. Hahn, *Extended-connectivity fingerprints.* J Chem Inf Model, 2010. **50**(5): p. 742-54.
58. Moore, T.W., et al., *Asymmetric synthesis of host-directed inhibitors of myxoviruses.* Beilstein J Org Chem, 2013. **9**: p. 197-203.
59. Andrews, S., *FastQC: a quality control tool for high throughput sequence data.* Available online at: http://www.bioinformatics.babraham.ac.uk/projects/fastqc, 2010.
60. Wingett, S.W. and S. Andrews, *FastQ Screen: A tool for multi-genome mapping and quality control.* F1000Res, 2018. **7**: p. 1338.
61. Aronesty, E., *Comparison of sequencing utility programs.* Open Bionf., 2013. **7**: p. 1-8.
62. Dobin, A., et al., *STAR: ultrafast universal RNA-seq aligner.* Bioinformatics, 2013. **29**(1): p. 15-21.
63. Liao, Y., G.K. Smyth, and W. Shi, *featureCounts: an efficient general purpose program for assigning sequence reads to genomic features.* Bioinformatics, 2014. **30**(7): p. 923-30.
64. Robinson, M.D., D.J. McCarthy, and G.K. Smyth, *edgeR: a Bioconductor package for differential expression analysis of digital gene expression data.* Bioinformatics, 2010. **26**(1): p. 139-40.
65. Subramanian, A., et al., *Gene set enrichment analysis: a knowledge-based approach for interpreting genome-wide expression profiles.* Proc Natl Acad Sci U S A, 2005. **102**(43): p. 15545-50.
66. Liberzon, A., et al., *The Molecular Signatures Database (MSigDB) hallmark gene set collection.* Cell Syst, 2015. **1**(6): p. 417-425.
67. Liberzon, A., et al., *Molecular signatures database (MSigDB) 3.0.* Bioinformatics, 2011. **27**(12): p. 1739-40.

68. Tsai, P.L., et al., *Cellular RNA Binding Proteins NS1-BP and hnRNP K Regulate Influenza A Virus RNA Splicing.* PLoS pathogens, 2013. **9**(6): p. e1003460.
69. Solorzano, A., et al., *Mutations in the NS1 protein of swine influenza virus impair anti-interferon activity and confer attenuation in pigs.* J Virol, 2005. **79**(12): p. 7535-43.
70. Matera, A.G. and Z. Wang, *A day in the life of the spliceosome.* Nat Rev Mol Cell Biol, 2014. **15**(2): p. 108-21.
71. Robb, N.C. and E. Fodor, *The accumulation of influenza A virus segment 7 spliced mRNAs is regulated by the NS1 protein.* J Gen Virol, 2012. **93**(Pt 1): p. 113-8.
72. Bier, K., A. York, and E. Fodor, *Cellular cap-binding proteins associate with influenza virus mRNAs.* J Gen Virol, 2011. **92**(Pt 7): p. 1627-34.
73. Wang, W., et al., *Imaging and characterizing influenza A virus mRNA transport in living cells.* Nucleic Acids Res, 2008. **36**(15): p. 4913-28.
74. Fortes, P., A.I. Lamond, and J. Ortin, *Influenza virus NS1 protein alters the subnuclear localization of cellular splicing components.* J Gen Virol, 1995. **76 (Pt 4)**: p. 1001-7.
75. Zhang, L., et al., *Inhibition of pyrimidine synthesis reverses viral virulence factor-mediated block of mRNA nuclear export.* J Cell Biol, 2012. **196**(3): p. 315-26.
76. Wolff, T., R.E. O'Neill, and P. Palese, *NS1-binding protein (NS1-BP): A novel human protein that interacts with the influenza A virus nonstructural NS1 protein is relocalized in the nucleus of infected cells.* J. Virol., 1998. **72**: p. 7170-7180.
77. Tsai, P.L., et al., *Cellular RNA binding proteins NS1-BP and hnRNP K regulate influenza A virus RNA splicing.* PLoS Pathog., 2013. **9**(6): p. e1003460.
78. Cao, W., et al., *Control of alternative splicing by forskolin through hnRNP K during neuronal differentiation.* Nucleic Acids Res, 2012. **40**(16): p. 8059-71.
79. Marchand, V., et al., *Identification of protein partners of the human immunodeficiency virus 1 tat/rev exon 3 leads to the discovery of a new HIV-1 splicing regulator, protein hnRNP K.* RNA Biol, 2011. **8**(2): p. 325-42.
80. Motta-Mena, L.B., et al., *A disease-associated polymorphism alters splicing of the human CD45 phosphatase gene by disrupting combinatorial repression by heterogeneous nuclear ribonucleoproteins (hnRNPs).* J Biol Chem, 2011. **286**(22): p. 20043-53.
81. Venables, J.P., et al., *Multiple and specific mRNA processing targets for the major human hnRNP proteins.* Mol Cell Biol, 2008. **28**(19): p. 6033-43.
82. Sharma, A., et al., *Son is essential for nuclear speckle organization and cell cycle progression.* Mol Biol Cell, 2010. **21**(4): p. 650-63.
83. Lu, X., H.H. Ng, and P.A. Bubulya, *The role of SON in splicing, development, and disease.* Wiley Interdiscip Rev RNA, 2014. **5**(5): p. 637-46.
84. Karlas, A., et al., *Genome-wide RNAi screen identifies human host factors crucial for influenza virus replication.* Nature, 2010. **463**(7282): p. 818-22.
85. Hautbergue, G.M., et al., *Mutually exclusive interactions drive handover of mRNA from export adaptors to TAP.* Proc Natl Acad Sci U S A, 2008. **105**(13): p. 5154-9.
86. Gatfield, D., et al., *The DExH/D box protein HEL/UAP56 is essential for mRNA nuclear export in Drosophila.* Curr Biol, 2001. **11**(21): p. 1716-21.
87. Albert, B.J., et al., *Meayamycin inhibits pre-messenger RNA splicing and exhibits picomolar activity against multidrug-resistant cells.* Mol Cancer Ther, 2009. **8**(8): p. 2308-18.
88. Kaida, D., et al., *Spliceostatin A targets SF3b and inhibits both splicing and nuclear retention of pre-mRNA.* Nat Chem Biol, 2007. **3**(9): p. 576-83.
89. Schneider, J., et al., *Analysis of influenza B Virus NS1 protein trafficking reveals a novel interaction with nuclear speckle domains.* J Virol, 2009. **83**(2): p. 701-11.
90. Esparza, M., et al., *Chemical intervention of influenza virus mRNA nuclear export.* PLoS Pathog, 2020. **16**(4).
91. Amorim, M.J., et al., *Nuclear export of influenza A virus mRNAs requires ongoing RNA polymerase II activity.* Traffic, 2007. **8**(1): p. 1-11.

92. Wisskirchen, C., et al., *The cellular RNA helicase UAP56 is required for prevention of double-stranded RNA formation during influenza A virus infection.* J Virol, 2011. **85**(17): p. 8646-55.
93. Caruthers, J.M. and D.B. McKay, *Helicase structure and mechanism.* Curr Opin Struct Biol, 2002. **12**(1): p. 123-33.
94. Cordin, O., et al., *The DEAD-box protein family of RNA helicases.* Gene, 2006. **367**: p. 17-37.
95. Sengoku, T., et al., *Structural basis for RNA unwinding by the DEAD-box protein Drosophila Vasa.* Cell, 2006. **125**(2): p. 287-300.
96. Grzechnik, P. and J. Kufel, *Polyadenylation linked to transcription termination directs the processing of snoRNA precursors in yeast.* Mol Cell, 2008. **32**(2): p. 247-58.
97. Zhang, L., et al., *Influenza Virus NS1 Protein RNA-Interactome Reveals Intron Targeting.* J Virol, 2018.
98. Valcarcel, J., A. Portela, and J. Ortin, *Regulated M1 mRNA splicing in influenza virus-infected cells.* J Gen Virol, 1991. **72 (Pt 6)**: p. 1301-8.
99. Ilyinskii, P.O., et al., *Toxicity of influenza A virus matrix protein 2 for mammalian cells is associated with its intrinsic proton-channeling activity.* Cell Cycle, 2007. **6**(16): p. 2043-7.
100. Nayak, D.P., et al., *Influenza virus morphogenesis and budding.* Virus Res, 2009. **143**(2): p. 147-61.
101. Mor, A., et al., *Dynamics of single mRNP nucleocytoplasmic transport and export through the nuclear pore in living cells.* Nat Cell Biol, 2010. **12**(6): p. 543-52.
102. Cheng, H., et al., *Human mRNA export machinery recruited to the 5' end of mRNA.* Cell, 2006. **127**(7): p. 1389-400.
103. Luo, M.J. and R. Reed, *Splicing is required for rapid and efficient mRNA export in metazoans.* Proc Natl Acad Sci U S A, 1999. **96**(26): p. 14937-42.
104. Valencia, P., A.P. Dias, and R. Reed, *Splicing promotes rapid and efficient mRNA export in mammalian cells.* Proc Natl Acad Sci U S A, 2008. **105**(9): p. 3386-91.
105. Nemeroff, M.E., et al., *Influenza virus NS1 protein interacts with the cellular 30 kDa subunit of CPSF and inhibits 3' end formation of cellular pre-mRNAs.* Mol. Cell, 1998. **1**: p. 991-1000.
106. Qiu, Y. and R.M. Krug, *The influenza virus NS1 protein is a poly(A)-binding protein that inhibits nuclear export of mRNAs containing poly(A).* J Virol, 1994. **68**(4): p. 2425-32.
107. Zhang, L., et al., *Inhibition of Pyrimidine Synthesis Reverses Viral Virulence Factor-Mediated Block of mRNA Nuclear Export* J. Cell Biol., 2012 **196**: p. 315-26.
108. Girard, C., et al., *Post-transcriptional spliceosomes are retained in nuclear speckles until splicing completion.* Nat Commun, 2012. **3**: p. 994.
109. Kornblihtt, A.R., et al., *Alternative splicing: a pivotal step between eukaryotic transcription and translation.* Nat Rev Mol Cell Biol, 2013. **14**(3): p. 153-65.
110. Tilgner, H., et al., *Deep sequencing of subcellular RNA fractions shows splicing to be predominantly co-transcriptional in the human genome but inefficient for lncRNAs.* Genome Res, 2012. **22**(9): p. 1616-25.
111. Valcarcel, J., P. Fortes, and J. Ortin, *Splicing of influenza virus matrix protein mRNA expressed from a simian virus 40 recombinant.* J Gen Virol, 1993. **74 (Pt 7)**: p. 1317-26.
112. Carmody, S.R. and S.R. Wente, *mRNA nuclear export at a glance.* J Cell Sci, 2009. **122**(Pt 12): p. 1933-7.
113. Diamond, M.S., *IFIT1: A dual sensor and effector molecule that detects non-2'-O methylated viral RNA and inhibits its translation.* Cytokine Growth Factor Rev, 2014. **25**(5): p. 543-50.
114. Wang, S., et al., *Tyrosine 132 phosphorylation of influenza A virus M1 protein is crucial for virus replication by controlling the nuclear import of M1.* J Virol, 2013. **87**(11): p. 6182-91.
115. Kumar, N., et al., *Receptor tyrosine kinase inhibitors block multiple steps of influenza a virus replication.* J Virol, 2011. **85**(6): p. 2818-27.
116. Sun, A., et al., *Host-directed Inhibitors of Myxoviruses: Synthesis and in vitro Biochemical Evaluation.* ACS Med Chem Lett, 2011. **2**(11): p. 798-803.